Politecnico di Torino

POLITECNICO DI TORINO

Department of Environment, Land and Infrastructure Engineering

Master's Degree Program in

Agritech Engineering

Master's Thesis

Managed Aquifer Recharge for Climate-Resilient Agriculture: A Sensitivity-Based Design Framework

Supervisor:

Prof. Tiziana Anna Elisabetta Tosco

Candidate:

Khatereh Mehryari

Co-supervisor:

Prof. Alessandro Casasso

September 2026

Abstract

Water scarcity, climate change, and increasing agricultural water demand are key challenges for climate-resilient water management. Managed Aquifer Recharge (MAR) can help address these challenges by intentionally storing available water in aquifers for later use, especially during dry periods when irrigation demand is higher. This role is important under climate change, which can intensify the mismatch between water availability and crop-water demand. However, the feasibility of infiltration-based MAR depends on aquifer response, particularly groundwater mounding beneath recharge areas. Estimating water-table rise and dissipation is important for assessing water availability after recharge and avoiding excessive water-level rise, which may cause waterlogging, salinity risks, and reduced crop yield. Therefore, recharge geometry, recharge rate, and aquifer properties should be assessed before detailed site-specific design. This thesis presents a preliminary, sensitivity-based assessment of infiltration-based MAR configurations for climate-resilient agricultural water management. The study focused on groundwater mounding beneath basin-type and trench/strip-type recharge systems and compared how recharge geometry, recharge intensity, aquifer transmissivity, and selected transient parameters influence the magnitude and persistence of recharge-induced mounding. The thesis was carried out in four stages: analytical groundwater-mounding calculations, steady-state simulations in Visual MODFLOW Classic, selected transient assessment using MOUNDSOLV and one representative transient simulation in Visual MODFLOW Classic. The analytical calculations estimated water-table rise for basin-type and trench/strip-type recharge systems, the Visual MODFLOW simulations examined the spatial hydraulic-head response and were compared with analytical estimates, the MOUNDSOLV cases evaluated mound development and dissipation over time, and the representative transient Visual MODFLOW simulation was compared with the corresponding MOUNDSOLV response. The results showed that aquifer transmissivity is the main control on mound development. Under constant total recharge conditions, the trench configuration produced lower water-table rise than the circular basin, showing that long and narrow recharge geometries can reduce groundwater mounding. The strip sensitivity analysis showed that recharge intensity strongly affected mound development, while redistributing the same total recharge over different widths caused only small differences. The MOUNDSOLV results indicated that transient mound development and dissipation depend on hydraulic conductivity, specific yield, recharge-area distribution, and recharge duration, and that under low-conductivity conditions recharge-induced mounding may persist for several years after recharge stops. Overall, the study confirmed that analytical calculations, steady-state numerical simulations, and selected transient assessments provide a useful preliminary framework for comparing infiltration-based MAR alternatives. The results should be interpreted as preliminary guidance rather than a final site-specific design, and further investigation is required to evaluate aquifer heterogeneity, unsaturated-zone processes, clogging, water quality, monitoring needs, and practical implementation constraints.

Keywords: Managed Aquifer Recharge; groundwater mounding; Visual MODFLOW; MOUNDSOLV; transmissivity; recharge geometry; climate-resilient agriculture.

Acknowledgments

First and foremost, I would like to express my sincere and profound gratitude to my supervisor, Professor Tiziana Anna Elisabetta Tosco, for her invaluable guidance, constant availability, and encouragement throughout the development of this thesis. Her expertise, patience, and dedication have been a true source of inspiration, and I am deeply grateful for the trust she placed in me and for everything I have learned under her supervision. I would also like to extend my sincere thanks to my co-supervisor, Professor Alessandro Casasso, for his valuable advice, insightful suggestions, and contribution to this work.

I owe my deepest gratitude to my beloved family, whose unconditional love has accompanied me through every stage of this experience. To my dear mother and father, words can hardly express how thankful I am for all the sacrifices you have made, for your endless encouragement, and for always believing in me. Your love has been my greatest source of strength, your presence my comfort, and your faith in me has given me the courage to keep moving forward, even during the most difficult moments.

I would also like to express my heartfelt appreciation to my dear siblings, whose love, understanding, and companionship have meant more to me than words can say. Having you beside me has brought reassurance and motivation, particularly during the more demanding times. Your kindness, patience, and constant presence have made this experience lighter and more special, and I feel truly fortunate to have you in my life.

I am sincerely grateful to my dear friends, who have filled these years with warmth, laughter, and unforgettable memories. Thank you for your kindness, for listening, and for being there whenever I needed a moment of encouragement or simply a reason to smile. Your friendship has made this chapter of my life richer and more memorable.

This achievement would not have been the same without all the people who believed in me, inspired me, and stood beside me along the way. To each one of you, I offer my heartfelt thanks.

Contents

Abstract ..... **i**
Acknowledgments ..... **ii**
List of Figures ..... **vi**
List of Tables ..... **viii**
1. Introduction **1**
1.1 Agricultural water security under climate change 1
1.2 Climate-resilient agriculture and groundwater storage 1
1.3 Managed Aquifer Recharge for climate-resilient agriculture 2
1.4 Problem statement and methodological gap 2
1.5 Aim, objectives and scope of the thesis 3
1.6 Structure of the thesis 4
2. State of the Art and Technical Background **6**
2.1 Groundwater recharge and aquifer storage in agriculture 6
2.2 Technical requirements for MAR 6
2.3 MAR techniques for agricultural applications 7
2.4 Recharge-induced groundwater mounding 9
2.5 Analytical groundwater-mound assessment 11
2.5.1 Groundwater-flow equations 11
2.5.2 Circular recharge formulation 12
2.5.3 Strip/trench recharge formulation 14
2.6 Transient analytical and numerical modeling approaches 15
2.6.1 MOUNDSOLV and transient analytical mound assessment 15
2.6.2 MODFLOW and Visual MODFLOW Classic 16
2.6.3 Complementary roles of the modeling approaches 16
2.7 Sensitivity analysis and uncertainty in preliminary MAR assessment 17
2.8 Synthesis of literature 17
3. Methodology **19**
3.1 Research framework and modeling sequence 19
3.2 Modeling methods and comparison criteria 20
3.2.1 Steady-state analytical groundwater-mounding calculations 20
3.2.2 Visual MODFLOW Classic model setup 20
3.2.2.1 Output metrics and comparison criteria 20
3.3 Steady-state scenario design 21

3.3.1 Benchmark and diagnostic scenarios 23
3.3.1.1 Literature-based circular reference scenario 23
3.3.1.2 Square diagnostic case 25
3.3.1.3 Literature-based strip reference scenario 27
3.3.2 Transmissivity sensitivity analysis for circular and trench scenarios 29
3.3.2.1 Circular basin transmissivity sensitivity scenario 29
3.3.2.2 Trench transmissivity sensitivity Scenario 31
3.3.3 Recharge-configuration sensitivity cases 33
3.3.3.1 Constant-total-recharge circular basin cases 34
3.3.3.2 Modified literature-based strip cases 34
3.3.3.3 Constant-total-recharge strip cases 35
3.3.3.4 Supplementary narrow-trench case 35
3.4 Transient simulations 36
3.4.1 MOUNDSOLV scenario design 36
3.4.2 Monitoring points and dissipation criterion 37
3.4.3 Transient Visual MODFLOW comparison case 37
4. Results and discussion 38
4.1 Benchmark and diagnostic results 38
4.1.1 Literature-based circular benchmark and diagnostic checks 38
4.1.2 Square diagnostic case 41
4.1.3 Literature-based strip benchmark 43
4.1.4 Explanation of analytical–numerical differences 46
4.2 Circular and trench transmissivity-sensitivity results 46
4.2.1 Circular basin transmissivity-sensitivity results 46
4.2.2 Trench transmissivity-sensitivity scenario 50
4.2.3 Circular–trench comparison 54
4.3 Steady-state sensitivity results 55
4.3.1 Cases with changing total recharge 55
4.3.2 Constant-total-recharge circular basin cases 60
4.3.3 Constant-total-recharge strip cases 62
4.3.4 Supplementary narrow-trench case 63
4.3.5 Summary of recharge-distribution effects 65
4.4 Transient MOUNDSOLV results 65
4.4.1 Effect of recharge duration 65

4.4.2 Hydraulic conductivity and specific yield 66
4.4.3 Constant-diffusivity comparison 68
4.4.4 Recharge-area distribution 69
4.4.5 Distance-dependent response and dissipation 71
4.5 MOUNDSOLV–Visual MODFLOW comparison 73
4.6 Main findings of chapter 4 75
5. Conclusion 77
References 80
APPENDIX A. Additional figures for the circular recharge scenarios. 82
APPENDIX B. Additional figures for the strip/trench recharge scenarios. 84
APPENDIX C. Supplementary MOUNDSOLV recovery simulations. 87

List of Figures

Figure 2.1. Schematic representation of different Managed Aquifer Recharge infrastructure types. 8
Figure 2.2. Conceptual representation of recharge-induced groundwater mounding beneath a surface-infiltration area. 10
Figure 2.3. Geometry and symbols used to estimate groundwater mounding beneath a circular infiltration area 13
Figure 2.4. Geometry and symbols used to estimate groundwater mounding beneath a long infiltration strip 14
Figure 3.1. Summary of the methodological workflow adopted in this study. 19
Figure 3.2. Numerical setup of the corrected literature-based circular recharge reconstruction .. 25
Figure 3.3. Numerical setup of the square recharge scenario 26
Figure 3.4. Numerical setup of the literature-based strip recharge scenario 28
Figure 3.5. Numerical setup of the circular recharge scenario 31
Figure 3.6. Numerical setup of the trench scenario 33
Figure 4.1. Simulated hydraulic-head distribution for the corrected literature-based circular recharge scenario. 40
Figure 4.2. Central hydraulic-head profiles for the corrected unconfined model (case 1), constant-transmissivity diagnostic case (case 3), and analytical reference value. 41
Figure 4.3. Simulated hydraulic head distribution for the square recharge scenario. 42
Figure 4.4. Central hydraulic-head profiles for the corrected circular and square recharge scenarios. 43
Figure 4.5. Simulated hydraulic-head distribution for the literature-based strip recharge scenario. 45
Figure 4.6. Comparison of analytical and Visual MODFLOW water-table rise under different transmissivity conditions for the circular-basin sensitivity scenario. 47
Figure 4.7. Comparison of simulated plan-view hydraulic head distributions for the circular transmissivity-sensitivity scenario at different transmissivity values. 48
Figure 4.8. Comparison of simulated hydraulic head profiles along the central cross-section for the circular transmissivity-sensitivity scenario under different transmissivity values. 49
Figure 4.9. Comparison of analytical and Visual MODFLOW water-table rise under different transmissivity conditions for the trench transmissivity-sensitivity scenario. 51
Figure 4.10. Comparison of simulated plan-view hydraulic head distributions for the trench transmissivity-sensitivity scenario at different transmissivity values. 52
Figure 4.11. Comparison of simulated hydraulic head profiles along the central cross-section perpendicular to the trench axis for the trench transmissivity-sensitivity scenario at different transmissivity values. 53
Figure 4.12. Simulated hydraulic head distribution for the modified recharge-rate strip case. 57
Figure 4.13. Simulated hydraulic head distribution for the modified strip-width case. 58
Figure 4.14. Comparison of simulated hydraulic head profiles along the central cross-section for the preliminary strip sensitivity cases. 60
Figure 4.15. Effect of recharge area on simulated water-table rise for the constant-total-recharge circular basin cases. 61
Figure 4.16. Comparison of simulated hydraulic head profiles along the central cross-section for the constant-total-recharge strip sensitivity cases. 63

Figure 4.17. Comparison of simulated hydraulic-head profiles along the central cross-section perpendicular to the trench axis for the baseline trench and supplementary narrow-trench cases under selected transmissivity conditions. 64
Figure 4.18. Long-term transient development of water-table rise for the reference MOUNDSOLV scenario. 66
Figure 4.19. Transient water-table rise for hydraulic-conductivity and specific-yield scenarios. 67
Figure 4.20. Transient water-table rise for constant-diffusivity MOUNDSOLV scenarios. 68
Figure 4.21. Transient water-table rise at the recharge-basin center for the constant-total-recharge scenarios. 69
Figure 4.22. Water-table rise profiles along the x-axis at (y=0) after 365 days for the constant-total-recharge scenarios MS-1, MS-5, and MS-6. 70
Figure 4.23. Transient water-table rise at different monitoring distances from the recharge-basin edge for the reference scenario. 71
Figure 4.24. Mound dissipation after recharge stopped at 365 days for different monitoring distances from the recharge-basin edge. 72
Figure 4.25. Comparison of MOUNDSOLV and transient Visual MODFLOW water-table rise profiles after 365 days for the reference recharge case. 74
Figure 4.26. Transient Visual MODFLOW water-table rise at the recharge-basin center and at monitoring points located approximately 40, 90, and 200 m from the basin edge. 75

List of Tables

Table 2.1. Study-oriented classification of MAR techniques and their relevance to agricultural MAR assessment..... 9
Table 3.1. Overview of the steady-state scenarios and comparison framework..... 22
Table 3.2. Input data and derived parameters for the literature-based circular scenario. 23
Table 3.3. Numerical model settings for the corrected literature-based circular recharge scenario. 25
Table 3.4. Input data and derived parameters for the literature-based strip recharge scenario. ... 27
Table 3.5. Numerical model settings for the literature-based strip recharge scenario..... 29
Table 3.6. Input data and derived parameters used for the circular transmissivity-sensitivity scenario. 30
Table 3.7. Input data and derived parameters for the trench transmissivity-sensitivity scenario. 32
Table 3.8. Recharge-area and recharge-rate configurations for the constant-total-recharge circular basin cases..... 34
Table 3.9. Configuration of the constant-total-recharge strip sensitivity cases. 35
Table 3.10. Numerical settings for the baseline and supplementary narrow-trench cases. 36
Table 3.11. Summary of MOUNDSOLV scenario groups used in the transient assessment. 37
Table 4.1. Analytical value and numerical diagnostic checks for the literature-based circular recharge scenario. 40
Table 4.2. Summary of numerical model outputs for the square recharge scenario..... 41
Table 4.3. Comparison of the numerical results for the corrected circular and square recharge scenarios..... 43
Table 4.4. Analytical results for the literature-based strip recharge scenario..... 44
Table 4.5. Numerical outputs for the literature-based strip recharge scenario. 44
Table 4.6. Comparison of analytical and numerical water-table rise results for the literature-based strip recharge scenario. 45
Table 4.7. Comparison of analytical and Visual MODFLOW results for the circular transmissivity-sensitivity scenario at different transmissivity conditions. 47
Table 4.8. Comparison of analytical and Visual MODFLOW results for the trench scenario transmissivity-sensitivity under different transmissivity conditions. 50
Table 4.9. Comparison of numerical water-table rise results for the circular and trench transmissivity-sensitivity scenarios under the same total applied recharge rate..... 54
Table 4.10. Supplementary analytical calculations for the strip recharge scenario. 55
Table 4.11. Numerical model settings and simulated outputs for the modified recharge-rate strip case..... 56
Table 4.12. Numerical model settings for the modified strip-width case. 58
Table 4.13. Comparison of numerical settings and simulated outputs for the reference strip case and the two modified sensitivity cases..... 59
Table 4.14. Comparison of analytical and numerical water-table rise values for the preliminary strip sensitivity cases..... 59
Table 4.15. Numerical results for the supplementary constant-total-recharge circular basin sensitivity cases..... 61
Table 4.16. Numerical results for the constant-total-recharge strip sensitivity cases. 62
Table 4.17. Numerical results of the supplementary narrow-trench case under selected transmissivity case. 64

Table 4.18. Comparison of one-year, ten-year, and long-term transient water-table rise for the reference MOUNDSOLV scenario. 66
Table 4.19. Summary of transient MOUNDSOLV results for hydraulic-conductivity and specific-yield scenarios. 67
Table 4.20. Constant-diffusivity MOUNDSOLV scenarios with ($D = T/Sy$) maintained at 200 m^2/day. 68
Table 4.21. Effect of recharge-area size and infiltration intensity under constant total recharge rate. 69
Table 4.22. Simulated water-table rise at different monitoring distances after 365 days for the reference scenario. 71
Table 4.23. Dissipation time after recharge stopped based on the adopted 0.10 m threshold. 73
Table 4.24. Comparison of maximum water-table rise predicted by MOUNDSOLV and transient Visual MODFLOW after 365 days for the reference recharge case. 73

1. Introduction

1.1 Agricultural water security under climate change

Water is essential for agricultural production, food security, and rural livelihoods. Agricultural water security means having reliable access to enough water at the time when crops need it. However, this security is increasingly threatened by water scarcity, climate change, and growing competition among water users. Agriculture is the largest water-using sector worldwide and accounts for about 70% of global freshwater withdrawals. Water scarcity is not caused only by a physical lack of water; it can also result from poor allocation, inefficient use, limited infrastructure, and inadequate management of available resources (FAO, 2020; Ingrao et al., 2023).

The scale of the problem is considerable. According to FAO, approximately 3.2 billion people live in agricultural areas affected by high or very high water shortages or scarcity, including 1.2 billion people living under very high water constraints (FAO, 2020). More recent assessments show that water stress levels vary widely across countries and regions (FAO & UN-Water, 2024). Agriculture is particularly vulnerable because crop production depends not only on the total amount of available water but also on its timing during the growing season.

Climate change further reduces the reliability of agricultural water supplies. Changes in precipitation patterns, rising evapotranspiration, longer droughts, and more intense rainfall events affect both the amount and seasonal distribution of water resources (Caretta et al., 2022; Turral et al., 2011). Recent observations show that many river basins experience conditions that are either wetter or drier than normal, indicating increasing variability in the global water cycle (WMO, 2025). As a result, water may be abundant during wet periods but insufficient during hot and dry seasons, when irrigation demand is usually highest.

Future warming may further increase the gap between renewable water availability and human water demand, particularly in major agricultural regions (Rosa & Sangiorgio, 2025). Therefore, climate-resilient agriculture requires more than increasing water supply or improving irrigation efficiency. It also requires strategies that manage seasonal variability and make water available when crop demand is highest.

1.2 Climate-resilient agriculture and groundwater storage

Climate-resilient agriculture aims to maintain agricultural production under climate variability and water-related stress. From a water-management perspective, resilience depends on reliable access to water during dry periods and critical stages of crop growth. A reliable irrigation supply can therefore reduce the vulnerability of agricultural systems to drought and irregular rainfall (Caretta et al., 2022; Turral et al., 2011).

Groundwater can improve this reliability by providing water when rainfall and surface-water supplies are insufficient. It can act as an important buffer against short-term variations in precipitation and support crop production during dry periods. However, excessive groundwater abstraction can reduce aquifer storage, lower groundwater levels, and weaken the long-term adaptive capacity of agricultural systems (Caretta et al., 2022). Maintaining groundwater levels within an appropriate range can also reduce the propagation of meteorological drought into agricultural drought, as observed in the Huaibei Plain (Xu et al., 2024).

The long-term contribution of groundwater to agricultural resilience therefore depends on sustainable management. Where surplus water is available during wetter periods, Managed Aquifer Recharge (MAR) can be used to store water underground for later use during dry periods. MAR does not create additional water; instead, it changes the time and location of water storage and can complement measures such as efficient irrigation and improved irrigation scheduling (Alley et al., 2022; Dillon et al., 2009).

1.3 Managed Aquifer Recharge for climate-resilient agriculture

Managed Aquifer Recharge (MAR) involves deliberately directing water into an aquifer so that it can be recovered later or provide environmental benefits. In agricultural areas, this approach allows excess water from wet periods to be stored underground and made available during dry periods, when irrigation demand is typically greater. By improving the seasonal availability and reliability of groundwater resources, MAR can contribute to more climate-resilient agricultural water management (Alley et al., 2022; Dillon et al., 2009).

MAR may be implemented through surface-infiltration facilities or recharge wells. The suitability of each method depends on factors such as local water availability, land and soil characteristics, aquifer properties, and water quality (Bouwer, 2002; Dillon et al., 2009). The main MAR methods and the technical factors affecting their suitability are discussed in Chapter 2.

This thesis focuses on infiltration-based MAR and, specifically, on groundwater mounding beneath simplified basin- and trench-type recharge systems. When water is applied faster than the aquifer can transmit and redistribute it, the groundwater table may rise locally beneath the recharge area. Evaluating this hydraulic response is important because excessive mounding can restrict system performance (Bouwer, 2002; Bouwer et al., 1999). It therefore provides the basis for the problem statement and research objectives presented in the following sections.

1.4 Problem statement and methodological gap

The preliminary assessment of Managed Aquifer Recharge for agricultural water management involves several challenges. The amount of water available for recharge and the irrigation demand may change considerably during the year. At the same time, detailed information about aquifer properties and boundary conditions is often limited during the early planning stage. Therefore, an initial quantitative assessment is needed to estimate the possible groundwater response and identify the parameters that require further investigation.

The main gap addressed in this thesis lies between general MAR feasibility guidance and detailed site-specific groundwater modeling. General MAR guidance identifies requirements including suitable source water, appropriate aquifer conditions, accessible land, operational capability, and monitoring requirements (Alley et al., 2022; Dillon et al., 2009). Nonetheless, these general criteria do not directly quantify the groundwater-level rise expected for a selected recharge setup. Detailed numerical models can provide more site-specific results, but they require a precisely defined conceptual model, reliable hydrogeological data, suitable boundary conditions, and enough observations for calibration (Barnett et al., 2012). Such information is often incomplete during the preliminary assessment stage.

For infiltration-based MAR systems, the main question at the preliminary stage is whether the suggested recharge conditions could produce an unacceptable rise in groundwater levels. Although the main controls on groundwater mounding are generally known, their combined effects may vary

considerably with recharge geometry and aquifer conditions. Recharge rate, recharge-area dimensions, transmissivity, storage properties, and boundary conditions may all influence the magnitude and spatial extent of mound development (Bouwer, 2002; Bouwer et al., 1999; Hantush, 1967). A quantitative screening method is therefore needed to compare alternatives and determine which factors have the greatest influence on mound development.

To address this gap, the thesis develops an integrated preliminary framework that combines analytical calculations, simplified numerical simulations, and selected transient assessments. The framework compares basin- and trench-type recharge configurations, assesses groundwater-mounding behavior, and identifies the assumptions and parameters that most strongly affect the results. Its purpose is not to produce a final engineering design, but to support preliminary comparison and indicate where further field-data collection and site-specific studies are required.

1.5 Aim, objectives and scope of the thesis

The main aim of this thesis is to develop a preliminary, sensitivity-based framework for assessing groundwater mounding beneath infiltration-based Managed Aquifer Recharge systems in support of climate-resilient agricultural water management. The framework is intended for the early assessment stage, when detailed site-specific information may still be limited.

The study examines simplified basin-type and trench-type recharge configurations using analytical calculations, numerical simulations at steady-state, and selected transient assessments. It focuses on the magnitude, spatial distribution, and persistence of groundwater mounding. In the constant-total-recharge comparisons, the distribution of recharge areas refers to variations in the size or width of recharge areas while the recharge rate is modified to maintain the total applied recharge rate (Q) unchanged.

The specific objectives of this thesis are:

1. To review the main hydrogeological concepts relevant to infiltration-based MAR and to define simplified basin-type and trench-type recharge scenarios for preliminary comparison.
2. To apply analytical groundwater-mounding calculations to estimate water-table rise and examine the effects of recharge geometry, recharge rate, and aquifer transmissivity.
3. To simulate selected steady-state recharge scenarios using Visual MODFLOW Classic and compare the numerical groundwater-mound response with the corresponding analytical estimates.
4. To evaluate the sensitivity of groundwater-mound magnitude and spatial distribution to aquifer transmissivity, recharge rate, recharge geometry, and recharge-area distribution.
5. To assess transient mound development and dissipation using MOUNDSOLV, with attention to hydraulic conductivity, specific yield, recharge duration, recharge-area distribution, and distance from the recharge source, and to compare a representative basin-type case with a corresponding transient Visual MODFLOW simulation.
6. To integrate the analytical, steady-state numerical, and transient results into a preliminary screening approach for comparing infiltration-based MAR alternatives and identifying where further site-specific investigation is required.

Based on these objectives, the thesis addresses the following research questions:

1. How do aquifer transmissivity, recharge rate, recharge geometry, and recharge-area distribution influence the magnitude and spatial form of groundwater mounding under simplified infiltration-based MAR conditions?
2. How closely do steady-state Visual MODFLOW Classic simulations reproduce the groundwater-mound response estimates analytically for basin-type and trench-type recharge configurations, and what factors explain the differences between the two approaches?
3. How do hydraulic conductivity, specific yield, recharge duration, recharge-area distribution, and distance from the recharge source affect transient groundwater-mound development and dissipation in MOUNDSOLV?
4. How consistent are the transient groundwater-mound results obtained from MOUNDSOLV and Visual MODFLOW for a representative basin-type recharge case?
5. How can a combined sensitivity-based assessment support the preliminary screening of infiltration-based MAR alternatives when detailed site-specific data are not yet available?

The scope of this thesis is limited to a preliminary hydrogeological assessment under simplified aquifer conditions. The focus is on the aquifer's hydraulic response to selected recharge configurations. Water quality, clogging, detailed unsaturated-zone processes, cost-effectiveness, legal requirements, institutional structures, social factors, and site-specific engineering design for the site are not directly assessed. The findings should therefore be interpreted as support for preliminary comparison and further investigation, rather than as a final design or implementation strategy for a specific location.

1.6 Structure of the thesis

This thesis is organized into five chapters.

Chapter 1 introduces the research topic and explains the motivation for the study. It discusses agricultural water security under climate change, the role of groundwater storage, and the potential contribution of Managed Aquifer Recharge (MAR). It then presents the problem statement, knowledge gap, aim, research objectives, research questions, and scope of the thesis.

Chapter 2 provides the scientific and technical background of the study. It reviews groundwater recharge and aquifer storage, MAR techniques relevant to agriculture, and groundwater mounding as an important hydraulic constraint. It also introduces the analytical and numerical approaches used for steady-state and transient MAR assessment, together with the role of sensitivity analysis.

Chapter 3 describes the methodology used in the thesis. It presents the conceptual framework, the basin-type and trench-type recharge scenarios, and the analytical groundwater-mounding calculations. It then describes the steady-state Visual MODFLOW Classic simulations, the transient MOUNDSOLV assessments, the representative transient Visual MODFLOW comparison case, and the criteria used to compare the results.

Chapter 4 presents and discusses the results. It compares analytical and numerical groundwater-mound estimates and examines the effects of aquifer transmissivity, recharge rate, recharge geometry, and recharge-area distribution. It also evaluates transient mound development and dissipation and compares MOUNDSOLV with a corresponding transient Visual MODFLOW simulation for a representative basin-type case.

Chapter 5 summarizes the key results and responds to the research questions. It discusses the contribution and limitations of the preliminary assessment framework and provides recommendations for future site-specific investigation.

2. State of the Art and Technical Background

This chapter presents the scientific and technical background required for the preliminary assessment developed in this thesis. While Chapter 1 explains the motivation and research problem, this chapter focuses on the hydrogeological concepts and previous studies that support the assessment framework.

The chapter first reviews groundwater recharge and aquifer storage in agricultural water management. It then examines the main technical requirements and infiltration-based MAR techniques relevant to agricultural applications. Groundwater mounding is discussed as the main hydraulic constraint considered in this study. The chapter also reviews the analytical and numerical approaches used for steady-state and transient groundwater-mound assessment and explains the role of sensitivity analysis when detailed site-specific data are limited. These concepts provide the basis for the methodology presented in Chapter 3.

2.1 Groundwater recharge and aquifer storage in agriculture

Groundwater recharge is the process by which water moves from the land surface through the soil and unsaturated zone until it reaches the saturated aquifer. Recharge can occur naturally through the infiltration of rainfall, rivers, and other surface-water sources. It can also be intentionally increased through managed systems such as infiltration basins, recharge trenches, and recharge wells. In agricultural areas, irrigation losses, drainage, and land-management practices may also influence the amount and timing of groundwater recharge (Bouwer, 2002; Dillon et al., 2009).

In an unconfined aquifer, recharge increases groundwater storage and usually causes the water table to rise. The magnitude and timing of this response depend on the recharge rate and area, aquifer transmissivity, specific yield, initial groundwater depth, and hydraulic boundary conditions. Part of the recharged water may remain in storage, while another part may move laterally towards rivers, drains, wells, or other discharge boundaries. If the aquifer cannot transmit the added water efficiently, a local groundwater mound may develop beneath the recharge area (Bouwer, 2002; Bouwer et al., 1999).

Aquifer storage can offer several advantages for agricultural water management. Compared with surface reservoirs, underground storage is less directly exposed to evaporation and generally requires less large-scale surface-storage infrastructure. It may therefore provide a useful way to store water during periods of greater availability and make it accessible during later periods of higher irrigation demand. However, the practical value of aquifer storage depends on whether the water can remain available for a useful period and whether it can be recovered or used without causing unacceptable hydraulic or water-quality effects (Bouwer, 2002; Dillon et al., 2009).

These storage and transmission processes form the hydrogeological basis for evaluating the infiltration-based MAR systems discussed in the following sections.

2.2 Technical requirements for MAR

This section focuses on the main technical requirements for implementing Managed Aquifer Recharge, while the general concept and agricultural relevance of MAR were introduced in Chapter 1. For a MAR strategy to be effective, its objective, water source, recharge method, and local hydrogeological conditions must be compatible. In practice, this requires suitable recharge-

water quantity and quality, adequate land or infrastructure, permeable surface and vadose-zone materials, and an aquifer with enough capacity to store and transmit the added water without causing unacceptable hydraulic or water-quality effects (Bouwer, 2002; Dillon et al., 2009; Zheng et al., 2023).

The key hydrogeological factors for infiltration-based MAR are soil permeability, depth to groundwater, aquifer transmissivity, storage properties, and hydraulic boundary conditions. The soil and vadose zone must allow water to move downward, while the saturated aquifer must be able to redistribute the recharge without excessive groundwater mounding. These subsurface conditions are especially important because they are difficult to adjust once a site has been selected (Alkhatib et al., 2021; Bouwer, 2002; Bouwer et al., 1999).

Long-term performance also depends on operation and maintenance. Clogging of infiltration surfaces can reduce recharge efficiency and may require pretreatment, drying periods, scraping, or other maintenance procedures. In agricultural applications, crop tolerance, the timing of water availability, field accessibility, and the risk of shallow groundwater or waterlogging must also be considered (Levintal et al., 2023). MAR feasibility therefore depends on how water availability, recharge infrastructure, soil and aquifer properties, operation, and groundwater response interact. The following section reviews the main MAR techniques relevant to agricultural applications.

2.3 MAR techniques for agricultural applications

Managed Aquifer Recharge can be implemented through surface-infiltration, well-based, and induced-recharge methods. The choice of method depends on the purpose of the scheme, available source water, land availability, and local hydrogeological conditions. This thesis focuses on two surface-infiltration configurations: compact basin-type systems and elongated trench/strip-type systems. These configurations differ in land requirements, operation, monitoring needs, and dependence on soil and aquifer properties (Alley et al., 2022; Dillon et al., 2009).

The main MAR infrastructure types are schematically shown in Figure 2.1.

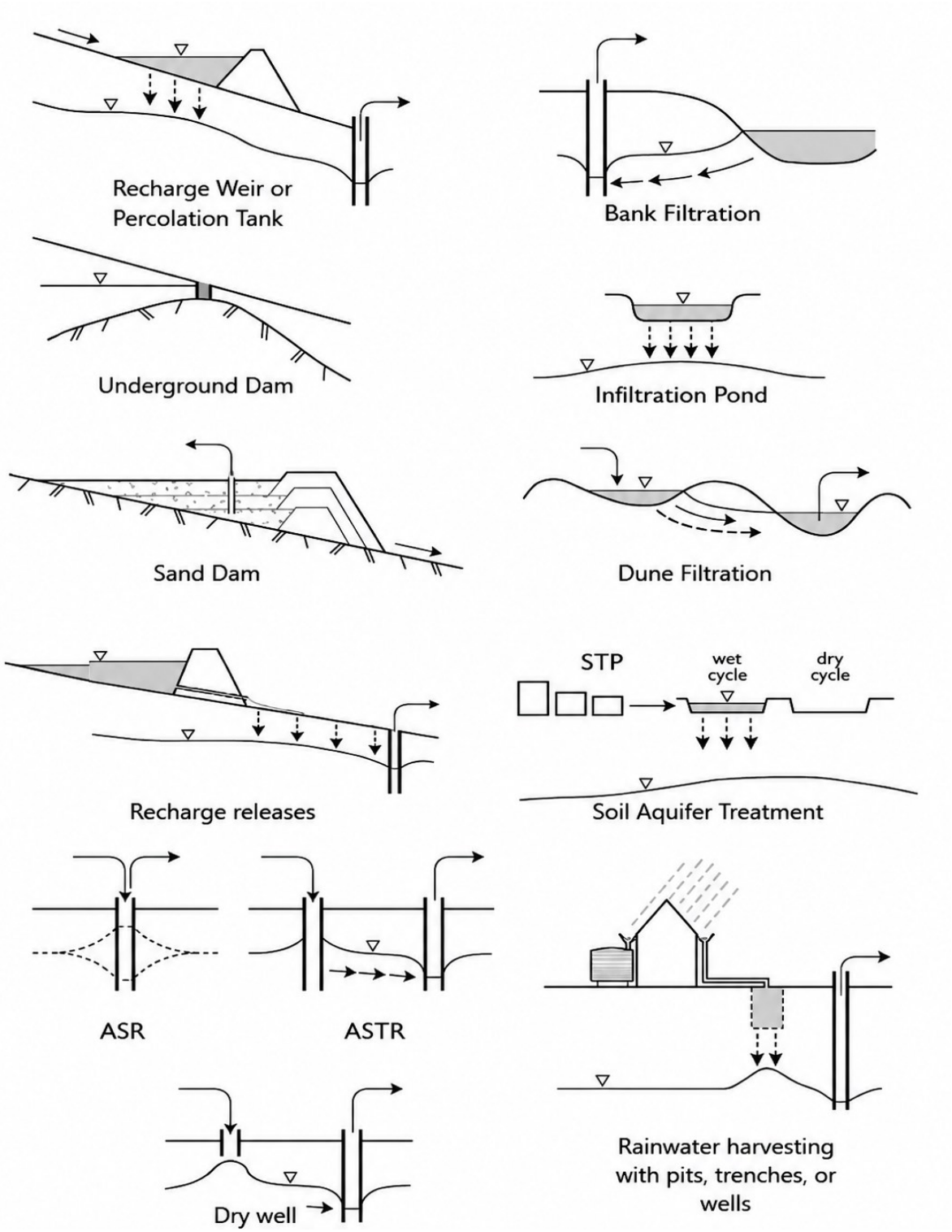

Figure 2.1. Schematic representation of different Managed Aquifer Recharge infrastructure types. The present thesis focuses on surface-infiltration configurations, particularly basin-type and trench/strip-type recharge systems (Source: Dillon et al. 2009).

Surface-infiltration methods are particularly relevant to agriculture because available land can be used to spread water over relatively large areas. Agricultural Managed Aquifer Recharge (Ag-MAR) extends this approach by applying excess water to fields, orchards, or other suitable land when crop and soil conditions allow. It is feasible depending on timing and quality of available water, soil and unsaturated-zone properties, groundwater response, crop tolerance and practical field limitations (Levintal et al., 2023).

The classification used in this thesis is summarized in Table 2.1.

Table 2.1. Study-oriented classification of MAR techniques and their relevance to agricultural MAR assessment.

MAR technique group	Typical examples	Relevance to agricultural MAR and this study
Compact surface-infiltration systems (basin-type)	Infiltration basins, recharge ponds, spreading areas, flooded agricultural fields	Suitable where adequate land and permeable surface materials are available; represented by the basin-type configurations examined in this thesis
Elongated surface-infiltration systems (trench/strip-type)	Recharge trenches, infiltration ditches, and strips	Recharge is applied over an elongated area; represented by the trench/strip-type configurations examined in this thesis
Well-based recharge systems	Injection wells, Aquifer Storage and Recovery (ASR), and Aquifer Storage Transfer and Recovery (ASTR)	Useful where surface infiltration is unsuitable or controlled recovery is required; not quantitatively modeled in this thesis
Induced-recharge systems	Bank filtration and river-connected recharge	Depend on a hydraulic connection with nearby surface-water bodies; included only as contextual MAR alternatives

Note: Compiled by the author based on Alley et al. (2022), Bouwer (2002), Dillon et al. (2009), and Levintal et al. (2023).

Surface-infiltration methods require suitable soil, vadose-zone, and aquifer conditions. Practical constraints such as clogging, recharge-water quality, and groundwater depth must also be considered, as discussed in Section 2.2. Among the available methods, basin- and trench/strip-type systems were selected because they represent two contrasting surface-infiltration geometries. Basin systems apply recharge over a compact area, whereas trench/strip systems distribute it over an elongated area (Dillon et al., 2009). The following section examines groundwater mounding as the main hydraulic response used to compare these configurations.

2.4 Recharge-induced groundwater mounding

Groundwater mounding is the local rise of the water table beneath and around a recharge area when water is added to an unconfined aquifer. Some increase in groundwater level is a normal response to recharge. However, excessive mounding can reduce the available unsaturated thickness, limit further infiltration, and increase the risk of waterlogging at the ground surface or in nearby areas. Groundwater mounding is therefore an important hydraulic constraint in the preliminary assessment of infiltration-based MAR systems (Bouwer, 2002; Bouwer et al., 1999). The formation of a recharge-induced groundwater mound is schematically illustrated in Figure 2.2.

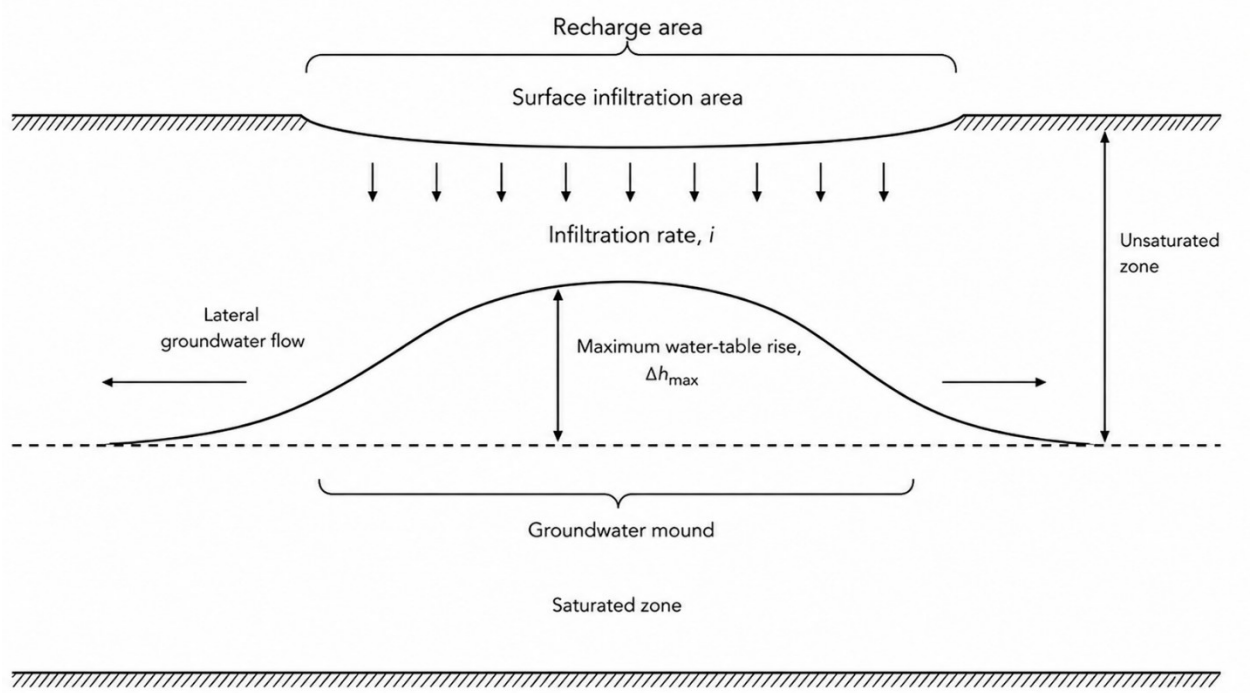

Figure 2.2. Conceptual representation of recharge-induced groundwater mounding beneath a surface-infiltration area. Redrawn by the author based on Thompson et al. (2007).

Groundwater-mound development has been examined using analytical and numerical approaches. The growth and decline of groundwater mounds beneath uniformly recharged circular and rectangular areas in unconfined aquifers were investigated using analytical solutions developed by Hantush (1967). These solutions allow the estimation of water-table rise during recharge and its decline after recharge stops.

In 1999, Bouwer et al. applied groundwater-mounding analysis to the planning of infiltration-based recharge systems. The design factors considered included infiltration rate, recharge-area dimensions, transmission through the unsaturated zone, and aquifer response. In addition, Bouwer (2002) also stated that an aquifer recharged through infiltration should have sufficient transmissivity to handle the additional water without excessive rise in the water table.

When the recharge rate remains constant, the magnitude and spatial extent of a mound are predominantly determined by recharge geometry, aquifer transmissivity, initial groundwater conditions, and hydraulic boundaries. A higher and more concentrated mound in a low-transmissivity aquifer generally means that the added water cannot spread easily away from the recharge area. In contrast, higher transmissivity causes the recharge-induced rise to spread over a wider area, which leads to a lower local mound height.

Transient mound behavior is influenced by both time and the properties of aquifers. The mound's development rate and duration after recharge depend on factors such as recharge duration, hydraulic conductivity, and storage-related parameters including specific yield. A mound may therefore continue to affect groundwater levels after the recharge period has ended, even when the maximum water-table rise during operation is acceptable (Bouwer et al., 1999; Hantush, 1967).

Groundwater mounding is particularly important in agricultural MAR. Recharge may be applied on or near cultivated land, where an excessive rise in groundwater level can reduce root-zone aeration and increase the risk of waterlogging. Preliminary assessment should therefore consider not only the volume of water that can be recharged, but also whether the expected groundwater response remains acceptable under the proposed operating conditions. Reviews of Ag-MAR similarly identify groundwater response, soil conditions, crop suitability, and practical field constraints as important feasibility considerations (Levintal et al., 2023).Recharge geometry also affects mound height and spatial distribution. This provides the basis for comparing the basin- and trench/strip-type configurations introduced in Section 2.3 (Bouwer et al., 1999).

The acceptable water-table rise is site-specific and depends on factors such as the initial depth to groundwater, the unsaturated thickness that must be maintained, crop-root conditions, and nearby infrastructure. Therefore, this thesis does not apply a universal operational water-table rise threshold; instead, the results are interpreted comparatively as part of a preliminary screening assessment.

Because groundwater mounding is the main hydraulic constraint considered in this thesis, a quantitative method is required to estimate water-table rise under different recharge and aquifer conditions. The following section reviews the analytical approaches used as the first step of this assessment.

2.5 Analytical groundwater-mound assessment

Analytical groundwater-mound assessment is used in this thesis to obtain reference estimates for the selected basin- and trench-type recharge configurations. Analytical solutions provide simplified mathematical descriptions of how recharge produces groundwater-level rise beneath and around a recharge area. This approach allows the effects of infiltration rate, recharge geometry, aquifer transmissivity, and selected boundary conditions to be examined before developing a numerical model. Because the analytical calculations are based on simplified aquifer and boundary conditions, the results are used as reference estimates rather than site-specific predictions (Bouwer et al., 1999; Hantush, 1967).

Previous analytical work provides the basis for the calculations used in this thesis. Hantush (1967) developed solutions for uniformly recharged circular and rectangular areas. Bouwer et al. (1999) later used related formulations for the preliminary assessment of infiltration-based recharge systems, while Zlotnik et al. (2017)extended mound analysis to aquifers with sloping bases. The Bouwer et al. (1999) formulations are used here for the basin- and strip/trench-type recharge configurations.

2.5.1 Groundwater-flow equations

Groundwater flow in saturated porous media is described by Darcy's law combined with conservation of mass. In its one-dimensional form, Darcy's law connects the volumetric flow rate to the difference in hydraulic-head along a flow path and can be expressed as (Harbaugh, 2005):

$$Q = \frac{KA(h1 - h2)}{L} \tag{2.1}$$

where Q is the volumetric flow rate, K is the hydraulic conductivity in the direction of flow, A is the cross-sectional area perpendicular to flow, $h_1 - h_2$ is the head difference along the flow path, and L is the length of the flow path.

When Darcy's law is combined with mass conservation, the three-dimensional transient groundwater-flow equation can be written as:

$$Ss\frac{\partial h}{\partial t} = \frac{\partial}{\partial x}\left(Kx\frac{\partial h}{\partial x}\right) + \frac{\partial}{\partial y}\left(Ky\frac{\partial h}{\partial y}\right) + \frac{\partial}{\partial z}\left(Kz\frac{\partial h}{\partial z}\right) + W \quad (2.2)$$

where S_s is specific storage, K_x, K_y, and K_z are hydraulic-conductivity components, W represents sources and sinks, and t is time. Under steady-state conditions, the storage term is equal to zero because hydraulic head does not vary with time. This is the general groundwater-flow equation solved numerically in MODFLOW using a finite-difference formulation (Harbaugh, 2005).

For groundwater-mound assessment in unconfined aquifers, the transient flow equation can be expressed in a simplified areal diffusivity form. Based on the linearized formulation of Zlotnik et al. (2017), and neglecting the slope-related advective term, the mound response can be written in simplified form as:

$$Sy\frac{\partial s}{\partial t} = T\left(\frac{\partial^2 s}{\partial x^2} + \frac{\partial^2 s}{\partial y^2}\right) + i \quad (2.3)$$

where S_y is specific yield, T is aquifer transmissivity, and i is the infiltration rate. In steady-state analytical calculations, the time derivative is neglected. In transient mound solutions, the storage term is retained, and the response depends on aquifer diffusivity, commonly expressed as T/S_y (Zlotnik et al., 2017).

The following subsections describe the steady-state circular and strip/trench formulations used in this study.

2.5.2 Circular recharge formulation

Circular recharge formulations represent infiltration over a circular or approximately compact recharge area. Under the assumptions used in the analytical approach, the aquifer is represented as homogeneous, isotropic, and unconfined, and recharge is applied uniformly under steady-state conditions. The groundwater response is treated as approximately axisymmetric, with the maximum mound generally occurring beneath the center of the recharge area.

The geometry and main parameters used in the circular recharge formulation are shown in Figure 2.3.

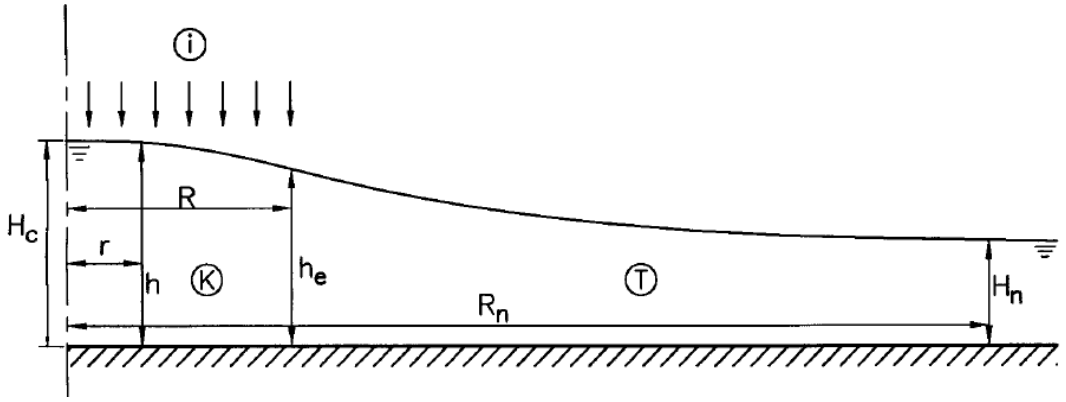

Figure 2.3. Geometry and symbols used to estimate groundwater mounding beneath a circular infiltration area (Source: Bouwer et al., 1999).

Following Bouwer et al. (1999), the total water-table rise beneath the center of a circular recharge area can be estimated by combining the head difference within the recharge area with the head difference between the edge of the recharge area and the distant control groundwater level.

For a circular recharge area, the head difference between the center and the edge of the recharge area is expressed as:

$$H_c - h_e = \frac{iR^2}{4T} \tag{2.4}$$

The head difference between the edge of the recharge area and the control groundwater level is given by:

$$h_e - H_n = \frac{iR^2}{2T} \ln\left(\frac{R_n}{R}\right) \tag{2.5}$$

Combining Equations 2.4 and 2.5 gives the total water-table rise beneath the center of the recharge area relative to the control groundwater level:

$$H_c - H_n = \frac{iR^2}{4T}\left(1 + 2\ln\frac{R_n}{R}\right) \tag{2.6}$$

where H_c is the groundwater head at the center of the mound, h_e is the groundwater head at the edge of the recharge area, H_n is the control groundwater level, R is the equivalent circular radius of the recharge area, R_n is the radial distance from the center of the recharge area to the control groundwater level, T is the aquifer transmissivity, and i is the gross infiltration rate.

When the recharge area is not exactly circular, an equivalent circular radius can be calculated from its area using:

$$R = \sqrt{(A/\pi)} \tag{2.7}$$

where A is the total recharge area. This conversion allows approximately square or other compact basin configurations to be represented by an equivalent circular geometry for preliminary analytical calculations.

According to this formulation, water-table rise increases with infiltration rate. For a fixed infiltration rate, increasing the recharge-area size also increases the total recharge applied to the

aquifer and generally increases water-table rise. Higher aquifer transmissivity generally reduces the maximum local water-table rise by allowing the added water to spread more efficiently (Bouwer et al., 1999). However, in the constant-total-recharge comparisons used in this thesis, recharge area and infiltration rate change together and should therefore be interpreted jointly.

In this thesis, the circular formulation is used to obtain reference mound estimates for basin-type recharge scenarios. These analytical results are later compared with numerical circular- and square-basin representations in Visual MODFLOW Classic to examine how grid representation and recharge geometry influence the predicted groundwater response.

2.5.3 Strip/trench recharge formulation

Strip and trench recharge systems represent elongated infiltration areas. In the analytical formulation, the recharge area is treated as a long strip with a uniform infiltration rate. Under the Dupuit–Forchheimer approximation, groundwater flow away from the recharge strip is assumed to be mainly horizontal, and the maximum water-table rise is expected near the center of the strip.

The geometry and main parameters used in the strip recharge formulation are shown in Figure 2.4.

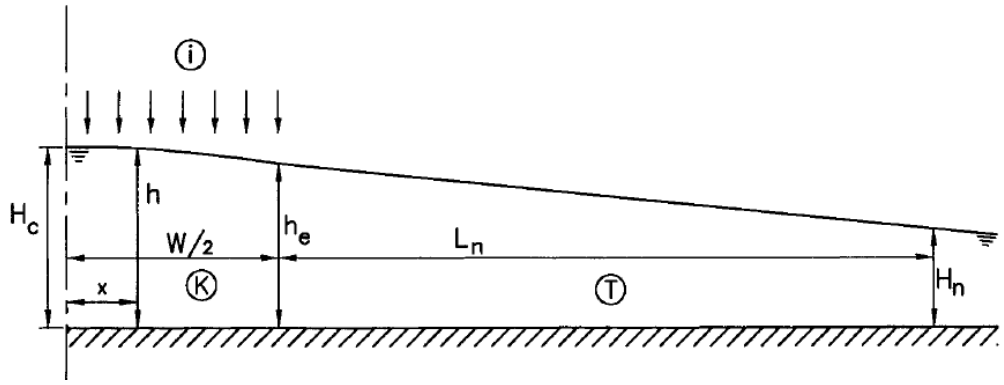

Figure 2.4. Geometry and symbols used to estimate groundwater mounding beneath a long infiltration strip (Source: Bouwer et al., 1999).

Following Bouwer et al. (1999), the total water-table rise beneath the center of a long recharge strip can be estimated by combining the head difference within the recharge area with the head difference between the strip edge and the distant control groundwater level.
For the strip recharge case, the head difference between the center of the strip and its edge is given by:

$$H_c - h_e = \frac{iW^2}{8T} \tag{2.8}$$

The head difference between the edge of the recharge strip and the control groundwater level is expressed as:

$$h_e - H_n = \frac{WiL_n}{2T} \tag{2.9}$$

Combining Equations 2.8 and 2.9, the total water-table rise beneath the center of the strip relative to the control groundwater level is obtained as:

$$H_c - H_n = \left(\frac{iW}{2T}\right)\left(\frac{W}{4} + L_n\right) \quad (2.10)$$

where H_c is the groundwater head at the center of the recharge strip, h_e is the groundwater head at the strip edge, H_n is the control groundwater level, W is the strip width, L_n is the distance from the strip edge to the control groundwater level, i is the gross infiltration rate, and T is the aquifer transmissivity.

According to this formulation, water-table rise increases with infiltration rate and distance to the control groundwater level. For a fixed infiltration rate, increasing strip width increases the recharge applied per unit strip length and generally increases water-table rise. Higher transmissivity allows the added water to move more easily away from the recharge area and generally reduces the maximum local water-table rise (Bouwer et al., 1999). However, in the constant-total-recharge comparisons used in this thesis, strip width and infiltration rate change together and should therefore be interpreted jointly.

The analytical formulation corresponds to a long strip. The length is supposed to be large enough to neglect end effects. In contrast, the trench-type recharge configurations used in the numerical simulations of this thesis have a finite length. This geometric difference could affect the predicted groundwater behavior and must be considered when comparing results from the analytical and numerical approaches.

The strip-based model in this thesis is used to obtain reference estimates of groundwater mounding for both trench and strip recharge scenarios. These estimates are compared with the corresponding Visual MODFLOW results in Chapter 4.

2.6 Transient analytical and numerical modeling approaches

The methods used in this thesis differ mainly in the way the groundwater-flow equation is simplified and solved. The circular and strip/trench formulations provide steady-state analytical estimates for idealized recharge geometries. MOUNDSOLV extends the analytical assessment to transient mound development, whereas Visual MODFLOW Classic solves the groundwater-flow equation numerically using a finite-difference grid.

2.6.1 MOUNDSOLV and transient analytical mound assessment

Steady-state simulations represent the groundwater response that develops when recharge and boundary conditions remain constant for a sufficiently long period. However, agricultural recharge is often seasonal or applied only for a limited time. Steady-state modeling alone cannot show how quickly a mound develops or how long it remains after recharge stops.

Hantush-type solutions, such as those implemented in MOUNDSOLV, are used to describe transient mound growth and decline under recharge conditions (Hantush, 1967). MOUNDSOLV is a specialized analytical tool developed by HydroSOLVE, Inc. for estimating groundwater-mound development under steady-state and transient recharge conditions (HydroSOLVE, Inc., n.d.). It provides a relatively direct method for examining groundwater response beneath defined recharge areas without constructing a detailed site-specific numerical model.

In this thesis, MOUNDSOLV was used for selected transient basin-type recharge scenarios. The analysis examined groundwater-mound development during recharge and mound dissipation after recharge stopped. Hydraulic conductivity, specific yield, recharge duration, recharge rate,

recharge-area dimensions, and distance from the recharge source were also considered. The MOUNDSOLV storage input was treated as specific yield, S_y, for consistency with the transient Visual MODFLOW comparison.

Maximum water-table rise, changes in water-table rise over time, and groundwater-mound profiles at different distances were the main outputs. These outputs were used to examine the magnitude and persistence of recharge-induced groundwater mounding.

Because the aquifer and recharge conditions used in MOUNDSOLV are simplified, the model was not used to predict conditions at a specific site. It was applied only to selected representative scenarios and sensitivity tests.

2.6.2 MODFLOW and Visual MODFLOW Classic

MODFLOW is a three-dimensional groundwater-flow model developed by the U.S. Geological Survey. It uses the finite-difference method to divide the model domain into a grid of cells and calculate hydraulic head throughout the groundwater system. MODFLOW can simulate steady-state and transient groundwater flow in confined and unconfined aquifers and can represent stresses such as recharge, pumping wells, rivers, and drains (Harbaugh, 2005).

Visual MODFLOW Classic is a graphical environment for constructing, running, and examining MODFLOW-based models. It allows the user to define the model domain and grid, assign aquifer properties and boundary conditions, apply recharge to selected cells, and display the results as hydraulic-head maps, contour plots, and cross-sectional profiles (Schlumberger Water Services, n.d.).

In this thesis, Visual MODFLOW Classic was mainly used to construct simplified steady-state models for selected basin-type and trench-type recharge configurations. The models were used to examine the spatial groundwater response and to compare the maximum water-table rise and central groundwater profiles with the corresponding analytical estimates. A representative transient basin case was also simulated for comparison with MOUNDSOLV.

The numerical models were developed as controlled scenario-comparison tools rather than calibrated models of a specific agricultural site. Detailed groundwater modeling normally requires a reliable conceptual model, field observations, suitable boundary and initial conditions, calibration, and uncertainty assessment (Barnett et al., 2012). Because detailed site-specific data were not available, the models used simplified aquifer conditions and clearly stated assumptions. Detailed vadose-zone flow, clogging, water-quality processes, and site-specific aquifer heterogeneity were not explicitly simulated.

2.6.3 Complementary roles of the modeling approaches

The approaches used in this thesis have different but complementary roles. Analytical calculations provide reference estimates and show how recharge geometry, recharge rate, and aquifer transmissivity influence water-table rise. Visual MODFLOW Classic provides a spatial, grid-based representation of the groundwater response within a finite model domain. MOUNDSOLV shows how groundwater mounding develops and declines over time.

These methods help in the preliminary comparison of infiltration-based MAR setups. They also help identify which parameters and assumptions have the greatest effect on the results and may

require further site-specific investigation. The following section describes the sensitivity analysis used in this thesis.

2.7 Sensitivity analysis and uncertainty in preliminary MAR assessment

Preliminary assessment of Managed Aquifer Recharge (MAR) is often carried out when detailed site-specific information is limited. At this stage, aquifer properties, recharge conditions, and the most suitable recharge configuration may still be uncertain. Sensitivity analysis is therefore useful because it shows how changes in selected input parameters influence the predicted groundwater response and helps identify which parameters require further investigation.

Sensitivity analysis is different from a complete uncertainty analysis. A full uncertainty assessment normally considers possible parameter ranges, probability distributions, alternative conceptual models, and supporting field data. The modeling framework used in this thesis is intended for preliminary comparison rather than calibrated prediction for a specific site. Uncertainty is therefore acknowledged through controlled variation of selected parameters and clear discussion of the assumptions and limitations of the models (Barnett et al., 2012).

Previous MAR studies have shown that groundwater response can be sensitive to both hydrogeological and operational conditions. Alkhatib et al. (2021), for example, examined the influence of aquifer transmissivity and other subsurface properties on recharge performance. Earlier groundwater-mounding studies also showed that recharge rate, recharge geometry, and aquifer transmissivity strongly influence mound development (Bouwer et al., 1999; Hantush, 1967).

The maximum rise of the groundwater mound is used as the main response indicator. This is important because a substantial rise in the water table can reduce the remaining unsaturated thickness and increase the risk of waterlogging. The effects of recharge geometry, recharge rate, and aquifer transmissivity on the magnitude and spatial distribution of groundwater mounding are assessed using analytical calculations and steady-state Visual MODFLOW Classic simulations.

By analyzing the mound's development during recharge and its decline after stopping recharge, the transient assessment of MOUNDSOLV extends this comparison. The transient sensitivity analysis considers hydraulic conductivity, specific yield, recharge duration, recharge rate, recharge-area dimensions, and distance from the recharge source. These variables are examined to identify which ones have the greatest influence on the transient groundwater-mound response.

The sensitivity analysis is limited to the hydraulic response of the simplified MAR configurations considered in this thesis. It is used to compare scenarios and identify parameters that may require further site-specific investigation.

2.8 Synthesis of literature

The literature reviewed in this chapter shows that Managed Aquifer Recharge can support agricultural water management by storing water during periods of greater availability and making it available during periods of higher demand. However, MAR feasibility depends not only on the availability of recharge water, but also on the selected recharge method, local hydrogeological conditions, source-water characteristics, land and infrastructure constraints, and operational requirements (Alley et al., 2022; Dillon et al., 2009).

For agricultural applications, infiltration-based systems such as basins and trenches are particularly relevant where suitable land, permeable soils, and adequate subsurface conditions are available. Their performance is strongly controlled by groundwater mounding, which depends on recharge geometry, infiltration rate, aquifer transmissivity, storage properties, and boundary conditions (Bouwer et al., 1999; Hantush, 1967). Excessive water-table rise may reduce the available unsaturated thickness and increase the risk of shallow groundwater or waterlogging.

Based on this review, the assessment framework adopted in this thesis focuses on the hydraulic response of simplified basin-type and trench-type recharge configurations. Analytical formulations, MOUNDSOLV, and Visual MODFLOW Classic are used as complementary tools to compare groundwater-mound response under the selected recharge scenarios.

3. Methodology

This chapter explains the methods used to study groundwater mounding beneath selected Managed Aquifer Recharge systems. It introduces the overall research framework, the modeling methods, the scenario design, and the criteria used to compare the results.

3.1 Research framework and modeling sequence

This study was developed as a preliminary screening assessment under simplified hydrogeological conditions. The aim was not to provide a final site-specific design, but to compare groundwater-mounding responses and identify the main parameters controlling groundwater-mound response.

The assessment was organized into four modeling stages: steady-state analytical groundwater-mounding calculations, steady-state numerical simulations in Visual MODFLOW Classic, transient analytical assessment using MOUNDSOLV, and a representative transient numerical simulation in Visual MODFLOW Classic. The steady-state analytical calculations provided reference estimates of maximum water-table rise for basin-type and trench/strip-type recharge geometries, while the steady-state Visual MODFLOW simulations were used to examine spatial hydraulic-head distributions and groundwater-mound response**.** MOUNDSOLV evaluated time-dependent mound growth and dissipation and the transient Visual MODFLOW case was used for comparison with the corresponding MOUNDSOLV result. These modeling components were supported by benchmark and diagnostic checks, sensitivity analyses, and an integrated comparison of the results.

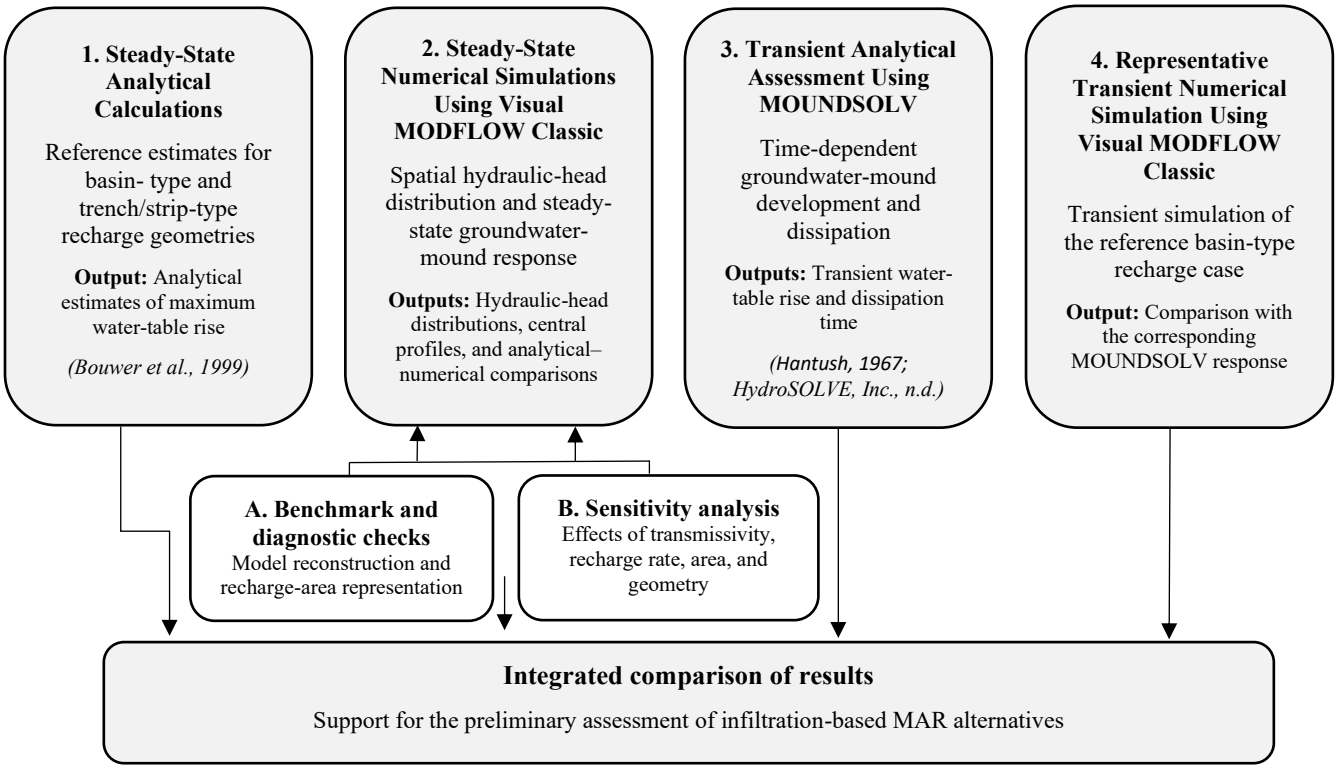

Figure 3.1. Summary of the methodological workflow adopted in this study.

3.2 Modeling methods and comparison criteria

3.2.1 Steady-state analytical groundwater-mounding calculations

Analytical groundwater-mounding calculations were used as the first quantitative step of the assessment. For basin-type scenarios, the circular recharge formulation of Bouwer et al. (1999) presented in Section 2.5.2, was applied using the recharge area, equivalent circular radius, infiltration rate, transmissivity and control distance defined for each case. For strip/trench-type scenarios, the corresponding long-strip formulation presented in Section 2.5.3 was applied using recharge width, infiltration rate, transmissivity and distance to the control groundwater level.

These calculations provided reference estimates of maximum water- table rise beneath the center of the recharge area. They were then used as a basis for comparison with the corresponding Visual MODFLOW simulations. Since the theoretical background and governing equations were already presented in Chapter 2, this section focuses only on how the formulations were applied to the selected scenarios, including input parameters, recharge geometry, and calculation procedures.

3.2.2 Visual MODFLOW Classic model setup

The steady-state numerical simulations were developed in Visual MODFLOW Classic as simplified single-layer, unconfined aquifer models. Visual MODFLOW Classic was used to construct finite-difference groundwater-flow simulations based on MODFLOW (Harbaugh, 2005). Each recharge configuration was represented by assigning recharge to the model cells corresponding to the selected basin, strip or trench area. Initial heads, hydraulic properties, recharge rates and boundary conditions were defined consistently within each comparison group so that the effect of the tested parameter or configuration could be isolated.

The numerical outputs used for comparison included maximum hydraulic head, maximum water-table rise, plan-view hydraulic-head distribution, and central cross-sectional hydraulic-head profiles. In this thesis, the Visual MODFLOW models were used as simplified scenario-comparison tools, rather than calibrated site-specific groundwater models.

Different boundary-condition configurations were used for basin-type and trench-type scenarios because their assumed flow patterns were different. For basin-type scenarios, constant-head boundaries were assigned along the outer model boundaries to represent a simplified surrounding groundwater level. For trench-type scenarios, constant-head boundaries were assigned on the boundaries perpendicular to the main lateral flow direction, while the remaining boundaries were treated as no-flow boundaries. This setup was used to approximate the dominant flow pattern assumed in each analytical formulation. The detailed settings for each scenario are presented in the following sections.

3.2.2.1 Output metrics and comparison criteria

The main output used to compare the simulations was maximum water- table rise. For each steady-state numerical simulation, water-table rise was calculated as the difference between the maximum simulated hydraulic head and the initial groundwater head:

$$\Delta h = h_{max} - h_0 \tag{3.1}$$

where Δh is the simulated water-table rise, h_{max} is the maximum hydraulic head obtained from the model, and h_0 is the initial groundwater head.

The numerical results were compared using maximum hydraulic head, water-table rise, plan-view hydraulic-head distribution, and central cross-sectional profiles. Where analytical estimates were available, the analytical and numerical water-table rise values were compared using absolute and relative differences.

The transient results were compared using water-table rise through time and the dissipation after recharge stopped. These criteria were used in Chapter 4 to compare the selected recharge configurations and to interpret the effects of transmissivity, recharge rate, recharge geometry, and transient parameters.

3.3 Steady-state scenario design

The steady-state scenarios were defined to compare groundwater-mounding responses under different basin-type and trench/strip-type recharge configurations. The scenarios were grouped according to their purpose in the study. Benchmark and diagnostic cases were used to check the modeling procedure and recharge-area representation before interpreting the main results. Transmissivity-sensitivity comparison cases were used to compare circular and trench-type recharge configurations under similar recharge and aquifer conditions. Recharge-configuration sensitivity cases were then used to examine the effects of recharge rate, recharge area, strip or trench width, and recharge geometry on water-table rise.

Table 3.1 summarizes the recharge configuration, parameters varied, conditions held constant, and purpose of each steady-state comparison. Detailed numerical values and model settings are presented in the corresponding subsections.

Table 3.1. Overview of the steady-state scenarios and comparison framework.

Scenario group	Recharge configuration	Parameter(s) varied	Key conditions held constant	Main purpose
3.3.1.1 Literature-based circular reference scenario	Circular recharge basin	None	Literature-based recharge geometry, aquifer assumptions, and analytical model settings	To provide an analytical benchmark and evaluate its consistency with the corresponding Visual MODFLOW reconstruction
3.3.1.2 Square diagnostic case	Square numerical recharge area	Recharge-area representation: circular versus square	Hydraulic properties, boundary conditions, initial head, model extent, and nominal recharge rate	To assess how the numerical representation of the recharge area affects the simulated groundwater-mounding response
3.3.1.3 Literature-based strip reference scenario	Long and narrow recharge strip	None	Literature-based strip geometry, aquifer assumptions, and analytical model settings	To provide an analytical reference for comparison with the corresponding Visual MODFLOW strip reconstruction
3.3.2.1 Circular-basin transmissivity sensitivity scenario	Circular recharge basin	Hydraulic conductivity and transmissivity	Recharge area, recharge rate, saturated thickness, boundary conditions, and other aquifer assumptions	To isolate the effect of aquifer transmissivity on groundwater mounding beneath a circular basin
3.3.2.2 Trench transmissivity sensitivity scenario	Rectangular recharge trench	Hydraulic conductivity and transmissivity	Recharge area, recharge rate, saturated thickness, boundary conditions, and other aquifer assumptions	To evaluate the effect of aquifer transmissivity beneath a trench and compare the response with the circular configuration
3.3.3.1 Constant-total-recharge circular-basin cases	Circular basins of different sizes	Recharge area and recharge rate; comparisons repeated at selected hydraulic-conductivity levels	Total applied recharge, model domain, grid, boundary conditions, initial head, and saturated thickness	To assess how distributing the same total recharge over different basin areas affects groundwater mounding
3.3.3.2 Modified literature-based strip cases	Literature-based recharge strip	Recharge rate or strip width, varied separately	Model domain, grid, layer configuration, hydraulic properties, initial head, boundary conditions, and strip length	To examine the individual effects of recharge-rate increase and strip-width enlargement
3.3.3.3 Constant-total-recharge strip cases	Recharge strips of different widths	Recharge rate and strip width, varied together	Recharge input per unit strip length, total applied recharge approximately constant, strip length, and other model settings	To assess how redistributing approximately the same recharge over different strip widths affects groundwater mounding
3.3.3.4 Supplementary narrow-trench case	Narrow rectangular recharge trench	Trench width and recharge rate	Total applied recharge approximately constant, trench length, hydraulic properties, boundary conditions, initial head, and saturated thickness	To assess whether a substantially narrower recharge trench changes the simulated groundwater-mounding response

3.3.1 Benchmark and diagnostic scenarios

The benchmark and diagnostic cases were used to check the modeling procedure before interpreting the main comparison scenarios. The literature-based circular and strip cases were based on Bouwer et al. (1999) and were used as reference cases for analytical–numerical comparison. The square recharge case was used as a diagnostic check to examine how numerical representation of the recharge area affected the simulated mound response.

3.3.1.1 Literature-based circular reference scenario

Scenario definition

This scenario was adopted from the circular recharge example presented by Bouwer et al. (1999) and was used as a literature-based analytical benchmark for evaluating groundwater mound development beneath a circular recharge area. The original example estimated the water-table rise and the control distance required to prevent excessive water-table rise beneath the recharge area.

The case was formulated for a steady-state, homogeneous, isotropic, unconfined aquifer, with no pumping wells or other groundwater discharge features. In this thesis, the scenario was used mainly as a methodological benchmark rather than as a site-specific MAR design. Some of the adopted values, particularly the high transmissivity and large permissible water-table rise, may be higher than those commonly expected in practical aquifer recharge applications. Therefore, the case was used to test the analytical formulation and to evaluate its consistency with the corresponding numerical reconstruction.

Input data and derived parameters

Table 3.2 presents the main input data and derived parameters used for the literature-based circular scenario. The hydraulic and recharge values were taken from the reference example of Bouwer et al. (1999). The recharge area and the equivalent circular radius were then calculated from the reported annual recharge volume and annual accumulated infiltration.

Table 3.2. Input data and derived parameters for the literature-based circular scenario.

Parameter	Symbol	Value	Unit
Transmissivity	T	930	m²/day
Initial groundwater depth below ground surface	—	91	m
Maximum permissible water-table rise	$\Delta h = Hc - Hn$	82	m
fillable porosity	n *(as reported by Bouwer et al., 1999)*	0.2	—
Annual recharge volume	Q	50,000,000	m³/year
Annual accumulated infiltration	I_{ann}	60	m/year
Daily equivalent infiltration	i	0.17	m/day
Recharge area	A	833,333	m²
Equivalent circular radius	R	515	m
Control distance	R_n	10	km

Note: The parameter values listed above were adopted from the example reported in Bouwer et al. (1999). In the original example, the value of 82 m represents the maximum permissible water-table rise ($Hc - Hn$), rather than to Hc alone. As discussed above, these values are used here as benchmark inputs for analytical–numerical comparison, rather than as typical practical design values.

Analytical calculation setup

The circular analytical formulation described in Section 2.5.2 was applied to the input values listed in Table 3.2. First, the recharge area was calculated from the reported annual recharge volume and annual accumulated infiltration. The calculated area was then converted into an equivalent circular radius for use in the analytical solution.

Using the adopted transmissivity, recharge rate, equivalent radius, and control-distance assumption, the analytical reference case provided a benchmark water-table rise value for comparison with the corresponding Visual MODFLOW Classic reconstruction. Since the initial groundwater level was defined relative to the adopted ground-surface datum, the analytical water-table rise was interpreted using the same reference level as the numerical model.

Numerical reconstruction in Visual MODFLOW Classic

Following the analytical calculation, the literature-based circular recharge scenario was reconstructed in Visual MODFLOW Classic under comparable aquifer and recharge conditions. A local ground-surface datum was adopted, with the ground surface assigned an elevation of 0 m. Therefore, the initial groundwater depth of 91 m below ground surface was represented as an initial head of −91 m. The constant-head boundaries were also assigned a value of −91 m, so all simulated heads in this scenario are reported relative to the adopted ground-surface datum.

The recharge basin was represented by assigning recharge to the grid cells located within the intended circular recharge area. Because the finite-difference model is discretized into square grid cells, the circular basin was represented numerically as an approximation of the intended circular geometry. In the initial reconstruction, the recharge zone was represented by 88 cells. Since this overrepresented the analytical recharge area, the recharge representation was corrected to 84 cells, giving an effective numerical recharge area of 840,000 m², which is closer to the analytical value of 833,333 m². The corrected numerical setup, including the full model domain and the discretized recharge area, is shown in Figure 3.2.

Because the analytical reference case is expressed in terms of transmissivity, the numerical reconstruction was defined using the corresponding equivalent transmissivity for consistency with the analytical formulation. In Visual MODFLOW Classic, hydraulic conductivity and layer thickness were entered as model inputs and related to transmissivity through $T = Kb$, where K is hydraulic conductivity and b is saturated thickness.

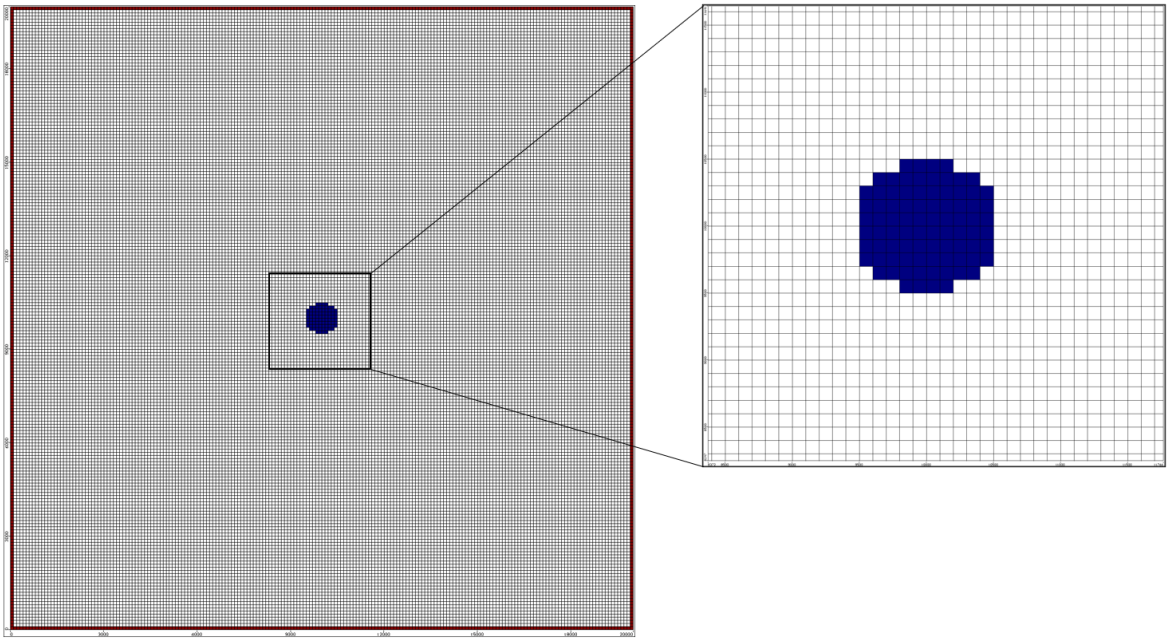

Figure 3.2. Numerical setup of the corrected literature-based circular recharge reconstruction, showing the full model domain and a magnified view of the discretized recharge area. The model domain was 20,000 × 20,000 m and was discretized using a 100 × 100 m finite-difference grid. The corrected recharge zone was represented by 84 recharge cells, corresponding to an effective numerical recharge area of 840,000 m².

The numerical model settings adopted for the corrected reconstruction are summarized in Table 3.3. The initial 88-cell reconstruction and the corrected 84-cell reconstruction were later compared in Chapter 4 to assess the effect of recharge-area representation on the analytical–numerical discrepancy.

Table 3.3. Numerical model settings for the corrected literature-based circular recharge scenario.

Parameter	Value	Unit
Initial groundwater head	-91	m
Constant head boundary	-91	m
Numerical recharge area	840,000	m²
Number of recharge cells	84	—
Model domain	20,000 × 20,000	m
Cell size	100 × 100	m

Note: Heads are reported relative to a ground-surface datum (z = 0), with an initial groundwater head of -91 m.

3.3.1.2 Square diagnostic case

Scenario definition

This scenario was developed to evaluate the influence of recharge-basin geometry on the simulated groundwater mound response. In contrast to the corrected circular recharge representation used in the reference case, the recharge area was represented using a square configuration. The main

hydraulic properties, model extent, boundary conditions, initial groundwater head distribution, and recharge rate were kept unchanged. Therefore, the purpose of this numerical case was to assess how replacing the circular recharge representation with a square recharge area affects the shape and magnitude of the simulated groundwater mound under otherwise comparable model conditions.

This comparison was not intended to define a separate literature-based case. Instead, it was used as a controlled numerical test within the same model setup. Only the shape of the recharge area was changed from circular to square. Because both recharge areas were represented using the square cells of the MODFLOW grid, their effective numerical areas were slightly different. This difference was considered when interpreting the comparison between the two scenarios.

Numerical implementation in Visual MODFLOW Classic

The square recharge scenario was implemented using the same MODFLOW model structure adopted for the corrected circular reference case. The model extent, cell size, layer configuration, hydraulic properties, initial groundwater head, and constant-head boundary conditions were kept unchanged in order to isolate the effect of recharge geometry.

The recharge basin was represented as a 9 × 9 cell square block located at the center of the model domain. This configuration corresponded to 81 recharge cells and an effective numerical recharge area of 810,000 m². The recharge rate assigned to the square basin was kept identical to that used in the circular recharge scenario. The resulting numerical setup is shown in Figure 3.3.

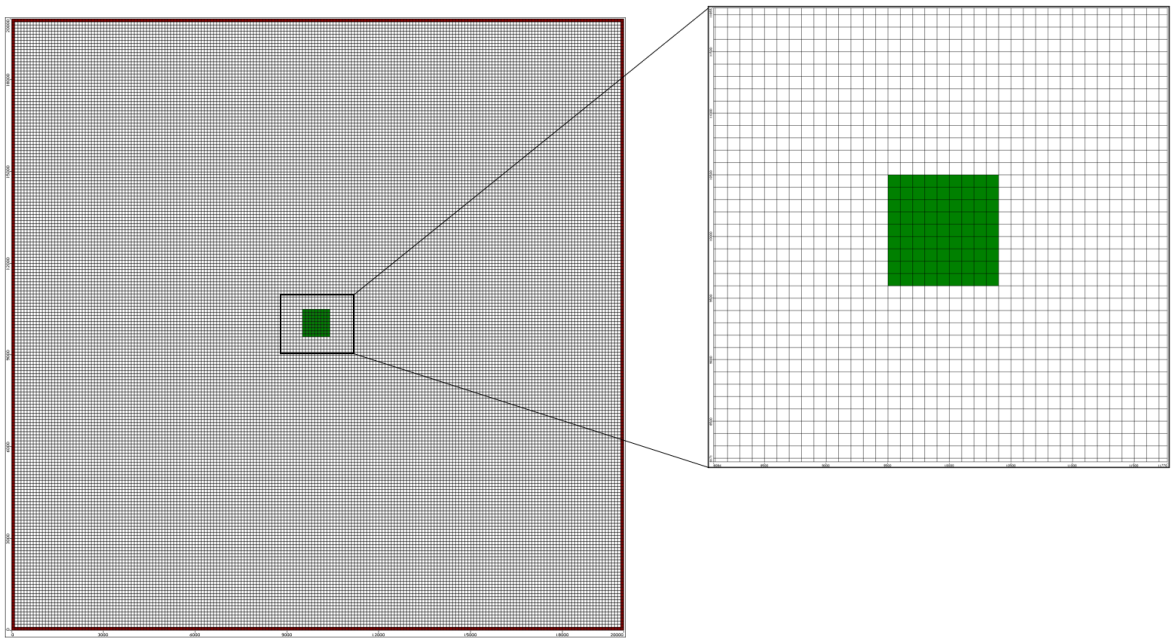

Figure 3.3. Numerical setup of the square recharge scenario, showing the full model domain and a magnified view of the discretized square recharge area. The model domain was 20,000 × 20,000 m and was discretized using a 100 × 100 m finite-difference grid. The square recharge zone was represented by a 9 × 9 cell block, corresponding to 81 recharge cells and an effective numerical recharge area of 810,000 m².

The simulated outputs of this scenario are presented and compared with the corrected circular scenario in Chapter 4.

3.3.1.3 Literature-based strip reference scenario

Scenario definition

This scenario was formulated based on the analytical relations for long infiltration areas presented by Bouwer et al. (1999). In contrast to the circular recharge case, the recharge area was represented as a long and narrow strip, and groundwater flow away from the recharge zone was evaluated using the analytical strip formulation.

The scenario was considered under steady-state conditions for a homogeneous, isotropic, unconfined aquifer. The main objective was to evaluate groundwater mounding beneath a recharge strip and to establish a literature-based analytical reference case for comparison with the numerical reconstruction in Visual MODFLOW Classic.

Input data and derived parameters

Table 3.4 summarizes the main input data and derived parameters used for the literature-based strip recharge scenario. The values were adopted from the analytical example presented by Bouwer et al. (1999) and were used to define the strip geometry, infiltration rate, transmissivity, permissible water-table rise, and required control distance for the analytical and numerical evaluations.

Table 3.4. Input data and derived parameters for the literature-based strip recharge scenario.

Parameter	Symbol	Value	Unit
Transmissivity	T	930	m²/day
Gross infiltration rate	i	0.02	m/day
Strip width	W	100	m
Half-width of strip	$W/2$	50	m
Maximum permissible water-table rise	$\Delta h = H_c - H_n$	2	m
Required control distance	L_n	1835	m

Note: The required control distance, *Ln*, was calculated using the strip analytical formulation and the input parameters listed in the table.

Numerical reconstruction in Visual MODFLOW Classic

Following the analytical formulation, the literature-based strip recharge scenario was reconstructed in Visual MODFLOW Classic to simulate groundwater mounding beneath a long recharge strip. The numerical model was developed under steady-state conditions for a homogeneous, isotropic, unconfined aquifer, consistent with the assumptions adopted in the analytical strip formulation.

A local ground-surface datum was adopted, with the ground surface assigned an elevation of 0 m. Accordingly, the initial groundwater depth of 91 m below ground surface was represented as an initial head of -91 m. The constant-head boundaries were also assigned a value of -91 m, so all simulated heads in this section were interpreted relative to the adopted ground-surface datum.

Because the analytical strip formulation is expressed in terms of transmissivity, the numerical implementation used equivalent hydraulic conductivity and saturated thickness values. A representative saturated thickness of 100 m was assumed for the strip reconstruction. Accordingly,

an equivalent hydraulic conductivity of 9.3 m/day was assigned using $K = T/b$ = 930/100. With the initial groundwater head fixed at -91 m and the saturated thickness set to 100 m, the aquifer bottom elevation was assigned as -191 m.

The model domain was defined as 4,000 × 4,000 m and discretized into a uniform finite-difference grid. A single unconfined layer was used. The recharge area was represented as a rectangular strip at the model center. Recharge was applied only to the strip cells. The strip width was set to 100 m, consistent with the analytical formulation, and the strip length was assigned as 1,000 m to approximate the long-strip condition. Since both the domain and the recharge strip were finite, the model should be interpreted as an approximate numerical reconstruction rather than an exact reproduction of the idealized analytical solution.

For the strip recharge reconstruction, constant-head boundaries were assigned only along the upper and lower model boundaries, representing the control groundwater direction perpendicular to the strip axis. The left and right model boundaries were treated as no-flow boundaries. This configuration was adopted to approximate the one-dimensional lateral flow assumption of the strip analytical formulation and to distinguish the strip model from the basin-type scenarios, where radial mound dissipation was represented using constant-head boundaries along the outer model boundaries. The resulting numerical setup is shown in Figure 3.4.

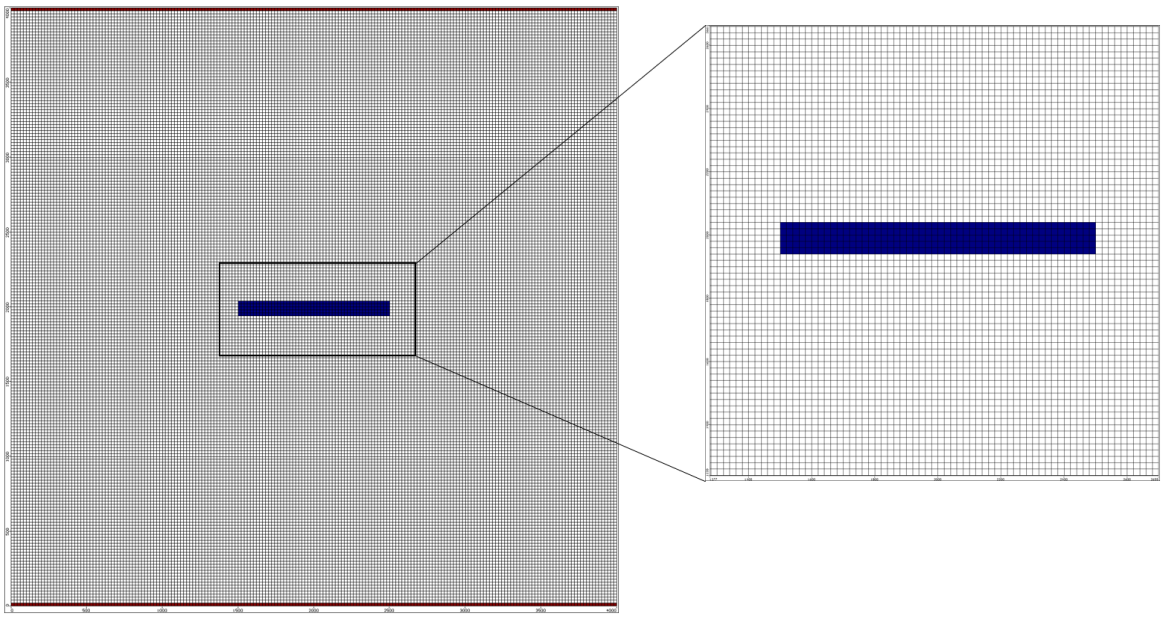

Figure 3.4. Numerical setup of the literature-based strip recharge scenario, showing the full model domain and a magnified view of the discretized strip recharge zone. The model domain is 4,000 × 4,000 m and was discretized using a uniform 20 × 20 m finite-difference grid. The recharge zone was represented as a 100 m wide and 1,000 m long strip, corresponding to a numerical recharge area of 100,000 m² and 250 recharge cells.

The numerical model settings adopted for the literature-based strip scenario are summarized in Table 3.5.

Table 3.5. Numerical model settings for the literature-based strip recharge scenario.

Parameter	Value	Unit
Initial groundwater head	-91	m
Constant head	-91	m
Numerical strip width	100	m
Numerical strip length	1000	m
Numerical recharge area	100000	m^2
Number of recharge cells	250	—
Model domain	4,000 × 4,000	m
Grid size	20 × 20	m
Boundary condition configuration	two constant-head boundaries + two no-flow boundaries	—

Note: Heads are reported relative to a ground-surface datum (z = 0), with an initial groundwater head of -91 m.

The numerical outputs, hydraulic-head distributions and comparison with the corresponding analytical estimate are presented and discussed in Chapter 4.

3.3.2 Transmissivity sensitivity analysis for circular and trench scenarios

3.3.2.1 Circular basin transmissivity sensitivity scenario

Scenario definition

The circular scenario was defined as a synthetic scenario to evaluate groundwater mound development beneath a circular recharge basin under simplified aquifer conditions. It used a regular 1,000 × 1,000 m model domain and a centrally located recharge area so that the analytical and numerical responses to be compared under consistent geometric and hydraulic assumptions.

The scenarios were formulated for a steady-state, homogeneous, isotropic, unconfined aquifer, with no pumping wells or additional groundwater discharge features. Hydraulic conductivity was varied over a selected range, while the recharge rate, recharge area, saturated thickness and boundary conditions were kept constant. This setup was used to isolate the influence of aquifer transmissivity on recharge-induced groundwater mounding.

Input data and derived parameters

The input parameters used for the circular scenario are summarized in Table 3.6. The recharge area was fixed at 10,000 m^2 and represented analytically by an equivalent circular basin with a radius of 56.42 m. A uniform recharge rate of 0.01 m/day was assigned in all cases. Hydraulic conductivity values were varied from 1 to 100 m/day, and the corresponding transmissivity values were calculated assuming a constant saturated thickness of 20 m.

Table 3.6. Input data and derived parameters used for the circular transmissivity-sensitivity scenario.

Parameter	Symbol	Value	Unit
Model domain	—	1,000 × 1,000	m
Initial groundwater depth below ground surface	—	10	m
Initial saturated thickness	b	20	m
Recharge rate	i	0.01	m/day
Recharge area	A	10,000	m²
Equivalent circular radius	R	56.42	m
Control distance	R_n	500	m
Hydraulic conductivity	K	**1**; 5; 10; 50; 100	m/day
Transmissivity	T	**20**; 100; 200; 1,000; 2,000	m²/day

Note: Bold values indicate the reference condition used for the circular scenario. Transmissivity values were calculated as $T = Kb$, with $b = 20$ m.

Analytical calculation procedure

The analytical calculation was performed using the steady-state circular recharge formulation described in Section 2.5.2. The input parameters listed in Table 3.6 were used consistently for all transmissivity cases.

For each case, the analytical expression was applied to estimate the water-table rise at the center of the recharge basin. This provided a set of analytical reference values to be compared with the corresponding steady-state numerical simulations. The calculated analytical water-table rise values are presented and discussed in Chapter 4.

Numerical model setup

The circular scenario was implemented in Visual MODFLOW Classic under steady-state conditions. The model domain was defined as a 1,000 × 1,000 m square and discretized using a uniform 10 × 10 m finite-difference grid. A single unconfined layer was considered, with the top elevation of 0 m and a bottom elevation of -30 m. The initial groundwater head was set to -10 m, corresponding to an initial groundwater depth of 10 m below the ground surface and an initial saturated thickness of 20 m.

Constant-head boundaries of -10 m were assigned along the outer edges of the model domain. The recharge basin was located at the center of the domain and represented as a discretized circular recharge zone. Recharge was applied uniformly at a rate of 0.01 m/day over 100 grid cells, corresponding to a numerical recharge area of 10,000 m².

The same model geometry, recharge rate, initial condition and boundary conditions were maintained for all simulations. Hydraulic conductivity was varied between 1 and 100 m/day, corresponding to transmissivity values of 20, 100, 200, 1,000 and 2,000 m²/day. The numerical setup adopted for this scenario is shown in Figure 3.5.

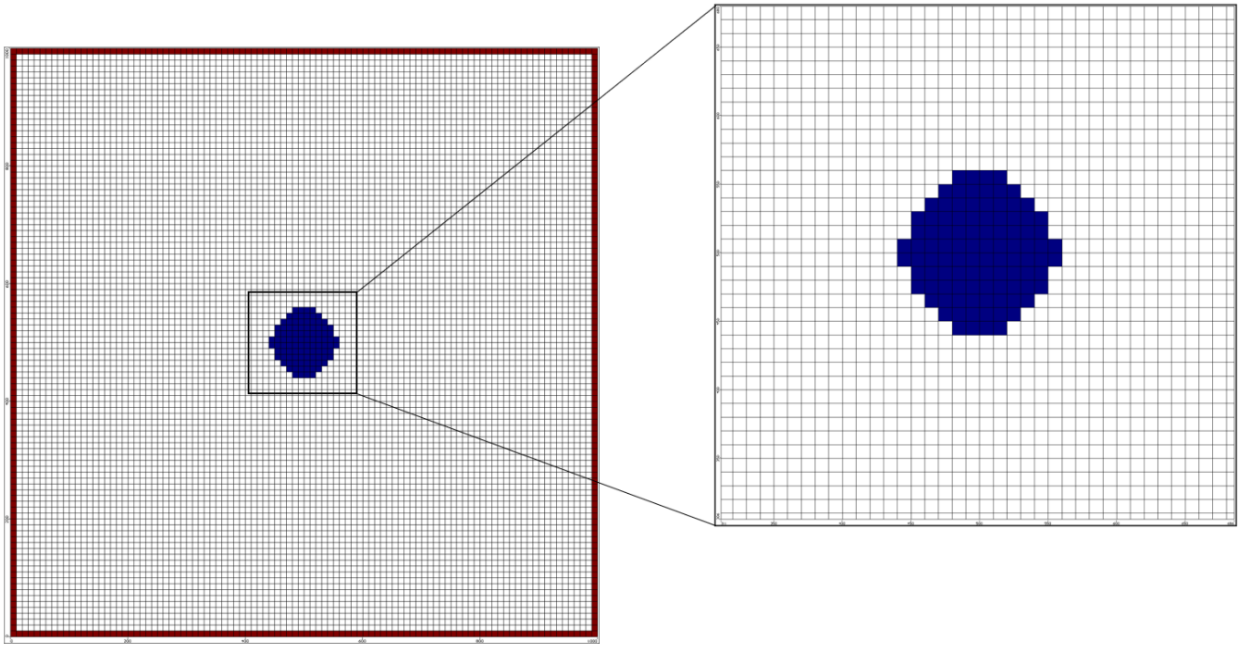

Figure 3.5. Numerical setup of the circular recharge scenario, showing the full model domain and a magnified view of the discretized circular recharge area. The model domain is 1,000 × 1,000 m and was discretized using a 10 × 10 m finite-difference grid. The recharge zone was represented by 100 recharge cells, corresponding to a numerical recharge area of 10,000 m².

3.3.2.2 Trench transmissivity sensitivity Scenario

Scenario definition

The trench case was defined as a synthetic scenario to evaluate groundwater mound development beneath a rectangular trench/strip recharge system under simplified aquifer conditions. It used the same regular 1,000 × 1,000 m model domain as the circular transmissivity-sensitivity scenario, but the recharge area was represented as a centrally located rectangular trench. This allowed the circular and trench-type recharge configurations to be compared under consistent hydraulic conditions while changing the recharge geometry.

The recharge area was fixed at 10,000 m². In the trench case, this area was represented by a 20 m wide and 500 m long rectangular recharge zone. The recharge rate was set to 0.01 m/day, giving a total applied recharge of 100 m³/day. This total recharge input was kept consistent with the corresponding circular scenario so that the effect of recharge geometry could be evaluated under comparable recharge conditions.

The scenarios were formulated for a steady-state, homogeneous, isotropic, unconfined aquifer, with no pumping wells or additional groundwater-discharge features. Hydraulic conductivity was varied over a selected range, while the recharge rate, recharge area, saturated thickness, and boundary conditions were kept constant. This setup was used to isolate the influence of aquifer transmissivity on recharge-induced groundwater mounding for the trench-type configuration.

Input data and derived parameters

The input data and derived parameters used for the trench scenario are summarized in Table 3.7. The baseline configuration consisted of a 20 m wide and 500 m long rectangular trench, corresponding to a recharge area of 10,000 m². Hydraulic conductivity was varied over a predefined range, and the corresponding transmissivity values were calculated by assuming a constant saturated thickness of 20 m.

Table 3.7. Input data and derived parameters for the trench transmissivity-sensitivity scenario.

Parameter	Symbol	Value	Unit
Model domain	—	1,000 × 1,000	m
Initial groundwater depth below ground surface	—	10	m
Initial saturated thickness	b	20	m
Recharge rate	i	0.01	m/day
Trench width	W	20	m
Trench half-width	$W/2$	10	m
Trench length	L_t	500	m
Recharge area	A	10,000	m²
Control distance	L_n	500	m
Hydraulic conductivity	K	**1**; 5; 10; 50; 100	m/day
Transmissivity	T	**20**; 100; 200; 1,000; 2,000	m²/day

Note: Bold values indicate the reference condition used for the trench scenario. Transmissivity values were calculated as $T = Kb$, with b = 20 m.

Analytical calculation procedure

For the trench scenario, analytical water-table rise was calculated using the steady-state trench/strip analytical relations described in Section 2.5.3. The calculations were performed for the selected transmissivity values derived from the tested hydraulic conductivity values and a constant saturated thickness of 20 m.

For each case, the analytical expression was applied to estimate water-table rise beneath the trench recharge area. This provided a set of analytical reference values for comparison with the corresponding steady-state numerical simulations. The calculated analytical water-table rise values are presented and discussed in Chapter 4.

Numerical model setup

The trench scenario was implemented in Visual MODFLOW Classic under steady-state conditions. The model domain was defined as a 1,000 × 1,000 m square and discretized using a uniform 10 × 10 m finite-difference grid. A single unconfined layer was considered, with the top elevation of 0 m and a bottom elevation of -30 m. The initial groundwater head was set to −10 m, corresponding to an initial groundwater depth of 10 m below the ground surface and an initial saturated thickness of 20 m.

Constant-head boundaries of -10 m were assigned to the two boundaries perpendicular to the main lateral flow direction from the trench, while the two remaining boundaries were treated as no-flow

boundaries. This boundary configuration was selected to approximate lateral mound dissipation away from the trench toward distant control heads. The recharge trench was represented as a centrally located rectangular zone, with recharge applied only within this area at a rate of 0.01 m/day. The trench was 20 m wide and 500 m long, corresponding to a recharge area of 10,000 m² and occupying 100 grid cells.

Hydraulic conductivity values of 1, 5, 10, 50, and 100 m/day were tested, corresponding to transmissivity values of 20, 100, 200, 1,000, and 2,000 m²/day. Therefore, the numerical model should be interpreted as a finite-length numerical reconstruction of the trench configuration rather than an exact reproduction of an idealized infinite strip. The numerical setup adopted for the trench transmissivity-sensitivity scenario is shown in Figure 3.6.

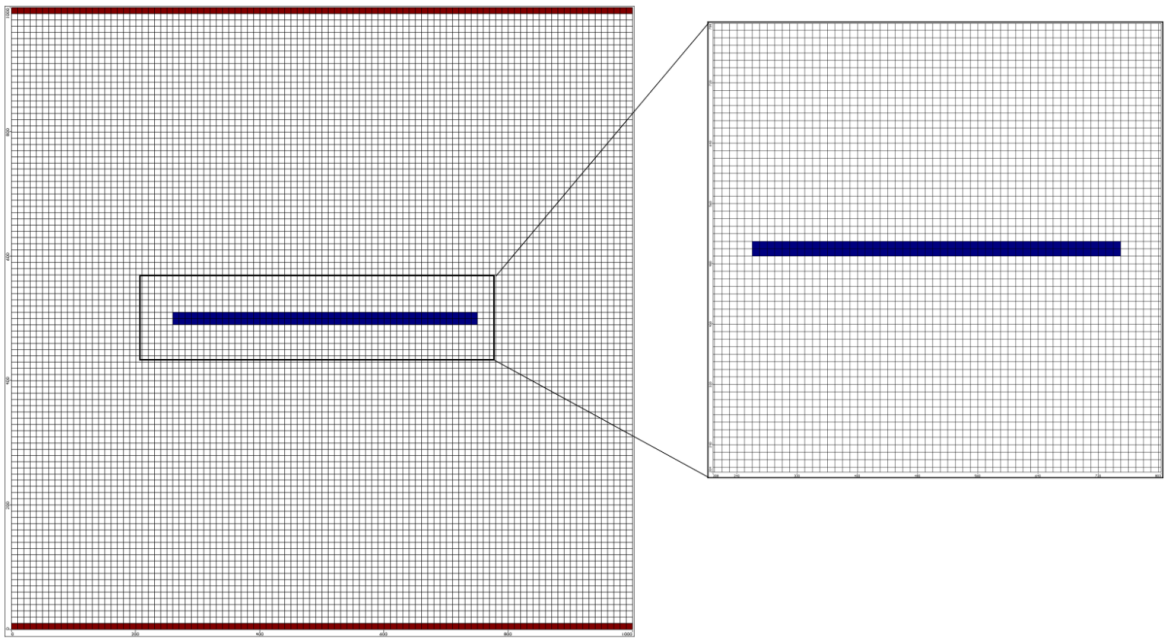

Figure 3.6. Numerical setup of the trench scenario, showing the full model domain and the discretized rectangular recharge trench. The model domain is 1,000 × 1,000 m and was discretized using a uniform 10 × 10 m finite-difference grid. The recharge trench was represented as a 20 m wide and 500 m long rectangular zone, corresponding to a recharge area of 10,000 m² and 100 recharge cells.

3.3.3 Recharge-configuration sensitivity cases

The recharge-configuration sensitivity cases were defined to examine how changes in recharge area, recharge rate, recharge width, recharge geometry, and transmissivity affected groundwater mound development. These cases were not intended as site-specific designs. Instead, they were used as controlled numerical tests to help interpret the main steady-state comparisons.

The sensitivity cases were divided into four groups. The first group examined circular basin cases with the same total recharge rate. The second group included modified literature-based strip cases, where either the recharge rate or the strip width was changed separately. In these cases, the total applied recharge also changed. The third group examined strip cases in which the recharge rate and strip width were changed together while keeping the recharge input per unit strip length

approximately constant. The fourth group included a supplementary narrow-trench case to test the effect of reducing trench width while keeping the total applied recharge approximately the same.

3.3.3.1 Constant-total-recharge circular basin cases

The constant-total-recharge circular basin cases were defined to evaluate how recharge-area distribution affects groundwater mound development when the total applied recharge is kept constant. In all cases, the total recharge rate was fixed at 100 m³/day by adjusting the recharge rate according to the recharge area.

Three configurations were compared: a smaller circular basin with higher recharge intensity, the baseline circular basin, and a larger circular basin with lower recharge intensity. The model domain, grid discretization, boundary conditions, initial head, saturated thickness, and aquifer properties were kept unchanged. Three selected hydraulic-conductivity values from the transmissivity-sensitivity circular scenario were used for these cases: 1, 10, and 100 m/day. The numerical results are presented in Chapter 4.

The recharge-area and recharge-rate configurations are summarized in Table 3.8.

Table 3.8. Recharge-area and recharge-rate configurations for the constant-total-recharge circular basin cases.

Case	Recharge area A (m²)	Recharge rate *i* (m/day)	Total *Q* (m³/day)
Smaller circular basin / higher intensity	5,000	0.020	100
Baseline circular basin	10,000	0.010	100
Larger circular basin / lower intensity	20,000	0.005	100

Note: The total applied recharge rate was kept constant at 100 m³/day in all cases by adjusting the recharge rate according to the recharge area.

3.3.3.2 Modified literature-based strip cases

Two preliminary strip sensitivity cases were defined based on the literature-based strip reference model. In the first case, the recharge rate was increased from 0.02 m/day to 0.10 m/day, while the strip geometry was kept unchanged. In the second case, the strip width was increased from 100 m to 300 m, while the recharge rate was kept equal to the reference value of 0.02 m/day.

These cases were used to examine the individual effects of recharge-rate increase and strip-width enlargement on groundwater mound development. Since changing the recharge rate or the strip width also changed the total applied recharge, these cases were interpreted as preliminary sensitivity tests rather than constant-total-recharge comparisons. For clarity, the three preliminary strip simulations were labelled STR-REF for the literature-based reference strip case, STR-RR for the modified recharge-rate case, and STR-SW for the modified strip-width case.

For both cases, the model domain, grid discretization, layer configuration, hydraulic properties, initial head, and boundary-condition configuration were kept identical to the literature-based strip reference model. The numerical model setup for the modified strip-width case is shown in Appendix B, Figure B.4. The numerical outputs and comparisons are presented in Chapter 4.

3.3.3.3 Constant-total-recharge strip cases

Additional strip sensitivity cases were defined to evaluate the effect of recharge distribution while maintaining approximately the same recharge rate per unit strip length. For the strip configuration, this condition was represented by keeping the product iW approximately constant, where i is the gross infiltration rate and W is the strip width. Since the strip length was kept constant in all cases, maintaining the same iW value also preserved approximately the same total applied recharge for the strip configurations.

Three strip configurations were compared: a narrow strip with higher recharge intensity, the reference strip, and a wide strip with lower recharge intensity. The reference strip used $i = 0.0200$ m/day and $W = 100$ m, giving $iW = 2$ m²/day per unit strip length. These cases were introduced to separate the effect of recharge area from the effect of total recharge rate.

In the numerical implementation, the model domain, grid discretization, hydraulic conductivity, saturated thickness, initial head, boundary-condition configuration, and strip length were kept identical to the reference strip scenario. Only the strip width and recharge rate were modified. The configuration of the constant-total-recharge strip sensitivity cases is summarized in Table 3.9.

Table 3.9. Configuration of the constant-total-recharge strip sensitivity cases.

Case	Description	i (m/day)	W (m)	iW (m²/day per unit length)	Recharge cells	Numerical recharge area (m²)
Narrow strip – higher intensity	Narrower recharge area	0.0333	60	2	150	60,000
Reference strip	Original parameter set	0.0200	100	2	250	100,000
Wide strip – lower intensity	Wider recharge area	0.0100	200	2	500	200,000

Note: The product iW was kept approximately constant in all cases. The strip length was kept equal to 1,000 m, while the strip width and recharge rate were modified to evaluate the effect of recharge distribution under the same total recharge input.

The analytical and numerical results of these cases are presented and discussed in Chapter 4.

3.3.3.4 Supplementary narrow-trench case

A supplementary narrow-trench case was defined to examine the effect of reducing trench width while maintaining approximately the same total applied recharge as the baseline trench scenario. The baseline trench had a width of 20 m, a length of 500 m, a recharge area of 10,000 m², and a recharge rate of 0.01 m/day, corresponding to a total recharge rate of 100 m³/day.

In the supplementary narrow-trench case, the effective trench width was reduced to approximately 3.75 m, while the trench length was kept equal to 500 m. An initial width of 10 m had first been considered for this scenario. However, during discussions with the supervisors, a width of about 2–3 m, and at most about 4 m, was considered more representative of a physical infiltration trench than the initial 10 m width or the 20 m baseline width. Since the model grid had been refined and the total applied recharge was kept approximately constant, it was not possible to assign an exact width of 2, 3, or 4 m while preserving the same recharge-volume constraint. Therefore, an effective numerical width of approximately 3.75 m was adopted for the supplementary narrow-trench case.

The value of 3.75 m should therefore be interpreted as an effective numerical width resulting from the refined model representation, rather than as a fixed standard design width. The recharge rate was increased to 0.0533 m/day to maintain a total recharge rate of approximately 100 m^3/day.

This case was used to evaluate whether a narrower recharge zone would substantially change the simulated mound response under approximately constant-total-recharge conditions. The numerical settings for the baseline trench and the supplementary narrow-trench case are summarized in Table 3.10.

Table 3.10. Numerical settings for the baseline and supplementary narrow-trench cases.

Parameter	Baseline trench	Supplementary narrow trench
Trench width (m)	20	≈ 3.75
Trench length (m)	500	500
Recharge area (m^2)	10,000	≈ 1,875
Recharge rate (m/day)	0.01	0.0533
Total applied recharge (m^3/day)	100	≈ 100

Note: The recharge rate was adjusted to keep the total applied recharge rate approximately equal to 100 m^3/day in both configurations.

3.4 Transient simulations

As described in Chapter 2, MOUNDSOLV was used to evaluate selected transient groundwater-mounding responses. This part of the assessment focused on basin-type recharge cases, because the aim was to examine how the mound develops during recharge and how it dissipates after recharge stops. The transient assessment complemented the steady-state Visual MODFLOW simulations, which represented the long-term response to continuous recharge.

The reference transient case was defined to remain consistent with the corresponding steady-state circular basin scenario used in the steady-state assessment. It used a 100 m × 100 m recharge basin, a recharge rate of 0.01 m/day, a total recharge input of 100 m^3/day, a hydraulic conductivity of 1 m/day, and a specific yield of 0.10.

3.4.1 MOUNDSOLV scenario design

The transient scenarios were selected to examine the time-dependent behavior of groundwater mounding under a limited number of representative conditions. The reference case was used first to evaluate how water-table rise changed with recharge duration. Then, selected hydraulic-conductivity and specific-yield values were tested to assess the influence of aquifer transmissivity and storage on transient mound development.

Additional cases were included to compare responses under similar diffusivity conditions, where transmissivity and specific yield were varied together. Constant-total-recharge cases were also used to examine the effect of changing the recharge area and recharge rate while keeping the total recharge input unchanged. Finally, monitoring points at different distances from the recharge area were used to assess how long the mound persisted after recharge stopped and how its effect changed with distance.

The MOUNDSOLV simulations were named using "MS" followed by a case number. Extra letters were added for specific cases, including long-term (LT), extended long-term (ELT), and constant-

diffusivity (CD) simulations. Table 3.11 summarizes the MOUNDSOLV scenario groups, the cases included in each group, and the purpose and main variable of each comparison.

Table 3.11. Summary of MOUNDSOLV scenario groups used in the transient assessment.

Scenario group	Cases included	Purpose	Main variable
Reference duration cases	MS-1, MS-1-LT, MS-1-ELT	To examine mound development over different recharge durations	Simulation duration
K and specific-yield cases	MS-1, MS-2, MS-3, MS-4	To examine the effect of hydraulic conductivity and specific yield on transient water-table rise	K and specific yield
Constant-diffusivity cases	MS-CD2, MS-CD3	To examine the combined role of transmissivity and specific yield when diffusivity is kept constant	T/S_y
Constant-total-recharge cases	MS-5, MS-1, MS-6	To examine the effect of recharge-area distribution while keeping total recharge constant	Recharge area and recharge rate
Dissipation cases	MS-1	To examine mound persistence at different distances after recharge stops	Time and distance

Note: MS-1 was used as the reference transient case and was therefore included in several comparison groups.

The corresponding transient results are presented and discussed in Chapter 4.

3.4.2 Monitoring points and dissipation criterion

The main outputs extracted from MOUNDSOLV were maximum water-table rise at the center of the recharge basin, time-series responses, and water-table rise profiles along the centerline of the recharge area. These outputs were used to evaluate the magnitude of groundwater mounding, its change over time, and its persistence after recharge stopped.

For the monitoring-distance analysis, responses were evaluated at the basin center and at selected distances from the recharge-basin edge. This made it possible to assess the transient response not only below the recharge area, but also at locations away from the recharge zone.

After recharge stopped, mound dissipation was evaluated using a practical threshold of 0.10 m. In this study, a remaining water-table rise of 0.10 m was considered small enough to be treated as negligible for a preliminary assessment. This threshold was used to estimate how long it took for the recharge-induced mound to dissipate after the end of recharge.

3.4.3 Transient Visual MODFLOW comparison case

A representative transient Visual MODFLOW simulation was used as an additional consistency check for the transient assessment. The comparison was based on the reference MOUNDSOLV basin case, using a 100 m × 100 m recharge area, a recharge rate of 0.01 m/day, hydraulic conductivity of 1 m/day, specific yield of 0.10, and a recharge duration of 365 days.

The comparison focused on the maximum water-table rise after 365 days and the water-table rise profile along the central cross-section of the recharge area. The purpose was not to calibrate the two models, but to check whether the MOUNDSOLV response was broadly consistent with a comparable transient Visual MODFLOW simulation. The results of this comparison are presented in Chapter 4.

4. Results and discussion

This chapter presents and discusses the results obtained from the analytical calculations, the steady-state Visual MODFLOW Classic simulations, and the selected transient MOUNDSOLV assessment. The results are organized according to the modeling sequence described in Chapter 3. First, the benchmark and diagnostic cases are presented to evaluate the consistency between the analytical and numerical approaches and to examine the effect of recharge-area representation. Then, the circular and trench transmissivity-sensitivity scenarios are discussed to assess the effects of aquifer transmissivity and recharge geometry under comparable recharge conditions. The recharge-rate and recharge-area sensitivity cases are then presented. Finally, the transient MOUNDSOLV results are discussed to evaluate mound development, persistence, and dissipation through time.

The discussion focuses on water-table rise, hydraulic-head distribution, analytical–numerical agreement, and the sensitivity of mound development to recharge geometry, recharge intensity, aquifer transmissivity, recharge-area distribution, and transient parameters.

4.1 Benchmark and diagnostic results

This section presents the benchmark and diagnostic results used to check the modeling procedure before interpreting the main comparison scenarios. The literature-based circular and strip cases were used to compare analytical estimates with Visual MODFLOW reconstructions, while the square case was used to examine the effect of recharge-area representation.

4.1.1 Literature-based circular benchmark and diagnostic checks

The literature-based circular recharge case was used as the first benchmark for comparing the analytical water-table rise estimate with the corresponding Visual MODFLOW Classic reconstruction. Using the input values defined in Chapter 3, the analytical calculation gave a water-table rise of approximately 82 m. Since the initial groundwater head was represented as −91 m relative to the adopted ground-surface datum, this corresponded to an analytical mound-center head of approximately −9 m. This water-table rise is extremely large from a physical perspective. Although the benchmark is based on a real aquifer system in the United States, it is a classical reference case and should not be considered representative of typical aquifer conditions, such as those commonly found in Europe or Central Asia. The following scenarios therefore use different aquifer parameters to examine more representative conditions.

In the corrected Visual MODFLOW reconstruction, the recharge area was represented by 84 recharge cells, corresponding to an effective numerical recharge area of 840,000 m². This value was close to the analytical recharge area of 833,333 m². The corrected numerical simulation produced a maximum hydraulic head of −26 m, corresponding to a water-table rise of 65 m above the initial groundwater head. The simulated hydraulic-head distribution showed the expected mound shape, with the highest head below the recharge area and decreasing heads toward the model boundaries.

Although the corrected recharge-area representation improved the consistency between the analytical and numerical setups, a clear difference remained between the two results. The analytical solution estimated a water-table rise of 82 m, whereas the corrected unconfined MODFLOW reconstruction produced a water-table rise of 65 m. Therefore, additional diagnostic

checks were carried out to examine whether this difference was related to recharge-area discretization, grid resolution, solver selection, or the treatment of transmissivity.

In the initial MODFLOW reconstruction, the circular recharge area was represented by 88 recharge cells, corresponding to an effective recharge area of 880,000 m². This was larger than the analytical recharge area. After correcting the recharge representation to 84 cells, the simulated water-table rise increased from 59 m to 65 m. This shows that part of the initial discrepancy was related to the discretized representation of the recharge area.

Grid refinement and solver selection did not substantially change the result. When the grid was refined around the recharge zone, the effective recharge area was kept approximately the same, and the maximum simulated head and water-table rise remained unchanged. A further solver checks also produced the same result. These checks indicate that the remaining difference was not mainly caused by grid resolution or solver selection.

The final diagnostic check examined the role of transmissivity treatment. The analytical formulation of Bouwer et al. (1999) is based on a fixed transmissivity assumption, while the unconfined MODFLOW reconstruction allows saturated thickness, and therefore effective transmissivity, to change as the water table rises. To test this effect, a constant-transmissivity diagnostic simulation was performed by assigning transmissivity directly. This diagnostic case produced a maximum simulated head of −5 m and a water-table rise of 86 m, which was much closer to the analytical water-table rise of 82 m.

This result suggests that the remaining analytical–numerical discrepancy was mainly related to the fixed-transmissivity assumption used in the analytical solution. The constant-transmissivity diagnostic case was used only as a numerical check and should not be interpreted as the physically preferred representation of the aquifer. The actual scenario was treated as an unconfined aquifer, where groundwater mounding changes both hydraulic head and saturated thickness. The very large water-table rise in this benchmark caused a major change in saturated thickness, which made the difference between the analytical and numerical results easier to see. For lower and more typical water-table rises, this difference would probably be smaller. However, this benchmark was useful for showing the limitation of the analytical approach. Table 4.1 summarizes the analytical reference value and the diagnostic checks for the literature-based circular recharge case.

Figure 4.1 shows the simulated hydraulic-head distribution for the corrected circular reconstruction, and Figure 4.2 compares the central hydraulic-head profiles for the corrected unconfined model, the constant-transmissivity diagnostic case, and the analytical reference value. The corresponding central cross-sectional hydraulic-head distribution is provided in Appendix A, Figure A.1.

Table 4.1. Analytical value and numerical diagnostic checks for the literature-based circular recharge scenario.

Case	Check	Grid	*T* / layer	Solver	Cells	Area (m²)	h_{max} (m)	Δh (m)	Diff. (%)
Analytical reference	Bouwer et al. (1999)	—	Fixed *T*	—	—	833,333	-9	82	—
Original MODFLOW	Initial reconstruction	100 × 100 m	Unconfined / variable *T*	WHS	88	880,000	-32	59	-28.0
Case 1	Area correction	100 × 100 m	Unconfined / variable *T*	WHS	84	840,000	-26	65	-20.7
Case 2a	Grid refinement	50 × 50 m near recharge	Unconfined / variable *T*	WHS	336	840,000	-26	65	-20.7
Case 2b	Solver check	50 × 50 m near recharge	Unconfined / variable *T*	PCG2	336	840,000	-26	65	-20.7
Case 3	Constant- *T* diagnostic	50 × 50 m near recharge	Specified constant *T*	WHS	336	840,000	-5	86	+4.9

Note: h_{max} is the maximum simulated head relative to the adopted ground-surface datum, and Δh is the water-table rise relative to the initial groundwater head and Diff. was calculated relative to the analytical water-table rise of 82 m.

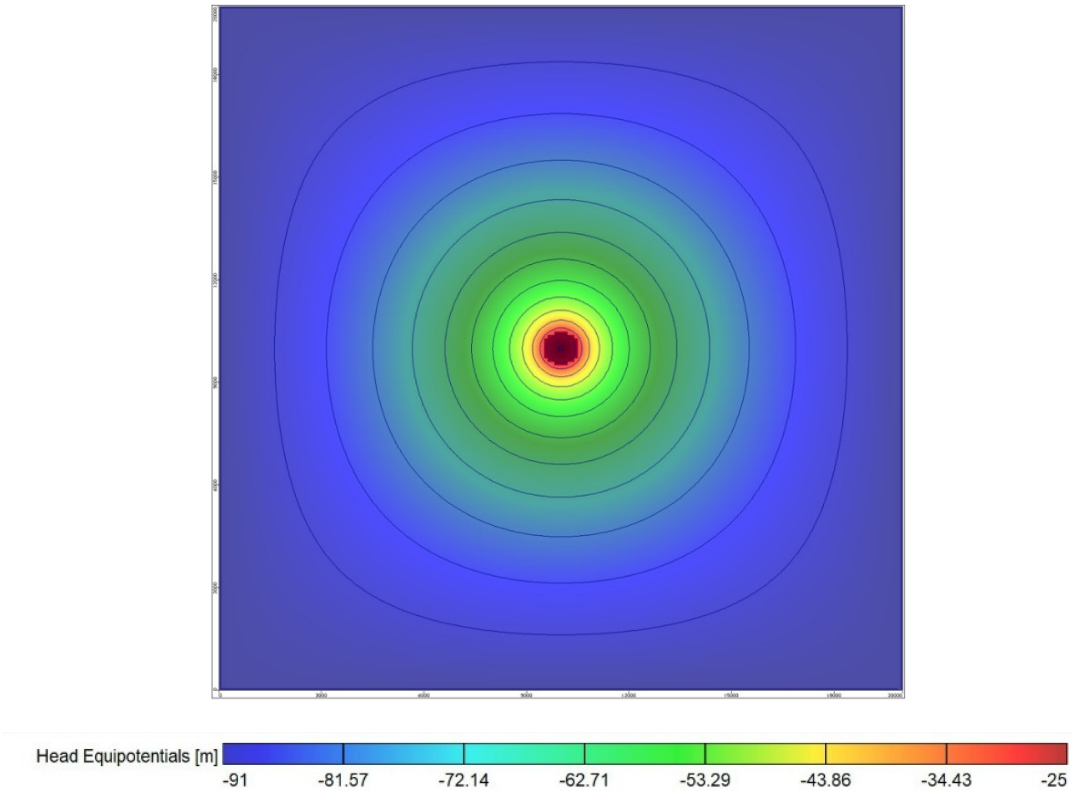

Figure 4.1. Simulated hydraulic-head distribution for the corrected literature-based circular recharge scenario.

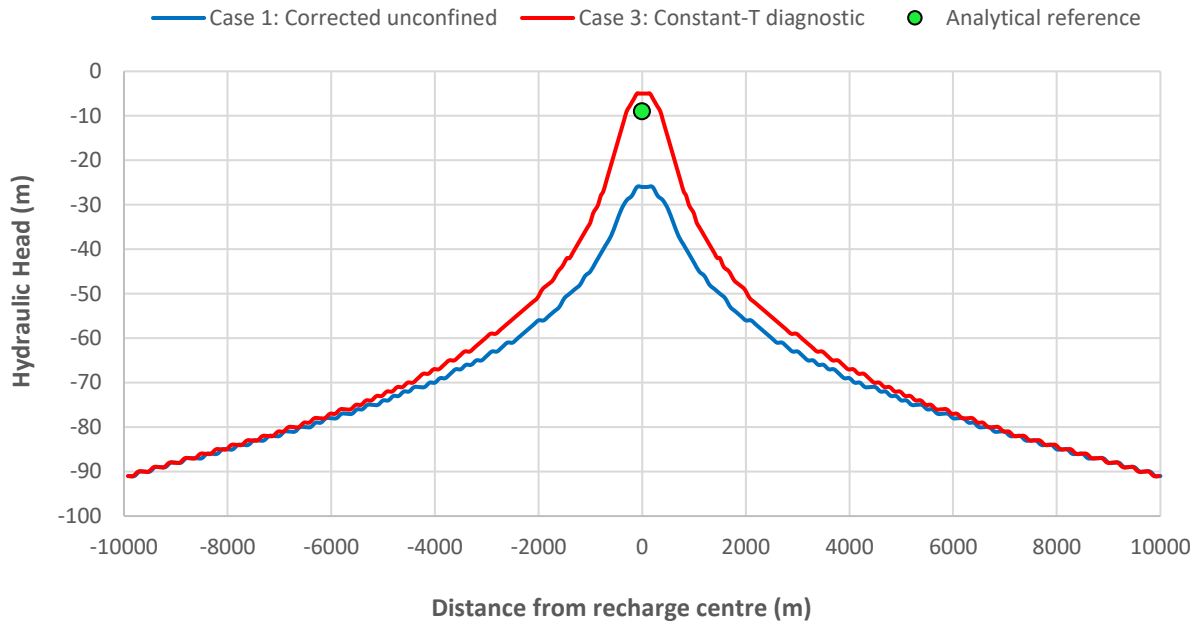

Figure 4.2. Central hydraulic-head profiles for the corrected unconfined model (case 1), constant-transmissivity diagnostic case (case 3), and analytical reference value. Case 1 gives a maximum head of −26 m and a water-table rise of 65 m, while Case 3 gives −5 m and 86 m. The analytical reference at the recharge center is approximately −9 m, corresponding to a water-table rise of 82 m.

Overall, the diagnostic checks show that the difference between the analytical and numerical results was not simply a numerical error. Instead, it reflected the limitation of applying a fixed-transmissivity analytical solution to a case with relatively large groundwater mounding.

4.1.2 Square diagnostic case

The square recharge case was used as a diagnostic test to examine how recharge-area representation affected the simulated groundwater mound response. The scenario was simulated under the same hydraulic properties, boundary conditions, initial groundwater head, and recharge rate used for the corrected circular reference case. The main numerical outputs of the square case are summarized in Table 4.2.

Table 4.2. Summary of numerical model outputs for the square recharge scenario.

Parameter	Value	Unit
Initial groundwater head	-91	m
Constant head	-91	m
Simulated maximum head	-35	m
Simulated water-table rise	56	m
Numerical recharge area	810,000	m²
Number of recharge cells	81	—

Note: Heads are reported relative to a ground-surface datum (z = 0), with an initial groundwater head of -91 m.

The square recharge scenario produced a maximum simulated head of −35 m, corresponding to a water-table rise of 56 m above the initial groundwater head of −91 m. The hydraulic-head distribution showed that the maximum mounding occurred beneath the recharge area and that hydraulic head decreased gradually toward the model boundaries. This behavior is consistent with the expected groundwater response to a localized recharge source. The simulated hydraulic-head distribution for the square recharge case is shown in Figure 4.3. The central cross-sectional hydraulic-head distribution for the square diagnostic case is shown in Appendix A**,** Figure A.2.

To evaluate the effect of recharge-area representation, the square case was then compared with the corrected circular recharge reconstruction. Both cases used the same hydraulic properties, boundary conditions, initial head, and hydraulic-head scale. The comparison focused on simulated maximum head, water-table rise, effective numerical recharge area, and number of recharge cells. The central hydraulic-head profiles are shown in Figure 4.4, and the main numerical indicators are summarized in Table 4.3.

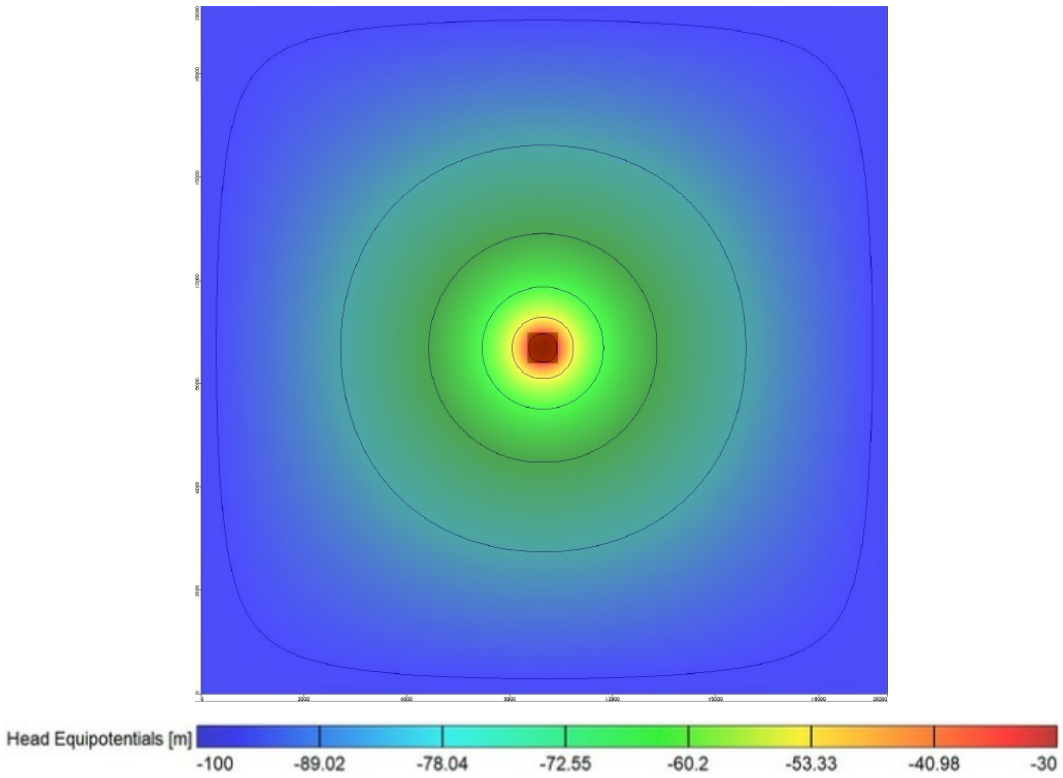

Figure 4.3. Simulated hydraulic head distribution for the square recharge scenario.

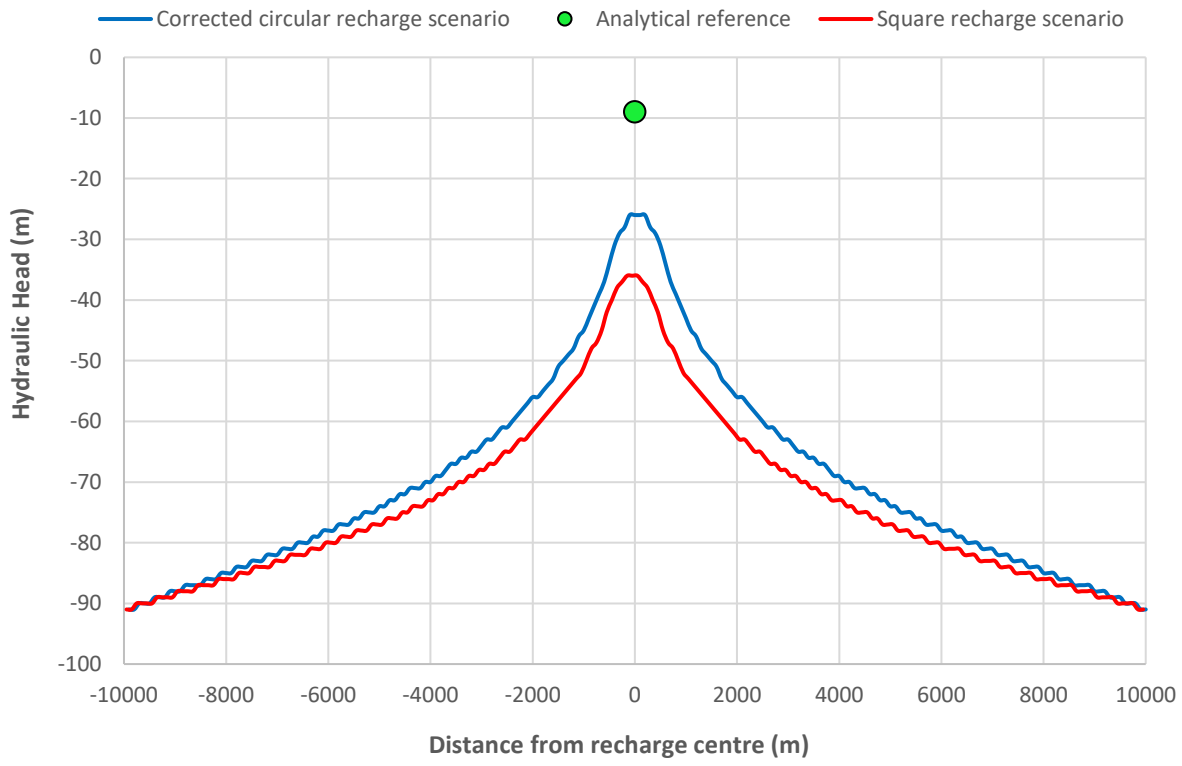

Figure 4.4. Central hydraulic-head profiles for the corrected circular and square recharge scenarios. The corrected circular scenario produced a higher water-table rise than the square scenario, with maximum heads of approximately −26 m and −35 m, respectively. The analytical reference value is shown at the recharge center, with a head of approximately −9 m and a water-table rise of 82 m.

Table 4.3. Comparison of the numerical results for the corrected circular and square recharge scenarios.

Parameter	Circular recharge scenario	Square recharge scenario
Simulated maximum head (m)	-26	-35
Simulated water-table rise (m)	65	56
Numerical recharge area (m²)	840,000	810,000
Number of recharge cells	84	81

4.1.3 Literature-based strip benchmark

The literature-based strip recharge case was used as the benchmark case for evaluating the analytical and numerical response of an elongated recharge configuration. This case was based on the strip/trench analytical formulation described in Chapter 2 and the numerical setup defined in Chapter 3.

Using the input values defined in Chapter 3, the analytical strip formulation gave a required control distance of approximately 1,835 m, or about 1.84 km. This means that, for the selected strip width, recharge rate, transmissivity, and permissible water-table rise, the control groundwater level would

need to be located at this distance from the strip edge to keep the total water-table rise beneath the strip center equal to 2 m. The main analytical results are summarized in Table 4.4.

Table 4.4. Analytical results for the literature-based strip recharge scenario.

Parameter	Symbol	Value
Total water-table rise (m)	$H_c - H_n$	2.000
Required control distance (m)	L_n	1835
Center-to-edge head rise (m)	$H_c - h_e$	0.027
Edge-to-control head difference (m)	$h_e - H_n$	1.973

The analytical results show that most of the total water-table rise occurred between the strip edge and the distant control groundwater level. In contrast, the head rise between the strip center and the strip edge was relatively small under the selected parameter values.

The same reference strip case was reconstructed in Visual MODFLOW Classic using the model domain, grid discretization, hydraulic properties, initial head, and boundary-condition configuration described in Chapter 3. The simulated water-table rise was calculated as the difference between the simulated maximum head and the initial groundwater head. The main numerical outputs are summarized in Table 4.5.

Table 4.5. Numerical outputs for the literature-based strip recharge scenario.

Parameter	Value	Unit
Initial groundwater head	-91	m
Constant head	-91	m
Simulated maximum head	-90.074	m
Simulated water-table rise	0.926	m
Numerical strip width	100	m
Numerical strip length	1000	m
Numerical recharge area	100,000	m^2
Number of recharge cells	250	—
Applied recharge rate	0.02	m/day

The numerical simulation produced a maximum hydraulic head of −90.074 m and a simulated water-table rise of 0.926 m above the initial groundwater head of −91 m. The simulated hydraulic-head distribution showed the expected mound pattern, with the maximum head occurring beneath the center of the recharge strip and decreasing gradually toward the model boundaries. The plan-view hydraulic-head distribution for the reference strip case is shown in Figure 4.5.

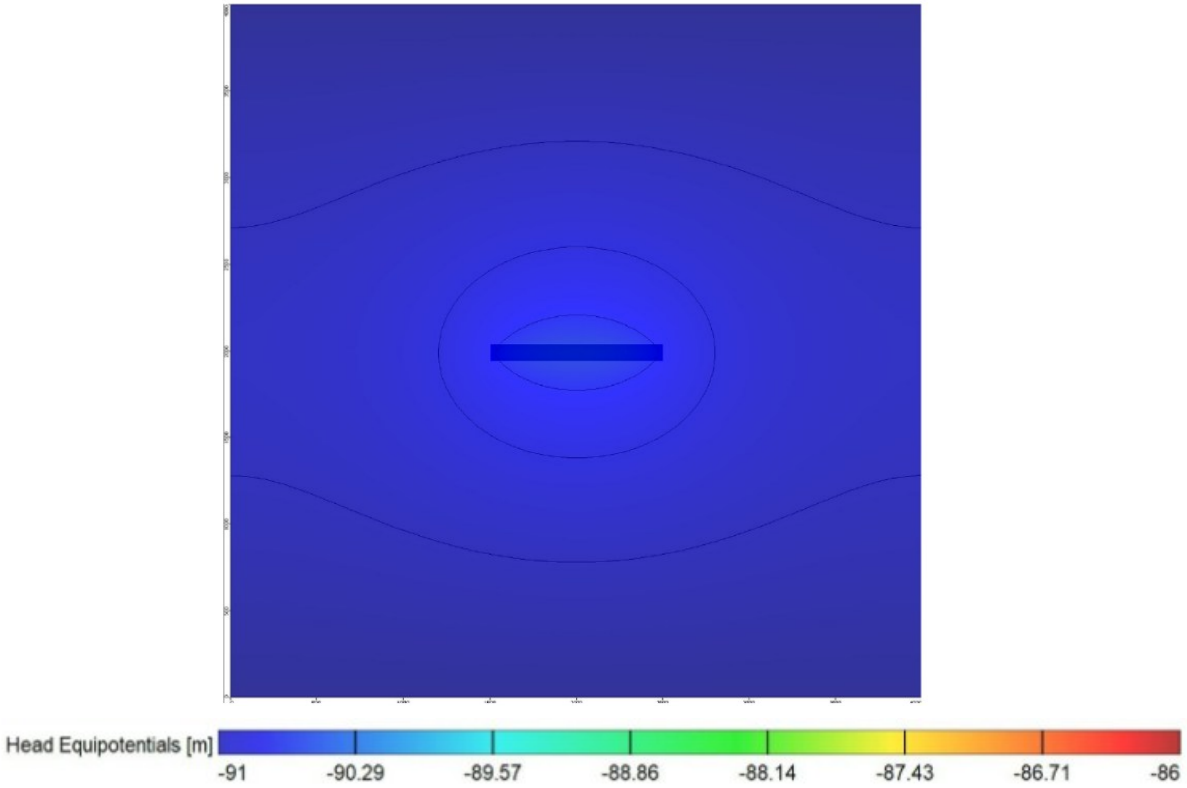

Figure 4.5. Simulated hydraulic-head distribution for the literature-based strip recharge scenario.

The corresponding central cross-sectional hydraulic-head distribution for the literature-based strip scenario is provided in Appendix B, Figure B.1. To evaluate the consistency between the analytical strip solution and the numerical reconstruction, the analytical and numerical water-table rise values were compared. The comparison is summarized in Table 4.6.

Table 4.6. Comparison of analytical and numerical water-table rise results for the literature-based strip recharge scenario.

Parameter	Analytical value	Numerical value
Initial/control groundwater head relative to datum (m)	-91.000	-91.000
Water-table rise, (H_c - H_n) (m)	2.000	0.926
Maximum head at mound center (m)	-89.000	-90.074
Difference in water-table rise (m)	—	-1.074
Relative difference (%)	—	-53.7

The numerical reconstruction produced a water-table rise of 0.926 m, which was lower than the analytical water-table rise of 2.000 m. This corresponds to a relative difference of approximately −53.7%. The difference is mainly related to the approximate nature of the numerical reconstruction, including the finite strip length, finite model domain, discretized representation of

the recharge strip, and boundary-condition implementation. Nevertheless, the numerical model reproduced the expected spatial pattern of groundwater mounding beneath the recharge strip.

4.1.4 Explanation of analytical–numerical differences

The benchmark cases showed that the analytical and numerical models produced the same general mound pattern, but not always the same water-table rise values. This difference was expected because the two approaches are based on different assumptions.

In the circular benchmark case, the main difference was related to the treatment of transmissivity. The analytical solution assumes a fixed transmissivity, while the unconfined MODFLOW model allows saturated thickness, and therefore effective transmissivity, to change as the water-table rises. This explains why the constant-transmissivity diagnostic case gave results closer to the analytical reference.

In the strip benchmark case, the numerical water-table rise was lower than the analytical estimate. This difference was mainly related to the simplified long-strip assumption used in the analytical formulation of Bouwer et al. (1999). In contrast, the Visual MODFLOW reconstruction represented the recharge area as a finite rectangular strip within a finite model domain. Therefore, finite strip length, grid discretization, and boundary-condition implementation affected the numerical response.

Overall, the analytical solutions were useful as reference estimates, but they should be interpreted together with their simplifying assumptions. The numerical models provided additional information on how recharge-area representation, model boundaries, and unconfined aquifer behavior affected the simulated mound response.

4.2 Circular and trench transmissivity-sensitivity results

The circular and trench transmissivity-sensitivity scenarios were used to examine the effect of aquifer transmissivity and recharge geometry under comparable hydraulic and recharge conditions. In both scenarios, the total recharge input was kept equal to 100 m^3/day, while hydraulic conductivity, and consequently transmissivity, was varied to evaluate its influence on groundwater mounding.

4.2.1 Circular basin transmissivity-sensitivity results

The circular transmissivity-sensitivity scenario was first used to evaluate the effect of aquifer transmissivity on groundwater mound development beneath a circular recharge basin. The recharge area, recharge rate, model domain, boundary conditions, and initial groundwater head were kept constant, while hydraulic conductivity was varied from 1 to 100 m/day. The corresponding transmissivity values ranged from 20 to 2,000 m^2/day.

The analytical and Visual MODFLOW results for the circular transmissivity-sensitivity scenario are summarized together in Table 4.7 to allow direct comparison. Both approaches show a clear decrease in water-table rise as transmissivity increases.

Table 4.7. Comparison of analytical and Visual MODFLOW results for the circular transmissivity-sensitivity scenario at different transmissivity conditions.

(K) (m/day)	(T) (m²/day)	Analytical results			Visual MODFLOW results		Absolute difference (m)	Relative difference (%)
		(H_c-h_e) (m)	(h_e-H_n) (m)	(H_c-H_n) (m)	Simulated maximum head (m)	Simulated water-table rise (m)		
1	**20**	0.3980	1.7360	2.1340	−7.9461	2.0538	0.0802	−3.8
5	**100**	0.0796	0.3472	0.4268	−9.5763	0.4236	0.0032	−0.7
10	**200**	0.0398	0.1736	0.2134	−9.7874	0.2125	0.0009	−0.4
50	**1,000**	0.0080	0.0347	0.0427	−9.9572	0.0427	0.0000	0.0
100	**2,000**	0.0040	0.0174	0.0213	−9.9786	0.0213	0.0000	0.0

Note: H_c-h_e represents the analytical center-to-edge head rise, h_e-H_n represents the analytical edge-to-control-head rise, and H_c-H_n represents the total analytical water-table rise. Heads are reported relative to a ground-surface datum (z = 0), with an initial groundwater head of -10 m. Relative difference (%) was calculated as (Numerical−Analytical)/Analytical×100. Negative values indicate that the numerical water-table rise value is lower than the analytical estimate.

Figure 4.6 compares the analytical and Visual MODFLOW water-table-rise results under the tested transmissivity conditions.

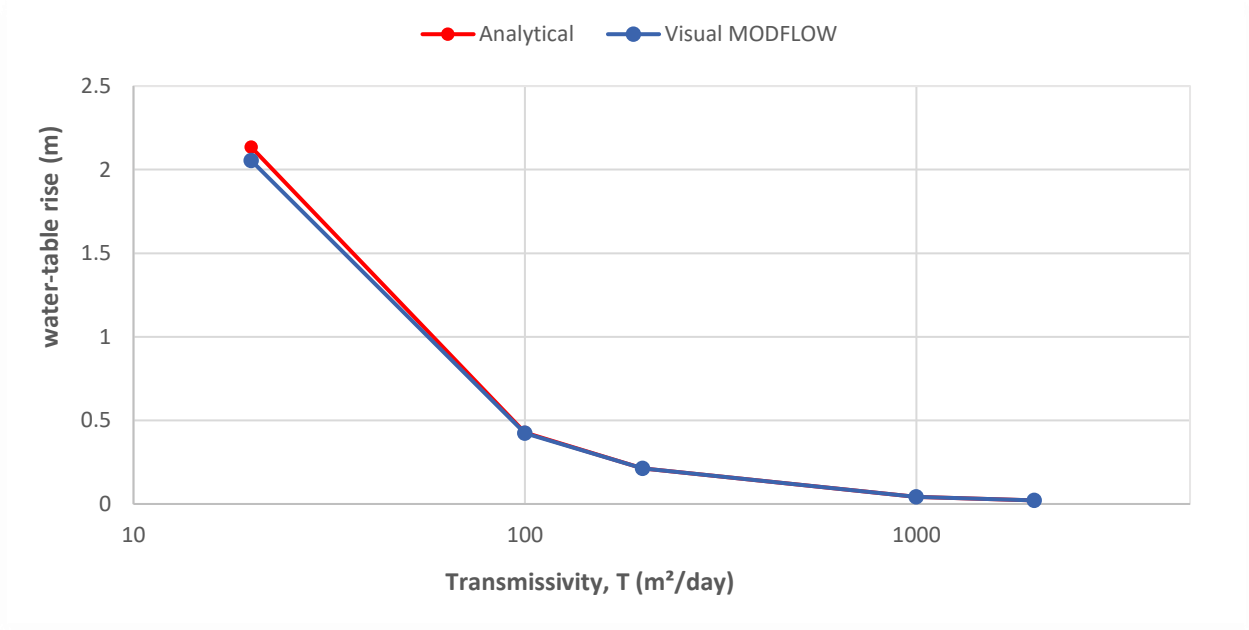

Figure 4.6. Comparison of analytical and Visual MODFLOW water-table rise under different transmissivity conditions for the circular-basin sensitivity scenario.

The analytical and Visual MODFLOW results showed a very similar trend. The largest difference occurred at T=20 m^2/day, where the Visual MODFLOW result was 3.8% lower. At higher transmissivity values, the difference was very small.

The spatial distribution of simulated hydraulic head is shown in Figure 4.7. A common color scale was used for all transmissivity cases to allow direct comparison. The lowest-transmissivity case produced the most pronounced mound beneath the recharge area, while the higher-transmissivity cases remained close to the initial groundwater head across most of the model domain.

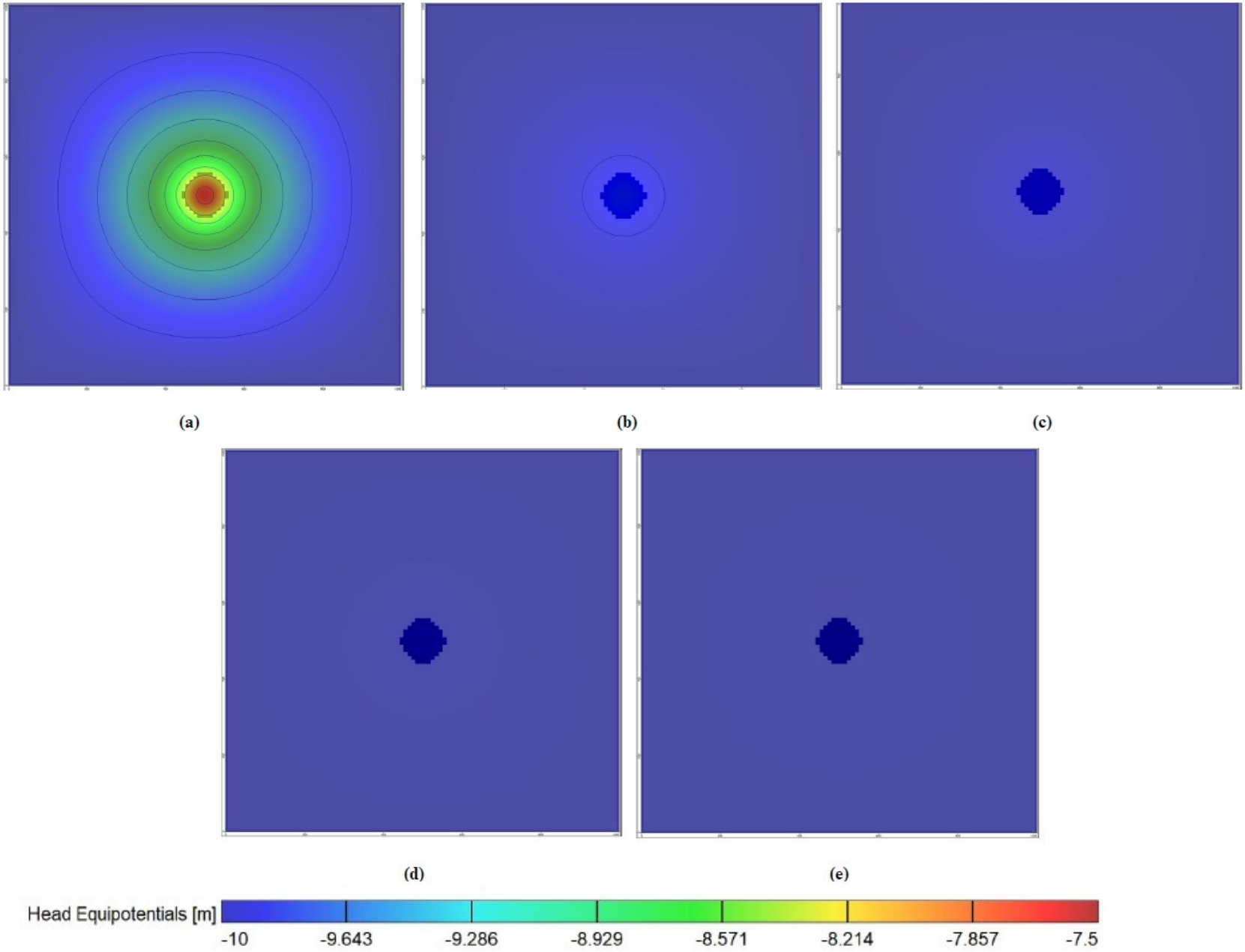

Figure 4.7. Comparison of simulated plan-view hydraulic head distributions for the circular transmissivity-sensitivity scenario at different transmissivity values.

(a) K = 1 m/day, T = 20 m²/day; (b) K = 5 m/day, T = 100 m²/day; (c) K = 10 m/day, T = 200 m²/day;

(d) K = 50 m/day, T = 1000 m²/day; and (e) K = 100 m/day, T = 2000 m²/day

To compare the spatial response more clearly, hydraulic-head profiles were extracted along the central cross-section of the model domain. The profiles show that increasing transmissivity reduced both the mound crest and the lateral extent of recharge-induced head buildup. The lowest-transmissivity case produced the highest and broadest mound response, whereas the higher-transmissivity cases showed only small departures from the initial groundwater head. Additional central cross-sectional hydraulic-head distributions for the circular transmissivity-sensitivity scenario under all transmissivity values are reported in Appendix A**,** Figure A.3.

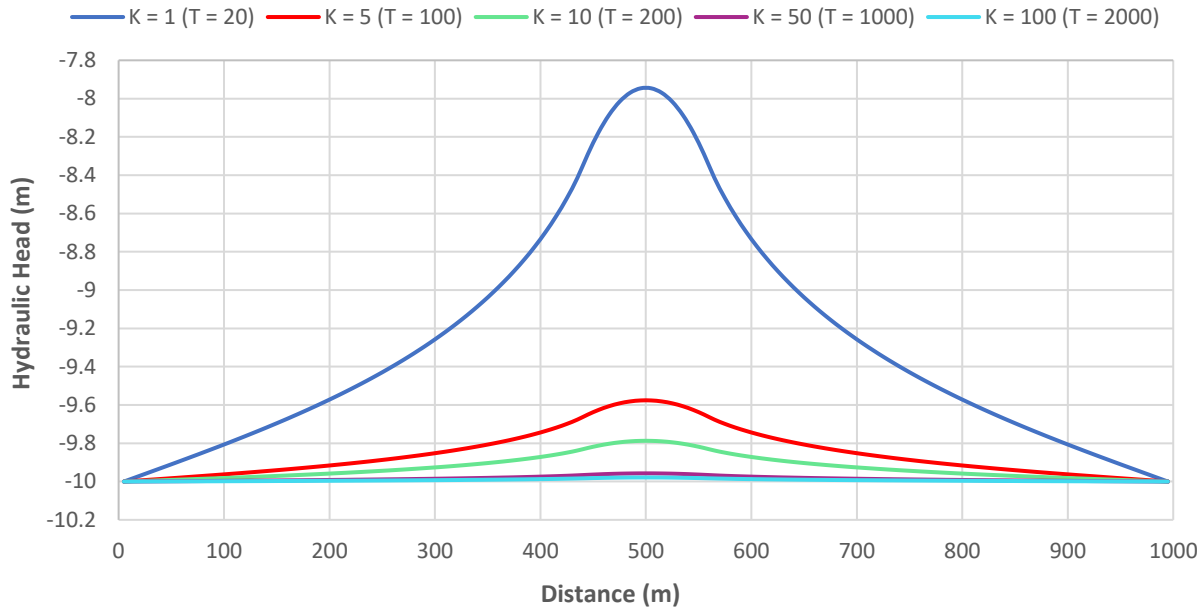

Figure 4.8. Comparison of simulated hydraulic head profiles along the central cross-section for the circular transmissivity-sensitivity scenario under different transmissivity values.

As shown in Table 4.7 and Figure 4.6 , the analytical and Visual MODFLOW results were in good agreement. Both approaches reproduced the same transmissivity-dependent response, with water-table rise decreasing as transmissivity increased. The Visual MODFLOW results were slightly lower than the analytical estimates for the lower-transmissivity cases. The largest relative difference was −3.8% at T=20 m^2/day, while the differences were negligible for the higher-transmissivity cases.

A local grid-refinement check was therefore performed for the T = 20 m^2/day case. The refined-grid simulation produced a water-table rise of approximately 1.998 m, compared with 2.054 m in the original numerical model and 2.134 m in the analytical calculation. Since grid refinement did not improve the agreement with the analytical value, the remaining difference was not considered to be primarily controlled by grid resolution.

Overall, the circular transmissivity-sensitivity scenario shows that transmissivity was the main control on groundwater mound development under the tested recharge conditions. Lower transmissivity produced greater water-table rise beneath the recharge basin, while higher

transmissivity allowed the recharge water to spread more effectively through the aquifer. The numerical model was able to reproduce both the magnitude and the overall trend of the analytical water-table rise response under the selected steady-state conditions.

4.2.2 Trench transmissivity-sensitivity scenario

The trench transmissivity-sensitivity scenario was used to evaluate groundwater mound development beneath a rectangular trench-type recharge configuration. The scenario used the same total recharge input as the circular transmissivity-sensitivity case, equal to 100 m^3/day, but the recharge was applied over a 20 m wide and 500 m long trench. Hydraulic conductivity was varied from 1 to 100 m/day, corresponding to transmissivity values from 20 to 2,000 m^2/day.

The analytical and Visual MODFLOW results for the trench transmissivity-sensitivity scenario are summarized together in Table 4.8 to allow direct comparison. Both approaches show a clear decrease in water-table rise as transmissivity increases.

Table 4.8. Comparison of analytical and Visual MODFLOW results for the trench scenario transmissivity-sensitivity under different transmissivity conditions.

(K) (m/day)	(T) (m^2/day)	Analytical results			Visual MODFLOW results		Absolute difference (m)	Relative difference (%)
		(H_c-h_e) (m)	(h_e-H_n) (m)	(H_c-H_n) (m)	Simulated maximum head (m)	Simulated water-table rise (m)		
1	**20**	0.0250	2.5000	2.5250	−8.4615	1.5393	0.9865	−39.0
5	**100**	0.0050	0.5000	0.5050	−9.6847	0.3153	0.1897	−37.6
10	**200**	0.0025	0.2500	0.2525	−9.8421	0.1578	0.0947	−37.5
50	**1,000**	0.0005	0.0500	0.0505	−9.9682	0.0317	0.0188	−37.2
100	**2,000**	0.0003	0.0250	0.0253	−9.9841	0.0158	0.0095	−37.5

Note: H_c-h_e represents the analytical center-to-edge head rise, h_e-H_n represents the analytical edge-to-control-head rise, and H_c-H_n represents the total analytical water-table rise. Heads are reported relative to a ground-surface datum (z = 0), with an initial groundwater head of -10 m. Relative difference (%) was calculated as (Numerical−Analytical)/Analytical×100. Negative values indicate that the numerical water-table rise value is lower than the analytical estimate.

Figure 4.9 compares the analytical and Visual MODFLOW water-table rise results under the tested transmissivity conditions.

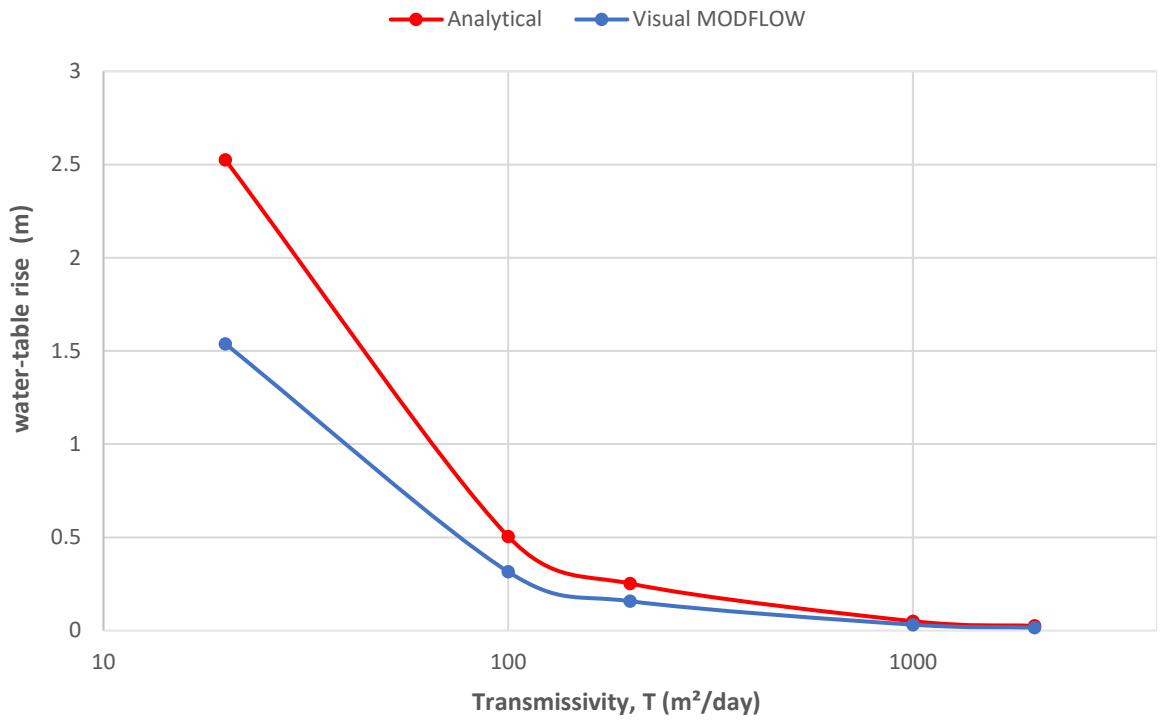

Figure 4.9. Comparison of analytical and Visual MODFLOW water-table rise under different transmissivity conditions for the trench transmissivity-sensitivity scenario.

The analytical and Visual MODFLOW results showed the same decreasing trend as transmissivity increased. However, the Visual MODFLOW values were consistently lower than the analytical estimates. The relative difference remained approximately 37–39% under all tested transmissivity conditions.

The spatial distribution of simulated hydraulic head was evaluated using plan-view hydraulic-head distributions. A common color scale was used for all transmissivity cases to support direct comparison. The lowest-transmissivity case produced the most visible mound response beneath and around the trench, while the higher-transmissivity cases remained close to the initial groundwater head across most of the model domain.

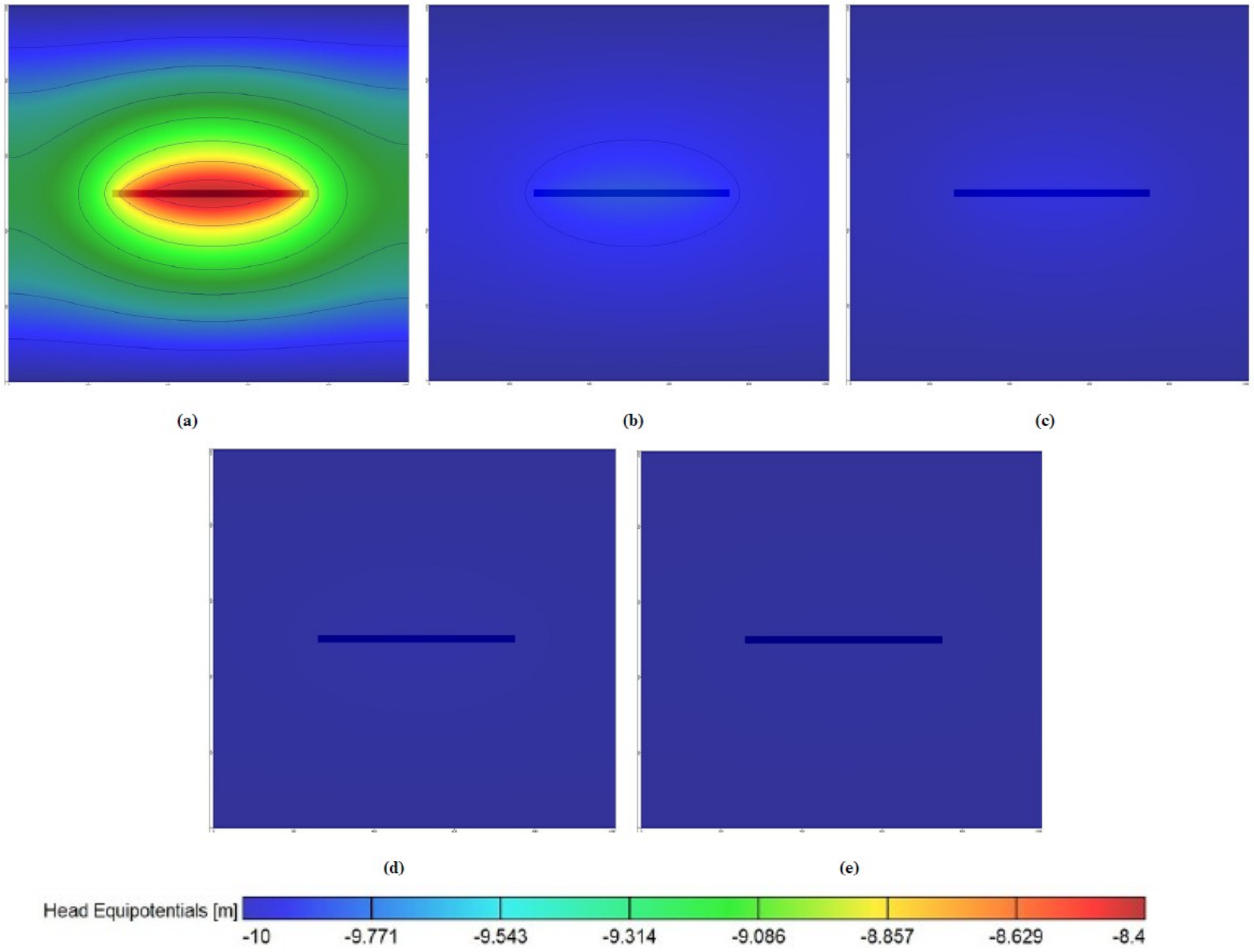

Figure 4.10. Comparison of simulated plan-view hydraulic head distributions for the trench transmissivity-sensitivity scenario at different transmissivity values.

(a) K = 1 m/day, T = 20 m²/day; (b) K = 5 m/day, T = 100 m²/day; (c) K = 10 m/day, T = 200 m²/day;

(d) K = 50 m/day, T = 1000 m²/day; and (e) K = 100 m/day, T = 2000 m²/day

To compare the spatial response more clearly, hydraulic-head profiles were extracted along the central cross-section perpendicular to the trench axis. The profile comparison confirmed that the lowest-transmissivity case produced the highest and most pronounced mound response. In contrast, the higher-transmissivity cases remained close to the initial groundwater head across most of the model domain.

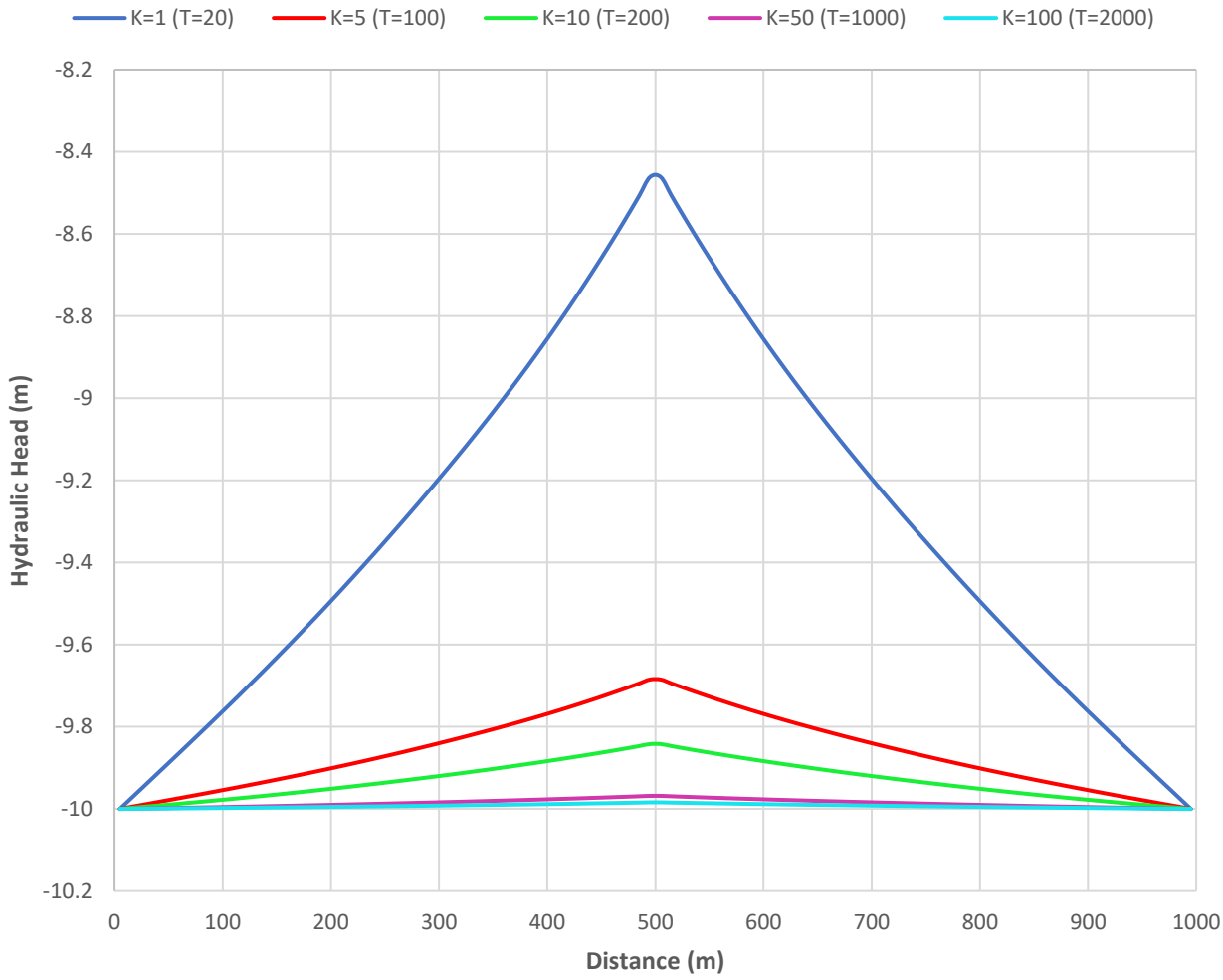

Figure 4.11. Comparison of simulated hydraulic head profiles along the central cross-section perpendicular to the trench axis for the trench transmissivity-sensitivity scenario at different transmissivity values.

Additional central cross-sectional hydraulic-head distributions for the trench transmissivity-sensitivity scenario at different transmissivity values are reported in Appendix B, Figure B.5. The analytical and Visual MODFLOW results are compared in Table 4.8 and Figure 4.9.

The comparison shows that the analytical and Visual MODFLOW results followed the same general trend. In all cases, water-table rise decreased as transmissivity increased. However, the Visual MODFLOW results were consistently lower than the analytical estimates, with relative differences of approximately −37% to −39%.

This systematic difference is mainly related to the different representation of the trench in the two approaches. The analytical solution is based on an idealized long-strip recharge condition, while

the numerical model represents a finite rectangular trench with a length of 500 m within a finite model domain. As a result, some additional lateral spreading can occur around the two finite ends of the trench, which may reduce the simulated water-table rise compared with the idealized analytical estimate. This interpretation is consistent with Bouwer et al. (1999), who describe the strip formulation for long and narrow recharge systems and note that groundwater mounding can be reduced by using longer and narrower recharge areas.

Additional checks were performed for the lowest-transmissivity case to examine whether the difference was mainly caused by grid resolution or solver settings. Grid refinement and solver changes did not substantially reduce the analytical–numerical difference. Therefore, the remaining difference was interpreted mainly as a result of the difference between the idealized analytical strip/trench formulation and the finite numerical representation in Visual MODFLOW.

Overall, the trench transmissivity-sensitivity scenario confirms that aquifer transmissivity was the main control on groundwater mound development beneath the trench configuration. Lower transmissivity limited lateral dissipation and produced greater water-table rise, while higher transmissivity allowed the applied recharge to spread more efficiently through the aquifer, resulting in smaller head increases.

4.2.3 Circular–trench comparison

The circular and trench transmissivity-sensitivity scenarios were compared to evaluate the effect of recharge geometry on simulated groundwater mound development. The two scenarios were defined using the same model domain, initial groundwater head, saturated thickness, hydraulic conductivity values, and transmissivity values. The total applied recharge was also kept the same in both scenarios.

In both cases, the total recharge input was 100 m³/day. For the circular case, recharge was applied over a compact circular basin, while for the trench case, the same total recharge input was distributed along a 20 m wide and 500 m long rectangular trench. Therefore, the comparison focused on the effect of recharge geometry and spatial recharge distribution rather than a difference in total applied recharge.

The numerical water-table rise results for the two configurations are summarized in Table 4.9.

Table 4.9. Comparison of numerical water-table rise results for the circular and trench transmissivity-sensitivity scenarios under the same total applied recharge rate.

K (m/day)	*T* (m²/day)	Circular water-table rise (m)	Trench water-table rise (m)	Difference, Circular − Trench (m)
1	**20**	2.0538	1.5385	0.5153
5	**100**	0.4236	0.3153	0.1083
10	**200**	0.2125	0.1578	0.0547
50	**1000**	0.0427	0.0317	0.0110
100	**2000**	0.0213	0.0158	0.0055

The results show that the circular transmissivity-sensitivity scenario produced larger water-table rise values than the trench transmissivity-sensitivity scenario for all tested transmissivity values. The largest difference occurred under the lowest-transmissivity condition. At T = 20 m²/day, the

circular scenario produced a water-table rise of 2.0538 m, compared with 1.5385 m for the trench scenario. As transmissivity increased, the difference between the two geometries became progressively smaller.

This indicates that recharge geometry affected both the magnitude and spatial concentration of groundwater mounding. The circular recharge configuration produced a more radially concentrated mound, while the trench configuration distributed the same total recharge input along an elongated recharge zone. As a result, the trench scenario produced lower water-table rise values than the circular scenario under the same total recharge volume.

However, the decreasing difference at higher transmissivity values shows that aquifer transmissivity remained the dominant control on the overall mound response. At high transmissivity, recharge water spread more easily through the aquifer, and the effect of recharge geometry became less pronounced.

4.3 Steady-state sensitivity results

4.3.1 Cases with changing total recharge

The first group of sensitivity cases examined the effect of changing recharge rate and strip width for the literature-based strip configuration. In these cases, the recharge rate or strip width was changed separately, while the other model settings were kept consistent with the reference strip case. Since changing either the recharge rate or the strip width also changed the total applied recharge, these cases were interpreted as preliminary sensitivity tests rather than constant-total-recharge comparisons. In this section, the reference strip, modified recharge-rate, and modified strip-width simulations are referred to as STR-REF, STR-RR, and STR-SW, respectively.

Supplementary analytical calculations were first performed to evaluate the expected effect of these parameter changes on groundwater mound development. In these calculations, the reference transmissivity, T = 930 m²/day, and the previously derived control distance, Ln = 1,835 m, were retained. The recharge rate and strip width were then varied individually under otherwise consistent analytical conditions. The results are summarized in Table 4.10.

Table 4.10. Supplementary analytical calculations for the strip recharge scenario.

Analytical configuration	Description	i (m/day)	W (m)	H_c-H_n (m)	H_c-h_e (m)	h_e-H_n (m)
Reference analytical strip case (STR-REF)	**Original parameter set**	0.02	100	2.000	0.027	1.973
Modified recharge-rate case (STR-RR)	**Recharge rate increased**	0.10	100	10.000	0.134	9.866
Modified strip-width case (STR-SW)	**Strip width increased**	0.02	300	6.160	0.242	5.918

The supplementary analytical results show that increasing either the recharge rate or the strip width produced a larger groundwater mound under the same reference control-distance assumption. The recharge-rate modification produced the largest water-table rise, increasing the total water-table rise to 10.0 m. Increasing the strip width also increased the water-table rise, but to a smaller extent,

with a total water-table rise of 6.16 m. These results indicate that the strip recharge response is sensitive to both recharge intensity and recharge geometry.

Modified recharge-rate case (STR-RR)

In the modified recharge-rate case, the recharge rate was increased from 0.02 m/day to 0.10 m/day, while the strip geometry, model domain, grid discretization, hydraulic conductivity, initial head, and boundary conditions were kept identical to the reference strip scenario. The numerical model settings and simulated outputs are summarized in Table 4.11.

Table 4.11. Numerical model settings and simulated outputs for the modified recharge-rate strip case.

Parameter	Value	Unit
Initial groundwater head	-91	m
Constant head	-91	m
Simulated maximum head	-86.430	m
Simulated water-table rise	4.570	m
Numerical strip width	100	m
Numerical strip length	1000	m
Numerical recharge area	100000	m^2
Number of recharge cells	250	—
Applied recharge rate	0.10	m/day

Note: The same ground-surface datum and head convention adopted for the reference strip case were used here.

The spatial response of the modified recharge-rate case was evaluated using the plan-view hydraulic-head distribution shown in Figure 4.12.

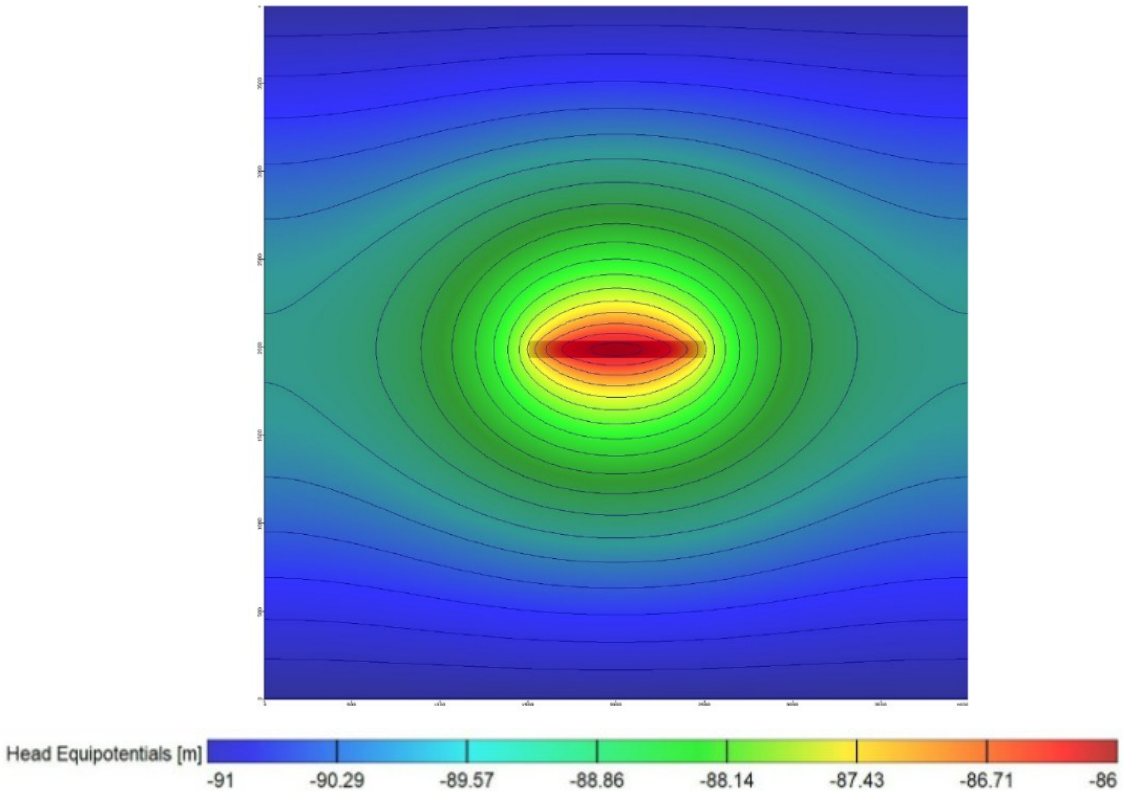

Figure 4.12. Simulated hydraulic head distribution for the modified recharge-rate strip case.

The numerical results show that increasing the recharge rate produced a substantially larger groundwater mound beneath the recharge strip. Compared with the reference strip case, the modified recharge-rate case generated a higher central head and a larger water-table rise. This indicates that recharge intensity strongly affected the simulated groundwater response under the tested conditions. The cross-sectional hydraulic-head distributions for the modified recharge-rate and modified strip-width cases are shown in Appendix B, Figure B.2. and Figure B.3. , respectively.

Modified strip-width case (STR-SW)

In the modified strip-width case, the strip width was increased from 100 m to 300 m, while the recharge rate was kept equal to the reference value of 0.02 m/day. The model domain, grid discretization, layer configuration, hydraulic conductivity, initial head, and boundary conditions were kept unchanged. The numerical model settings and simulated outputs are summarized in Table 4.12.

Table 4.12. Numerical model settings for the modified strip-width case.

Parameter	Value	Unit
Initial groundwater head	-91	m
Constant head	-91	m
Simulated maximum head	-88.384	m
Simulated water-table rise	2.616	m
Numerical strip width	300	m
Numerical strip length	1000	m
Numerical recharge area	300000	m^2
Number of recharge cells	750	—
Applied recharge rate	0.02	m/day

Note: The same ground-surface datum and head convention adopted for the reference strip case were used here.

The spatial response of the modified strip-width case was evaluated using the plan-view hydraulic-head distribution shown in Figure 4.13.

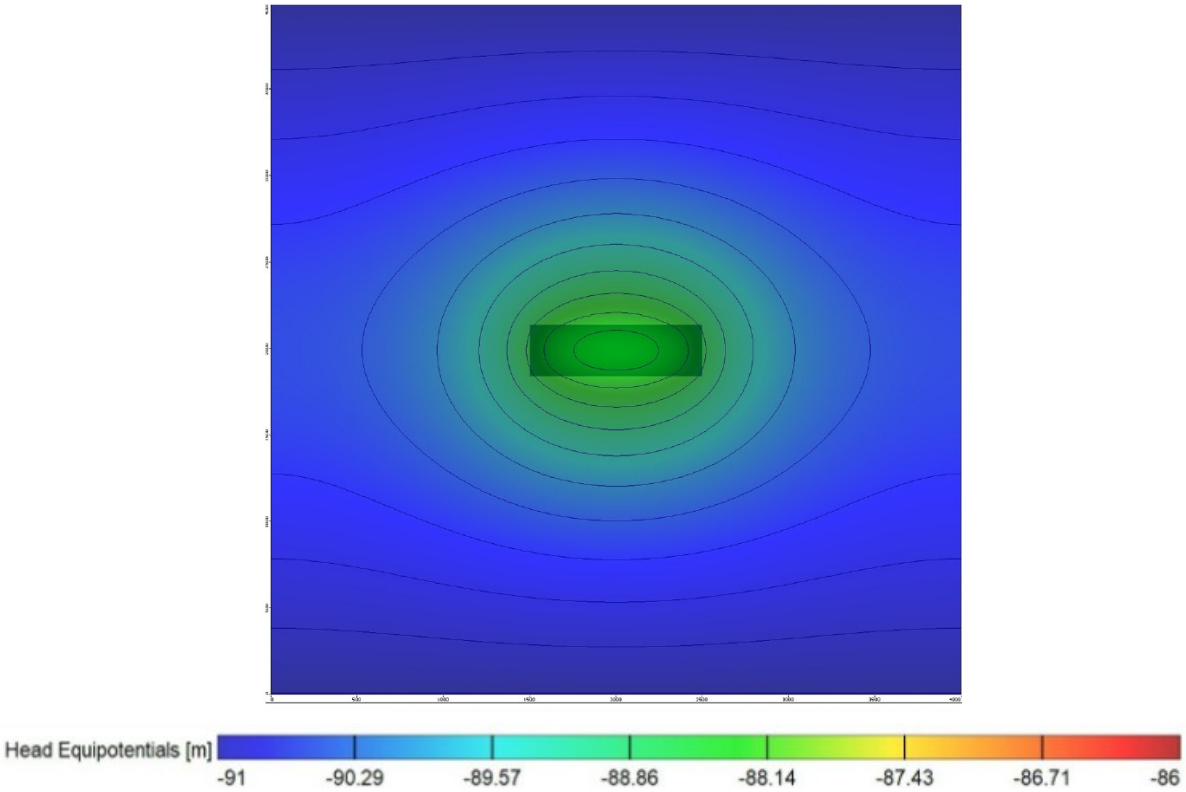

Figure 4.13. Simulated hydraulic head distribution for the modified strip-width case.

The modified strip-width case produced a larger simulated mound than the reference strip case. However, the increase in water-table rise was smaller than that obtained for the modified recharge-

rate case. This indicates that increasing recharge intensity had a stronger effect than strip-width enlargement under the tested conditions.

The STR-REF, STR-RR, and STR-SW cases were compared to evaluate the individual effects of recharge-rate increase and strip-width enlargement on groundwater mound development. These cases did not maintain the same total recharge input; therefore, the comparison should be interpreted as a preliminary sensitivity assessment rather than an isolated evaluation of recharge distribution. The numerical settings and outputs are summarized in Table 4.13.

Table 4.13. Comparison of numerical settings and simulated outputs for the reference strip case and the two modified sensitivity cases.

Parameter	Reference strip case (STR-REF)	Modified recharge-rate case (STR-RR)	Modified strip-width case (STR-SW)
Recharge rate (m/day)	0.02	0.10	0.02
Strip width (m)	100	100	300
Strip length (m)	1000	1000	1000
Simulated maximum head (m)	-90.074	-86.430	-88.384
Simulated water-table rise (m)	0.926	4.570	2.616
Numerical recharge area (m²)	100000	100000	300000
Number of recharge cells	250	250	750

To extend the analytical–numerical comparison beyond the reference strip case, the analytical and numerical water-table rise values were also compared for the three preliminary strip sensitivity cases. The comparison is summarized in Table 4.14.

Table 4.14. Comparison of analytical and numerical water-table rise values for the preliminary strip sensitivity cases.

Case	Analytical water-table rise (m)	Numerical water-table rise (m)	Difference (m)	Relative difference (%)
Reference strip (STR-REF)	2.000	0.926	-1.074	-53.7
Modified recharge-rate case (STR-RR)	10.000	4.570	-5.430	-54.3
Modified strip-width case (STR-SW)	6.160	2.616	-3.544	-57.5

The large difference between the analytical and MODFLOW results is likely related to the different representation of the recharge strip in the two methods. In the analytical method, the recharge area is assumed to be a long strip, with a length of at least ten times its width, and the effects of the strip ends are neglected (Bouwer et al., 1999). However, in MODFLOW, the strip has a finite length and is represented within a discretized model domain. Therefore, groundwater can spread in more directions in the numerical model, resulting in a lower simulated water-table rise.

The similar relative differences in all three scenarios indicate that the difference is mainly related to the two modeling approaches rather than only to changes in recharge rate or strip width. The slightly larger difference for STR-SW may be related to its greater width, because this case is less like the long and narrow strip assumed in the analytical model.

Figure 4.14 compares the hydraulic-head profiles along the central cross-section for the reference strip case and the two preliminary sensitivity cases.

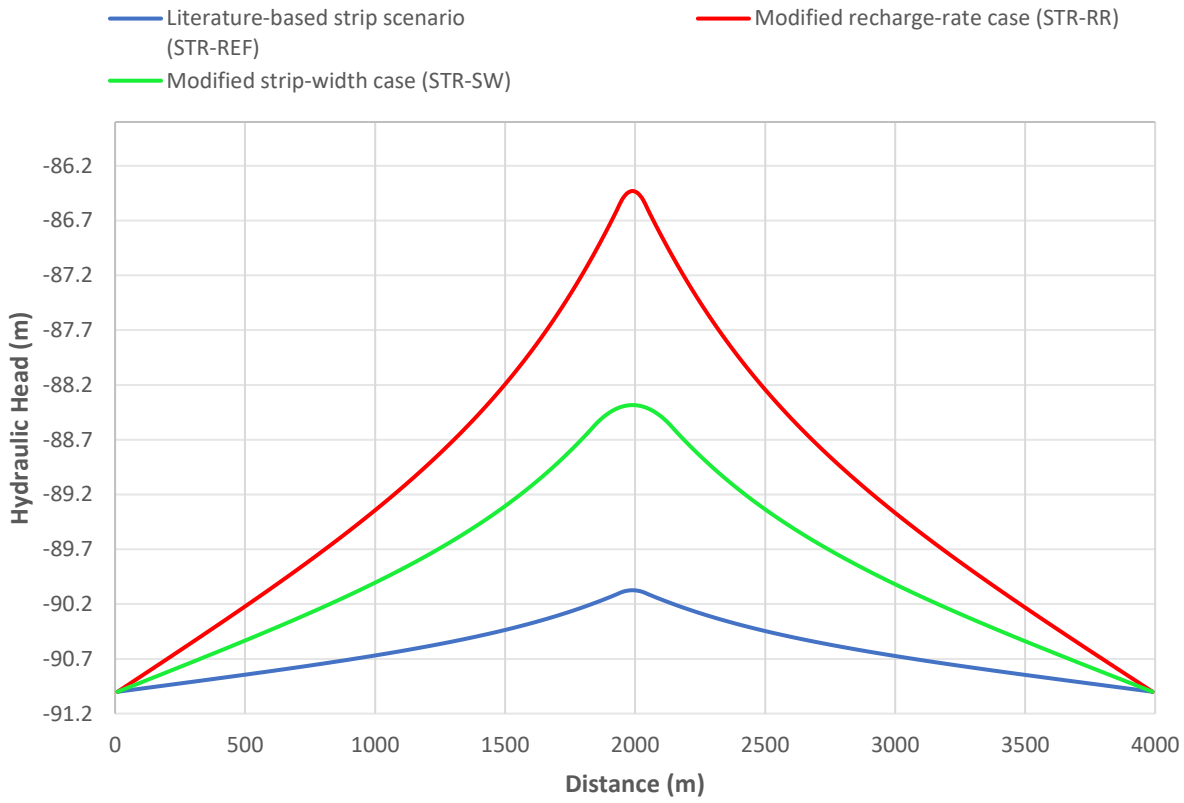

Figure 4.14. Comparison of simulated hydraulic head profiles along the central cross-section for the preliminary strip sensitivity cases. STR-REF: i = 0.02 m/day, W = 100 m, L = 1,000 m; STR-RR: i = 0.10 m/day, W = 100 m, L = 1,000 m; STR-SW: i = 0.02 m/day, W = 300 m, L = 1,000 m. In all cases, the initial groundwater head was -91 m and the same model domain, grid discretization, hydraulic properties, and boundary-condition configuration were used.

The comparison shows that both parameter modifications increased the simulated groundwater mound relative to the reference strip case. The modified recharge-rate case produced the strongest response, with the highest simulated head and the largest water-table rise. The modified strip-width case also produced a higher mound than the reference case, but its effect was smaller than that of the recharge-rate modification.

Overall, these preliminary sensitivity cases show that both recharge intensity and strip width affected the simulated mound response. However, because the total recharge input was not kept constant among these cases, additional constant-total-recharge comparisons were needed to isolate the effect of recharge distribution.

4.3.2 Constant-total-recharge circular basin cases

The constant-total-recharge circular basin cases were used to evaluate how changing the recharge area affected water-table rise while keeping the total recharge input constant at 100 m^3/day. In these

cases, the recharge area and recharge rate were adjusted together so that the same total recharge volume was applied in all configurations. The numerical results are summarized in Table 4.15.

Table 4.15. Numerical results for the supplementary constant-total-recharge circular basin sensitivity cases.

K (m/day)	Case	Recharge area (m²)	*i* (m/day)	*Q* (m³/day)	Water-table rise (m)
1	**Smaller basin**	5,000	0.020	100	2.265
	Baseline basin	10,000	0.010	100	2.054
	Larger basin	20,000	0.005	100	1.825
10	**Smaller basin**	5,000	0.020	100	0.235
	Baseline basin	10,000	0.010	100	0.213
	Larger basin	20,000	0.005	100	0.187
100	**Smaller basin**	5,000	0.020	100	0.024
	Baseline basin	10,000	0.010	100	0.021
	Larger basin	20,000	0.005	100	0.019

Figure 4.15 shows the effect of recharge area on simulated water-table rise for the constant-total-recharge circular basin cases.

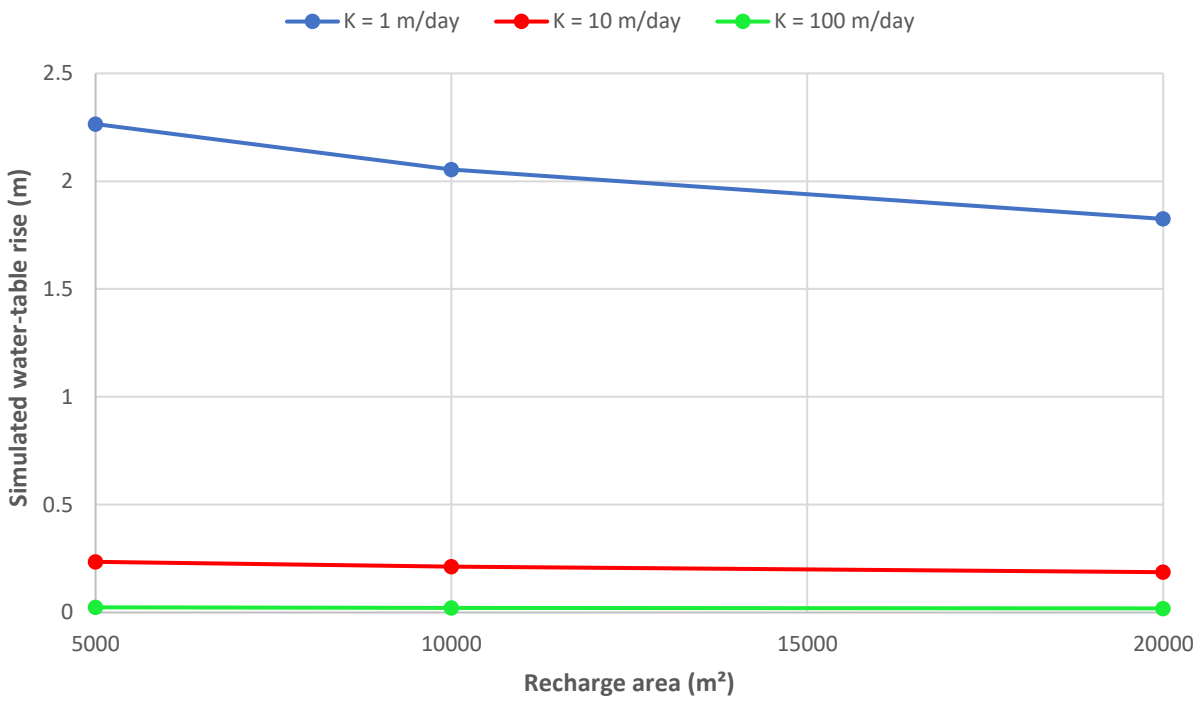

Figure 4.15. Effect of recharge area on simulated water-table rise for the constant-total-recharge circular basin cases. The total recharge input was kept constant at 100 m³/day.

The results show that basin size affected water-table rise while the total recharge rate was kept constant. For all tested hydraulic-conductivity values, the smaller basin produced the highest water-table rise, while the larger basin produced the lowest water-table rise. This means that applying the same recharge volume over a smaller area increased local head buildup, while spreading it over a larger area reduced the water-table rise. However, the effect of basin size became smaller as hydraulic conductivity increased, showing that hydraulic conductivity remained the main control on mound development.

4.3.3 Constant-total-recharge strip cases

The constant-total-recharge strip cases were used to evaluate the effect of recharge distribution independently from the total recharge input. In these cases, the product iW was kept approximately equal to 2 m²/day per unit strip length, while the recharge rate and strip width were varied. This allowed the same recharge input per unit strip length to be distributed over different strip widths. The numerical results are summarized in Table 4.16.

Table 4.16. Numerical results for the constant-total-recharge strip sensitivity cases.

Case	i (m/day)	W (m)	iW (m²/day per unit strip length)	Simulated maximum head (m)	Simulated Water-table rise (m)
Narrow strip – higher intensity	0.0333	60	2	-90.0631	0.93695
Reference strip	0.0200	100	2	-90.0738	0.92617
Wide strip – lower intensity	0.0100	200	2	-90.0977	0.90226

Note: The product iW was kept approximately constant to maintain the same recharge input per unit strip length in the three strip configurations.

Figure 4.16 compares the hydraulic-head profiles along the central cross-section for the constant-total-recharge strip sensitivity cases.

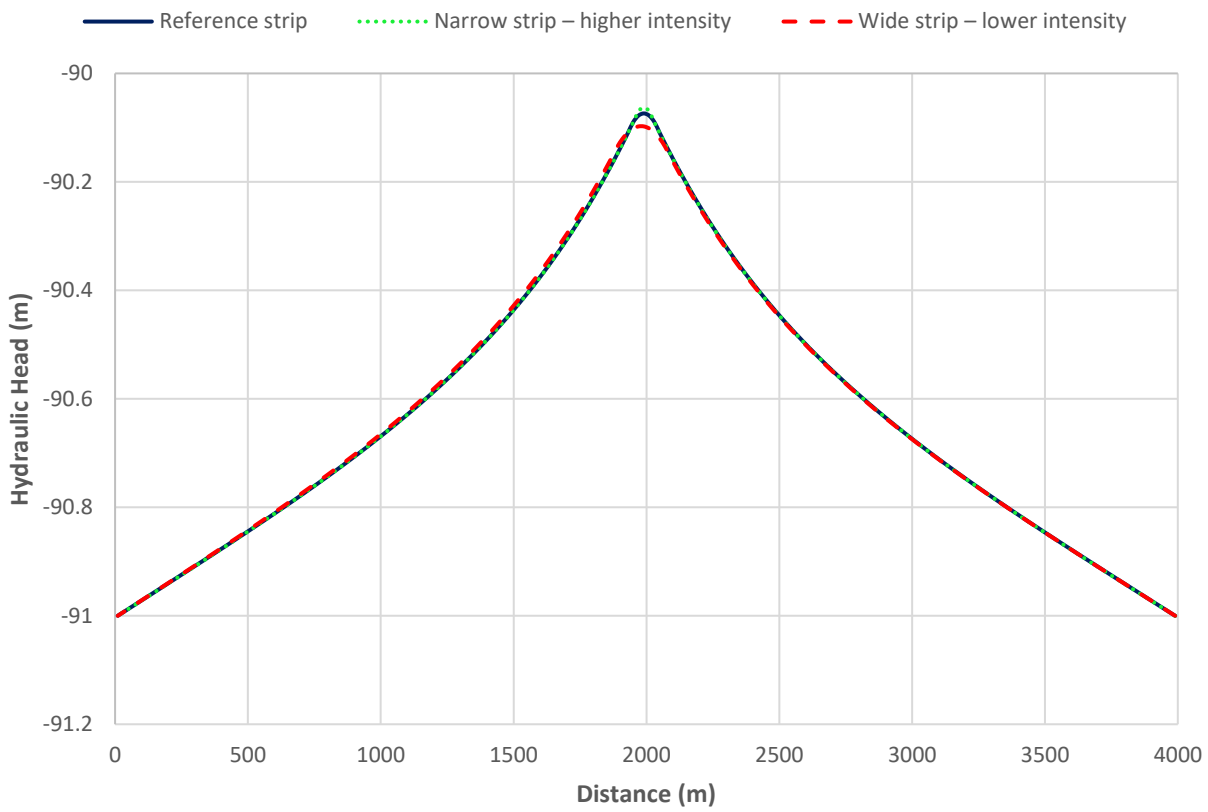

Figure 4.16. Comparison of simulated hydraulic head profiles along the central cross-section for the constant-total-recharge strip sensitivity cases. Reference strip: i = 0.0200 m/day, W = 100 m, L = 1,000 m; narrow strip – higher intensity: i = 0.0333 m/day, W = 60 m, L = 1,000 m; wide strip – lower intensity: i = 0.0100 m/day, W = 200 m, L = 1,000 m. In all cases, iW was kept approximately equal to 2 m²/day per unit strip length.

The comparison shows that the three hydraulic-head profiles were very similar because the recharge input per unit strip length was kept approximately constant. The narrow strip case produced the highest simulated water-table rise, while the wide strip case produced the lowest water-table rise. However, the differences among the three cases were small. This indicates that the total recharge input controlled the overall mound response more strongly than the redistribution of the same recharge over different strip widths under the tested conditions.

4.3.4 Supplementary narrow-trench case

The supplementary narrow-trench case was evaluated to examine the effect of reducing the effective trench width while maintaining approximately the same total applied recharge as the baseline trench configuration. The comparison was performed for selected transmissivity cases representing low, intermediate, and high aquifer conditions. In the supplementary case, the effective trench width was reduced from 20 m to approximately 3.75 m, while the trench length was kept equal to 500 m. The recharge rate was increased to keep the total recharge input approximately constant.

The numerical results for the baseline trench and supplementary narrow-trench cases are summarized in Table 4.17.

Table 4.17. Numerical results of the supplementary narrow-trench case under selected transmissivity case.

K (m/day)	*T* (m²/day)	Baseline water-table rise (m)	Narrow-trench water-table rise (m)	Difference (m)
1	**20**	1.5393	1.4637	-0.0756
10	**200**	0.1578	0.1488	-0.0090
100	**2000**	0.0158	0.0149	-0.0009

Figure 4.17 compares the simulated hydraulic-head profiles for the baseline trench and supplementary narrow-trench cases under the selected transmissivity conditions.

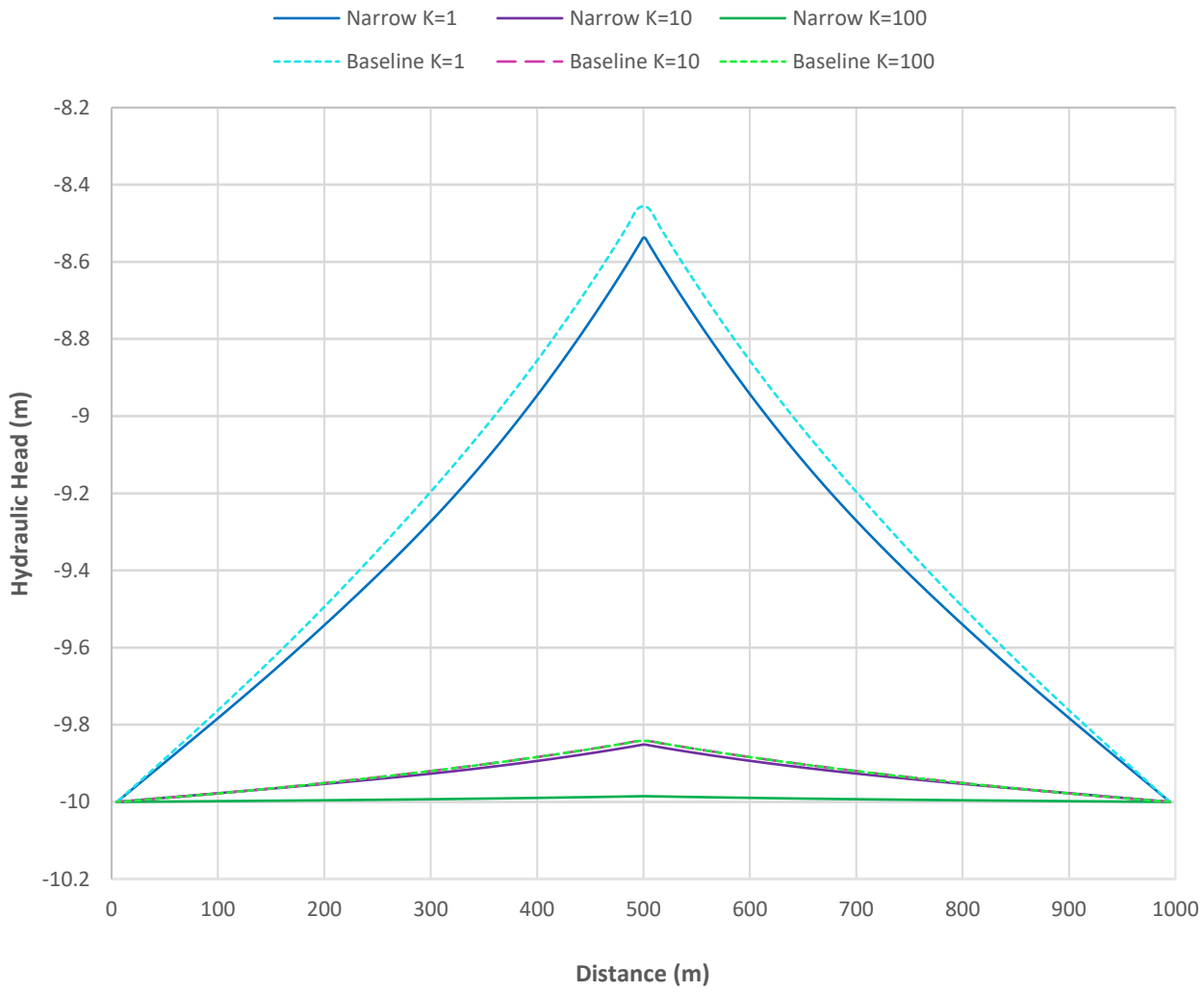

Figure 4.17. Comparison of simulated hydraulic-head profiles along the central cross-section perpendicular to the trench axis for the baseline trench and supplementary narrow-trench cases under selected transmissivity conditions. Baseline trench: $W = 20$ m, $L = 500$ m, $i = 0.01$ m/day, $Q = 100$ m³/day; supplementary narrow trench: effective $W \approx 3.75$ m, $L = 500$ m, $i = 0.0533$ m/day, $Q \approx 100$ m³/day. The comparison includes $K = 1$, 10, and 100 m/day, corresponding to $T = 20$, 200, and 2,000 m²/day. In all cases, the initial groundwater head was -10 m, and the same model domain, aquifer properties, and boundary-condition configuration were used.

The supplementary narrow-trench results show that reducing the effective trench width from 20 m to approximately 3.75 m, while keeping the total recharge input approximately constant, produced only small changes in simulated water-table rise. For all selected hydraulic-conductivity values, the narrow-trench case produced slightly lower water-table rise values than the baseline trench. The largest difference occurred for K = 1 m/day, where water-table rise decreased from 1.5392 m to 1.4637 m. For K = 10 and 100 m/day, the differences were very small.

These results indicate that using a narrower and more trench-like recharge width did not substantially change the overall mound response under the tested conditions. This is consistent with Bouwer et al. (1999), who noted that groundwater mounding can be reduced by using longer and narrower recharge areas. However, in the present simulations, the effect of reducing the recharge-zone width was small compared with the effect of hydraulic conductivity/transmissivity. Overall, water-table rise remained mainly controlled by aquifer hydraulic properties, while recharge-zone width produced only minor secondary changes under the constant-total-recharge condition.

4.3.5 Summary of recharge-distribution effects

The steady-state sensitivity results show that recharge-area distribution affected mound development, especially when the same total recharge was concentrated over a smaller area. In the circular basin cases, the smaller basin produced higher water-table rise, while spreading the same recharge over a larger basin reduced the water-table rise.

For the strip cases, the preliminary modified recharge-rate and modified strip-width cases showed that increasing the total recharge input increased water-table rise. However, when the recharge input per unit strip length was kept approximately constant, the differences between the strip profiles became small. This indicates that total recharge input had a stronger effect than redistributing the same recharge over different strip widths.

The supplementary narrow-trench case also produced only minor changes compared with the baseline trench case when the total recharge input was kept approximately constant. Overall, recharge geometry and recharge-area distribution influenced water-table rise, but aquifer hydraulic properties, especially hydraulic conductivity and transmissivity, remained the dominant controls on mound development.

4.4 Transient MOUNDSOLV results

This section presents the transient MOUNDSOLV results used to evaluate time-dependent groundwater mound development and dissipation. The results focus on recharge duration, hydraulic conductivity, specific yield, diffusivity, recharge-area distribution, monitoring distance, and mound dissipation after recharge stopped.

4.4.1 Effect of recharge duration

The reference MOUNDSOLV scenario was first used to evaluate the effect of simulation duration on transient mound development. The same input parameters were maintained, while the simulation time was increased from 365 days to 3,650 days and 36,500 days. The results are summarized in Table 4.18.

Table 4.18. Comparison of one-year, ten-year, and long-term transient water-table rise for the reference MOUNDSOLV scenario.

Scenario	Purpose	*t* (day)	*K* (m/day)	*Sy* (-)	*L* × *W* (m×m)	*Q* (m^3/day)	*q* (m/day)	Max rise, *s* (m)	*h* at center (m)
MS-1	One-year reference	365	1	0.10	100 × 100	100	0.01	1.960	21.96
MS-1-LT	Ten-year transient response	3650	1	0.10	100 × 100	100	0.01	2.874	22.87
MS-1-ELT	Long-term transient reference	36500	1	0.10	100 × 100	100	0.01	3.79	23.79

The results show that the maximum simulated water-table rise at the recharge-basin center increased from 1.960 m after 365 days to 2.874 m after 3,650 days and 3.790 m after 36,500 days. The corresponding hydraulic head at the basin center increased from 21.96 m to 22.87 m and 23.79 m, respectively.

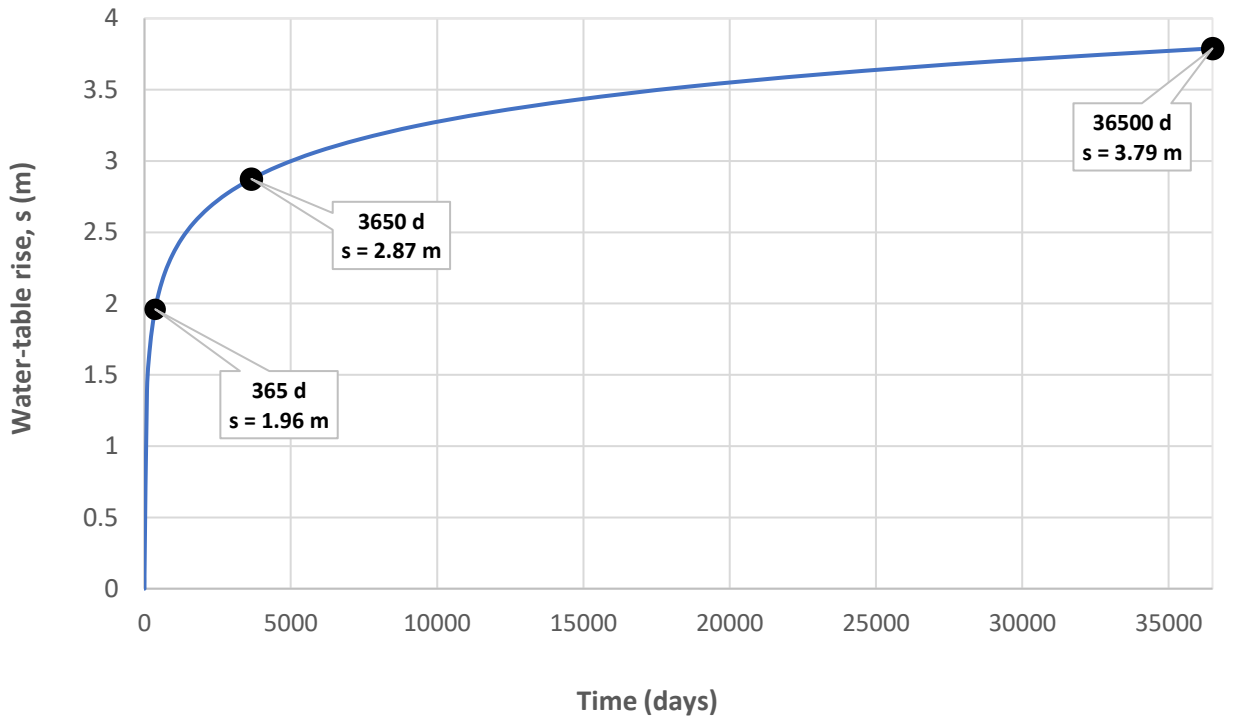

Figure 4.18. Long-term transient development of water-table rise for the reference MOUNDSOLV scenario. The simulated rise increased from 1.96 m at 365 days to 2.87 m at 3650 days and 3.79 m at 36500 days.

The response shows that water-table rise continued to increase with recharge duration, but the rate of increase became slower over time. This indicates that the transient mound gradually approached a long-term response under continuous recharge.

4.4.2 Hydraulic conductivity and specific yield

This scenario group was used to evaluate the influence of hydraulic conductivity and specific yield on transient recharge-induced mounding. The recharge-basin dimensions, total recharge input, recharge rate, initial saturated thickness, and simulation duration were kept constant, while

hydraulic conductivity and specific yield were varied. This allowed the influence of aquifer transmissivity and storage on transient mound development to be examined under the same recharge conditions. The results are summarized in Table 4.19.

Table 4.19. Summary of transient MOUNDSOLV results for hydraulic-conductivity and specific-yield scenarios.

Scenario	*K* (m/day)	*Sy* (-)	*T* (m²/day)	*t* (day)	Max rise, *s* (m)	*h* at center (m)
MS-1	1	0.10	20	365	1.960	21.96
MS-2	1	0.25	20	365	1.598	21.60
MS-3	100	0.10	2000	365	0.0379	20.04
MS-4	100	0.25	2000	365	0.03425	20.03

Note: All scenarios used a square recharge basin of 100 m × 100 m, $Q = 100$ m³/day, q = 0.010 m/day, and $h_0 = 20$ m. Transmissivity was calculated as $T=K\times h_0$, with h_0=20 m. The reported water-table rise corresponds to the recharge-basin center after 365 days.

The corresponding time-series responses are shown in Figure 4.19.

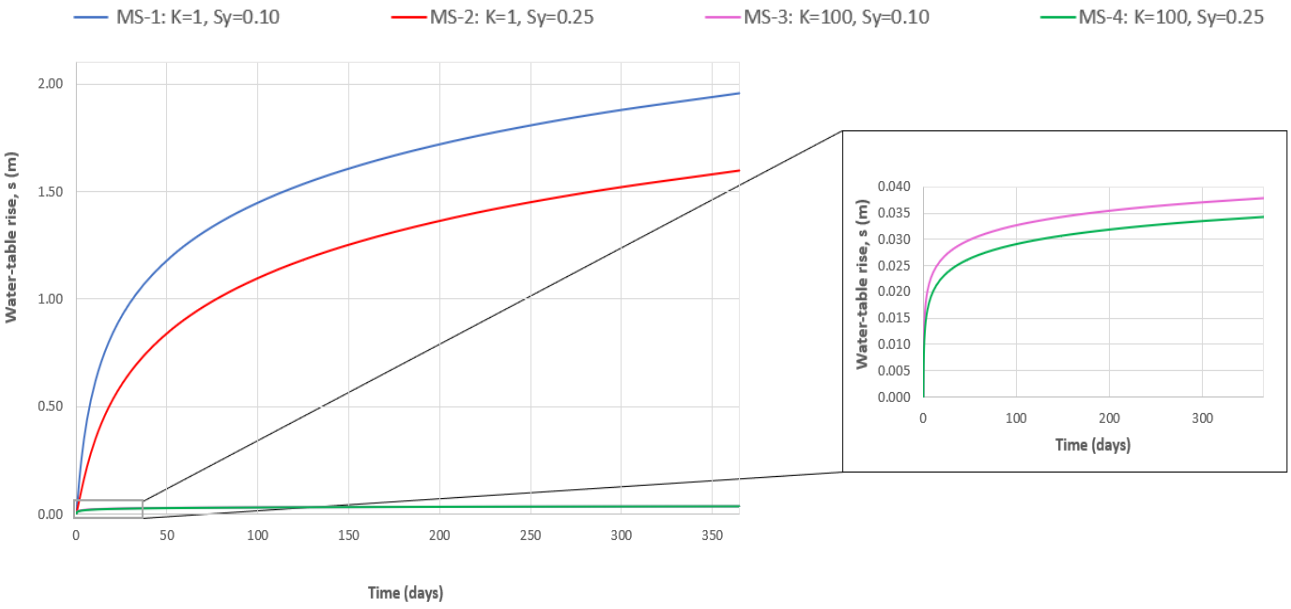

Figure 4.19. Transient water-table rise for hydraulic-conductivity and specific-yield scenarios. The inset highlights the low-magnitude responses for the high-conductivity scenarios MS-3 and MS-4.

The results show that both hydraulic conductivity and specific yield influenced the transient mound response, but their effects were different. Under the low-conductivity condition, increasing specific yield reduced the maximum simulated water-table rise from 1.960 m to 1.598 m after 365 days. This indicates that a higher specific yield increased the aquifer storage capacity, so a larger portion of the incoming recharge was stored within the aquifer and produced a smaller rise in the water table.

The effect of hydraulic conductivity was stronger. Increasing hydraulic conductivity from 1 m/day to 100 m/day reduced the maximum simulated water-table rise from 1.960 m to 0.0379 m for the same specific yield. This shows that transmissivity was the dominant control on the magnitude of

groundwater mounding in this comparison, while specific yield mainly affected the transient rate of mound development.

4.4.3 Constant-diffusivity comparison

A constant-diffusivity comparison was performed to further examine the combined role of transmissivity and specific yield on transient mound development. In these scenarios, hydraulic conductivity and specific yield were changed together so that the diffusivity ratio, $D = T/Sy$, remained constant. The recharge-basin dimensions, total recharge input, recharge rate, initial saturated thickness, and simulation duration were kept unchanged. The results are summarized in Table 4.20.

Table 4.20. Constant-diffusivity MOUNDSOLV scenarios with ($D = T/Sy$) maintained at 200 m²/day.

Scenario	K (m/day)	Sy (-)	T (m²/day)	$D = T/Sy$ (m²/day)	s at 365 d (m)	h at center (m)
MS-1	1	0.10	20	200	1.9600	21.96
MS-CD2	2	0.20	40	200	0.9798	20.98
MS-CD3	2.5	0.25	50	200	0.7838	20.78

Note: All scenarios used the same recharge basin of 100 m × 100 m, $Q = 100$ m³/day, $q = 0.010$ m/day, and $h_o = 20$ m. The diffusivity ratio ($D = T/S_y$) was kept constant at 200 m²/day.

The corresponding transient time-series responses are shown in Figure 4.20.

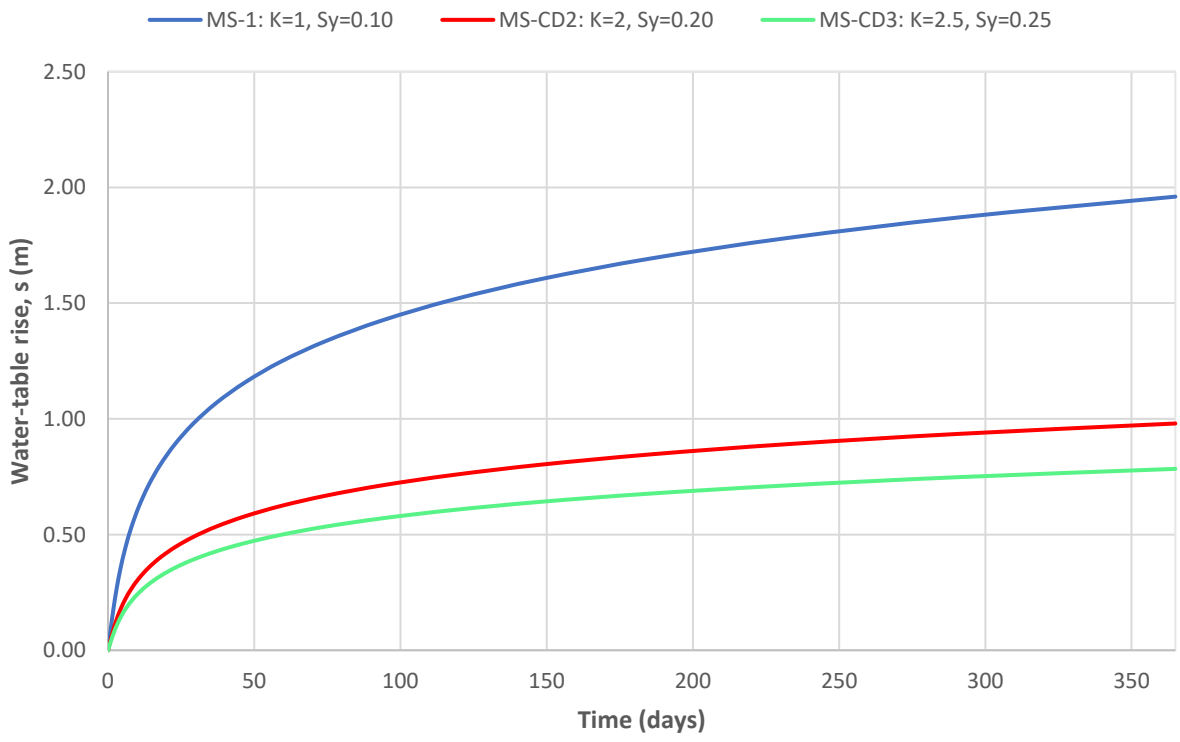

Figure 4.20. Transient water-table rise for constant-diffusivity MOUNDSOLV scenarios. The diffusivity ratio was kept constant at 200 m²/day, while hydraulic conductivity and specific yield were varied simultaneously.

The results show that keeping the diffusivity ratio constant reduced the contrast between the simulated responses compared with the original hydraulic-conductivity comparison. However, the curves did not collapse into a single response. The maximum simulated water-table rise still decreased from 1.960 m in the reference case to 0.9798 m and 0.7838 m in the constant-diffusivity cases.

This indicates that diffusivity was an important control on transient mound development, but it did not fully explain the simulated water-table rise by itself. The individual values of transmissivity and specific yield, together with the recharge-basin configuration, also influenced the transient response.

4.4.4 Recharge-area distribution

This scenario group was used to evaluate the effect of recharge-area distribution under a constant total recharge input. Three scenarios were compared: a larger recharge area with lower recharge intensity, the reference recharge area, and a smaller recharge area with higher recharge intensity. In all three cases, the total recharge input was kept constant at 100 m³/day, while recharge area and recharge intensity were varied. The input parameters and simulated results are summarized in Table 4.21.

Table 4.21. Effect of recharge-area size and infiltration intensity under constant total recharge rate.

Scenario	Purpose	$L \times W$ (m× m)	Area (m²)	Q (m³/day)	q (m/day)	K (m/day)	Sy (-)	t (day)	Max rise, s (m)	h at center (m)
MS-5	Large area, low intensity	200 × 100	20,000	100	0.005	1	0.10	365	1.634	21.63
MS-1	Reference area	100 × 100	10,000	100	0.010	1	0.10	365	1.960	21.96
MS-6	Small area, high intensity	100 × 50	5,000	100	0.020	1	0.10	365	2.182	22.18

The corresponding transient time-series responses at the recharge-basin center are shown in Figure 4.21.

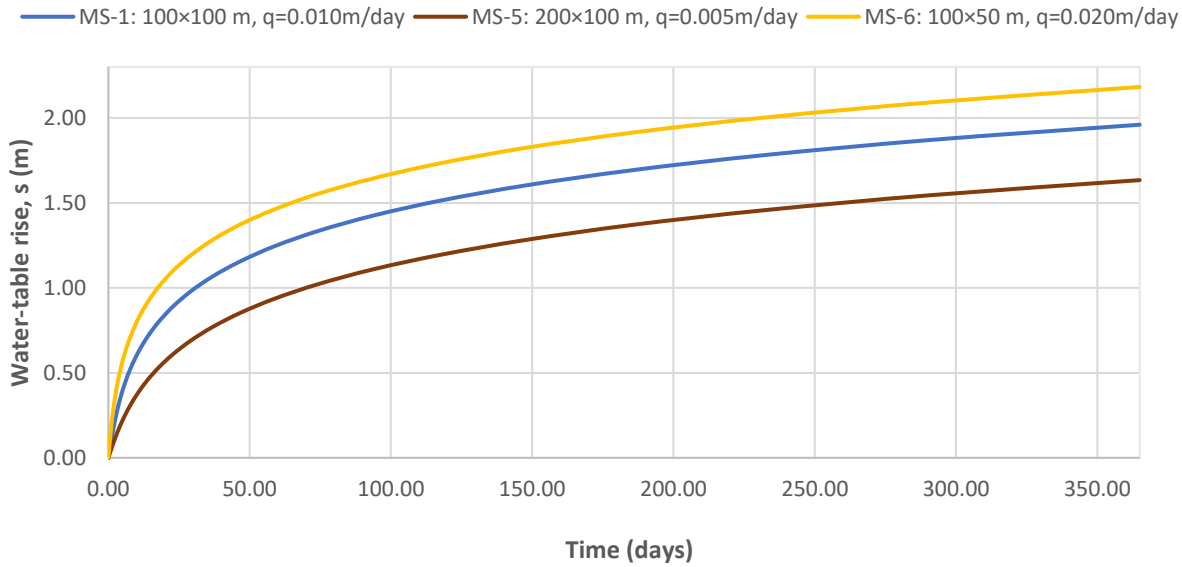

Figure 4.21. Transient water-table rise at the recharge-basin center for the constant-total-recharge scenarios.

Reducing the recharge area led to a more concentrated mound, with a higher peak below the basin center. After 365 days, the maximum simulated water-table rise was 1.634 m for the larger-area scenario, 1.960 m for the reference scenario, and 2.182 m for the smaller-area scenario. This indicates that concentrating the same total recharge over a smaller area produced a higher local mound, while distributing recharge over a larger area reduced the peak water-table rise.

To compare the spatial response more clearly, water-table-rise profiles were extracted along the centerline of the recharge basin after 365 days.

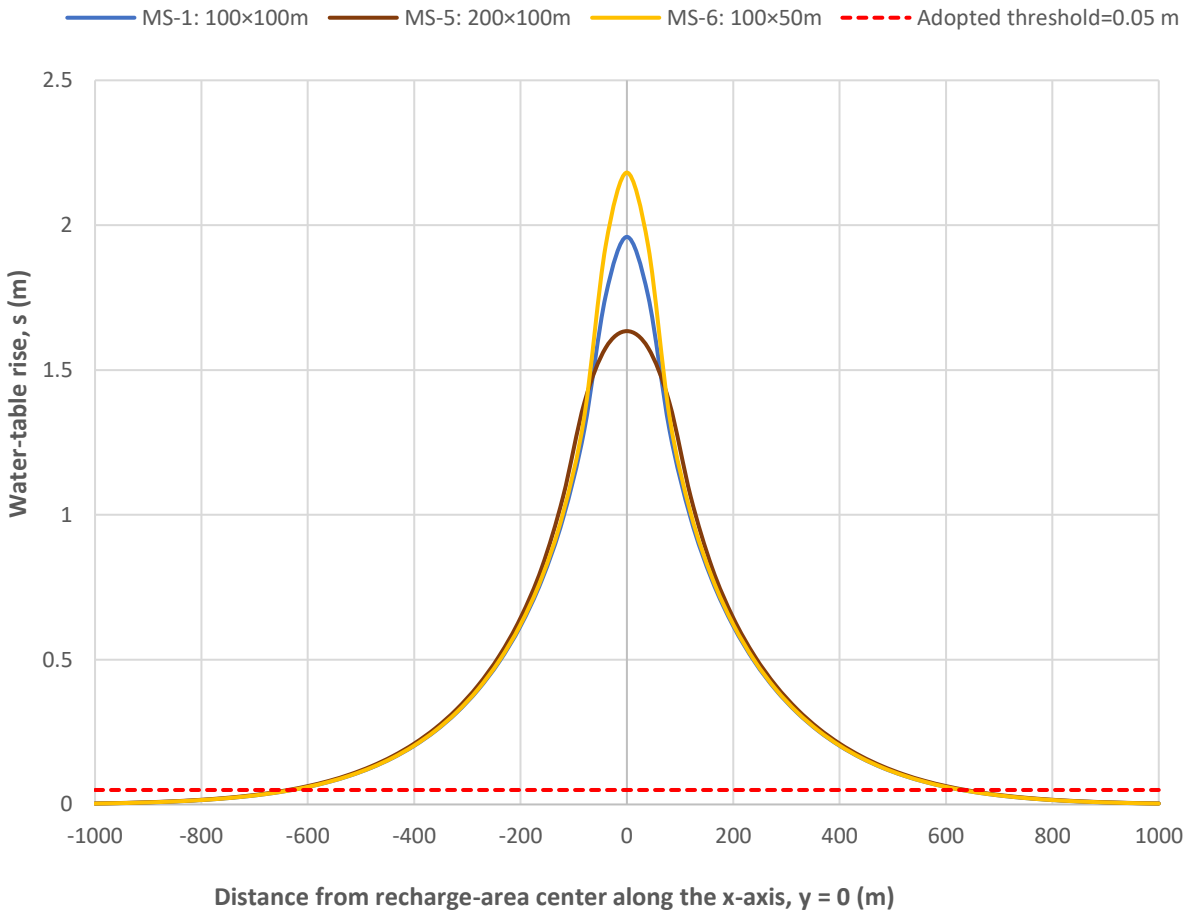

Figure 4.22. Water-table rise profiles along the x-axis at (y=0) after 365 days for the constant-total-recharge scenarios MS-1, MS-5, and MS-6. The dashed horizontal line indicates the adopted practical threshold of 0.05 m, and the recharge areas are centered at (x=0).

The profile comparison shows that the smaller recharge area produced the highest and most concentrated mound, while the larger recharge area produced a lower but more laterally distributed mound. Overall, the results indicate that recharge-area size and distribution influenced both the magnitude and the spatial form of transient groundwater mounding.

4.4.5 Distance-dependent response and dissipation

Distance-dependent mound response

To evaluate how the mound response changed away from the recharge basin, additional monitoring points were added to the reference scenario. These points were located at the basin center and at distances of 40 m, 90 m, and 200 m from the recharge-basin edge.

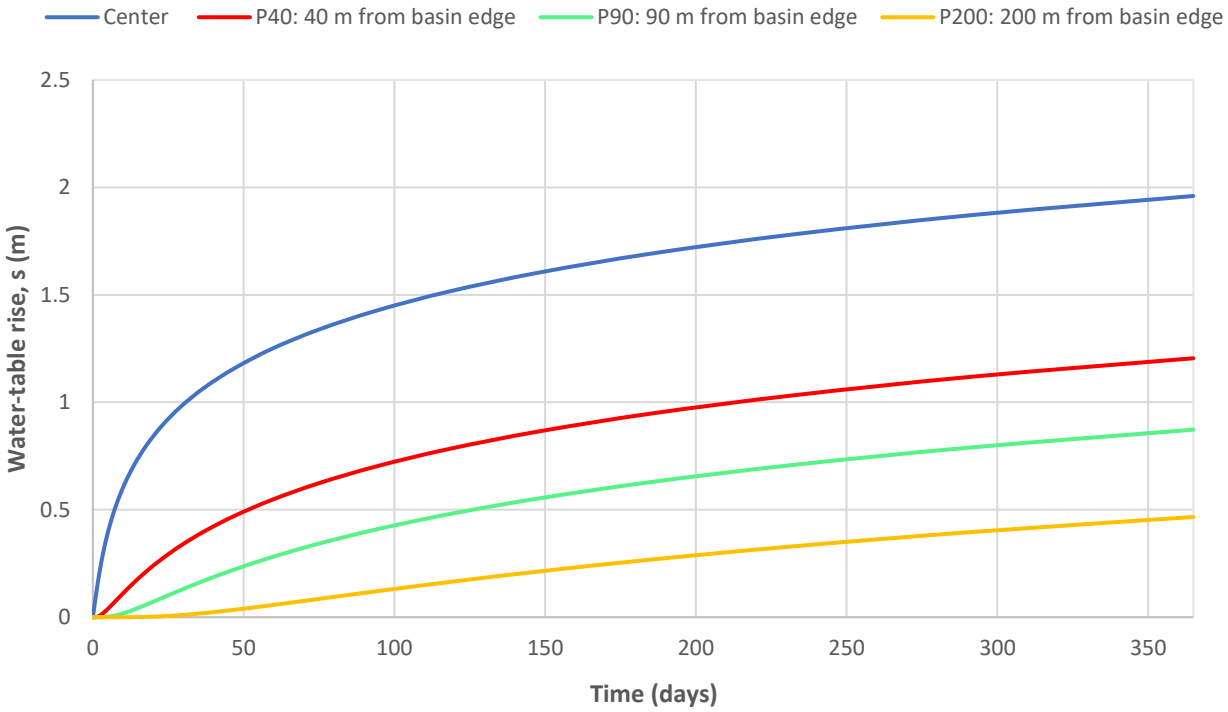

Figure 4.23. Transient water-table rise at different monitoring distances from the recharge-basin edge for the reference scenario.

The results show that water-table rise decreased with increasing distance from the recharge basin. The highest response occurred at the basin center, while the water-table rise became smaller and developed more gradually at larger distances. This indicates that the effect of recharge-induced mounding was spatially attenuated away from the recharge area. The simulated water-table rise values after 365 days are summarized in Table 4.22.

Table 4.22. Simulated water-table rise at different monitoring distances after 365 days for the reference scenario.

Monitoring point	Location	s at 365 days (m)
Center	x = 0 m, y = 0 m	1.960
P40	40 m from basin edge	1.206
P90	90 m from basin edge	0.676
P200	200 m from basin edge	0.466

Dissipation after stopping recharge

To evaluate mound dissipation after recharge stopped, the reference MOUNDSOLV scenario was simulated with recharge active during the first 365 days and then stopped. The response was evaluated at the recharge-basin center and at the three monitoring points located 40 m, 90 m, and 200 m from the recharge-basin edge. These monitoring points were used to assess how long the recharge-induced mound remained above a practical threshold after recharge stopped.

A preliminary threshold of 0.05 m was first considered to represent a very small residual water-table rise. However, the extended recovery simulation showed that a small residual mound remained at the end of the 36,500-day simulation, with late-time residual values of about 0.09 m. Therefore, the mound did not fall below the 0.05 m threshold within the simulated period. For this reason, an adopted practical threshold of 0.10 m was used for the final dissipation assessment. This threshold was selected because it was slightly higher than the late-time residual water-table rise and provided a practical basis for comparing dissipation times at different monitoring locations. Preliminary recovery simulations were first performed over 1095 days and then extended to 3650 days to evaluate whether the mound approached the adopted dissipation threshold. These supplementary recovery simulations are shown in Appendix C, Figure C.1 and Figure C.2.

The dissipation curves are shown in Figure 4.24. For clarity, only the first 5,000 days of the recovery period are shown. The dashed horizontal line represents the adopted practical dissipation threshold of 0.10 m.

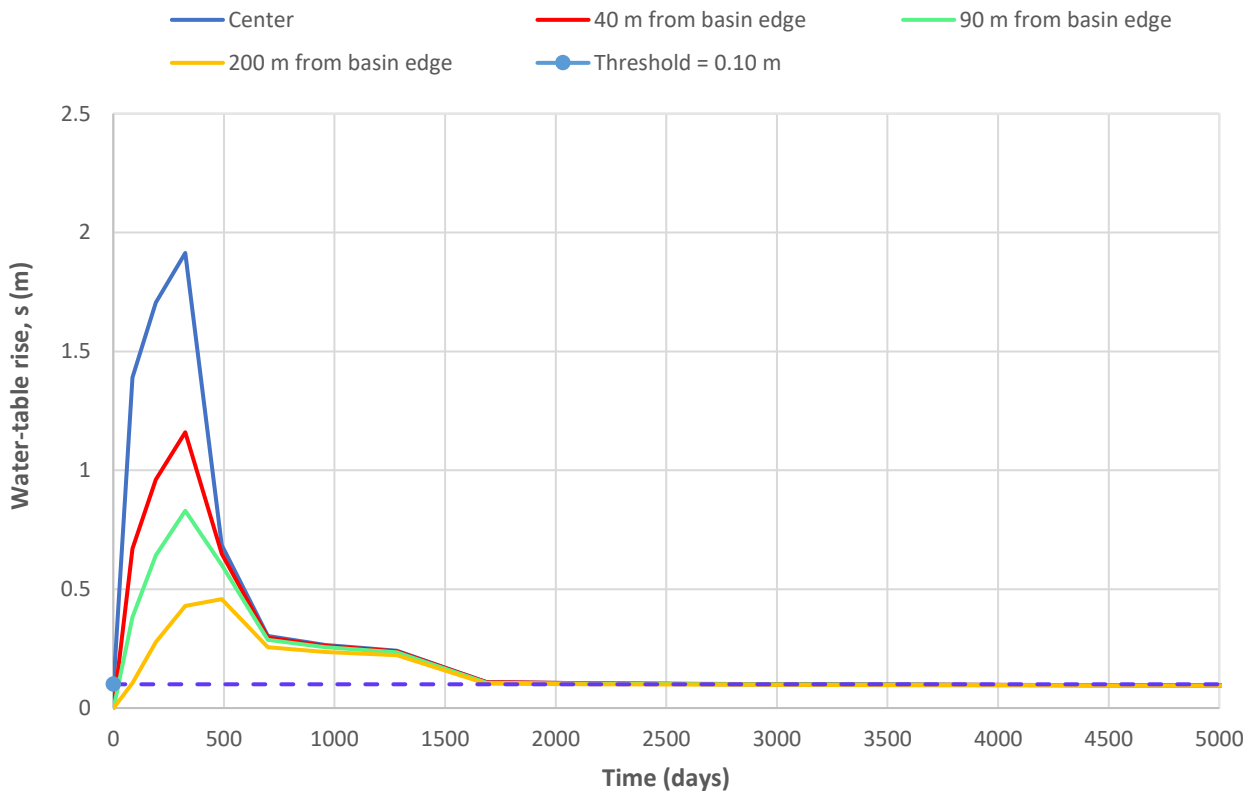

Figure 4.24. Mound dissipation after recharge stopped at 365 days for different monitoring distances from the recharge-basin edge. The dashed horizontal line represents the adopted practical dissipation threshold of 0.10 m.

The dissipation times estimated using the adopted 0.10 m threshold are summarized in Table 4.23.

Table 4.23. Dissipation time after recharge stopped based on the adopted 0.10 m threshold.

Monitoring point	Maximum rise at 365 d (m)	Late-time residual at 36500 d (m)	Time below 0.10 m (d)	Dissipation time after stop (d)
Center	1.960	0.090	3617	3252
40 m from basin edge	1.206	0.089	2826	2461
90 m from basin edge	0.676	0.090	2826	2461
200 m from basin edge	0.466	0.090	2193	1828

The results show that mound dissipation was slowest at the recharge-basin center, where the adopted threshold was reached 3,252 days after recharge stopped. At 40 m and 90 m from the basin edge, the threshold was reached after 2,461 days. The 200 m monitoring point reached the threshold earlier, after 1,828 days, because the simulated water-table rise at this distance was smaller. Overall, these results show that recharge-induced mounding can persist for several years after recharge stops, particularly near the recharge area. The dissipation response also shows that distance from the recharge basin affects both the magnitude and the time required for the mound to become practically negligible.

4.5 MOUNDSOLV–Visual MODFLOW comparison

The reference MOUNDSOLV scenario was compared with a corresponding transient Visual MODFLOW simulation to provide an additional consistency check for the transient assessment. The comparison was performed after 365 days of recharge and focused on the maximum water-table rise beneath the recharge area and the water-table-rise profile along the central cross-section of the recharge basin.

The maximum water-table rise values predicted by MOUNDSOLV and transient Visual MODFLOW are compared in Table 4.24.

Table 4.24. Comparison of maximum water-table rise predicted by MOUNDSOLV and transient Visual MODFLOW after 365 days for the reference recharge case.

Model	Maximum water-table rise after 365 days (m)	Difference relative to MOUNDSOLV (m)	Relative difference (%)
MOUNDSOLV MS-1	1.960	—	—
Transient Visual MODFLOW	1.862	-0.098	-5.0

MOUNDSOLV predicted a maximum water-table rise of 1.960 m after 365 days, while the transient Visual MODFLOW simulation produced a maximum water-table rise of 1.862 m. The difference between the two results was −0.098 m, corresponding to a relative difference of approximately −5.0% with respect to the MOUNDSOLV value. This indicates that the MODFLOW result was slightly lower than the MOUNDSOLV estimate, but the difference remained small.

The corresponding water-table-rise profiles along the central cross-section are shown in Figure 4.25.

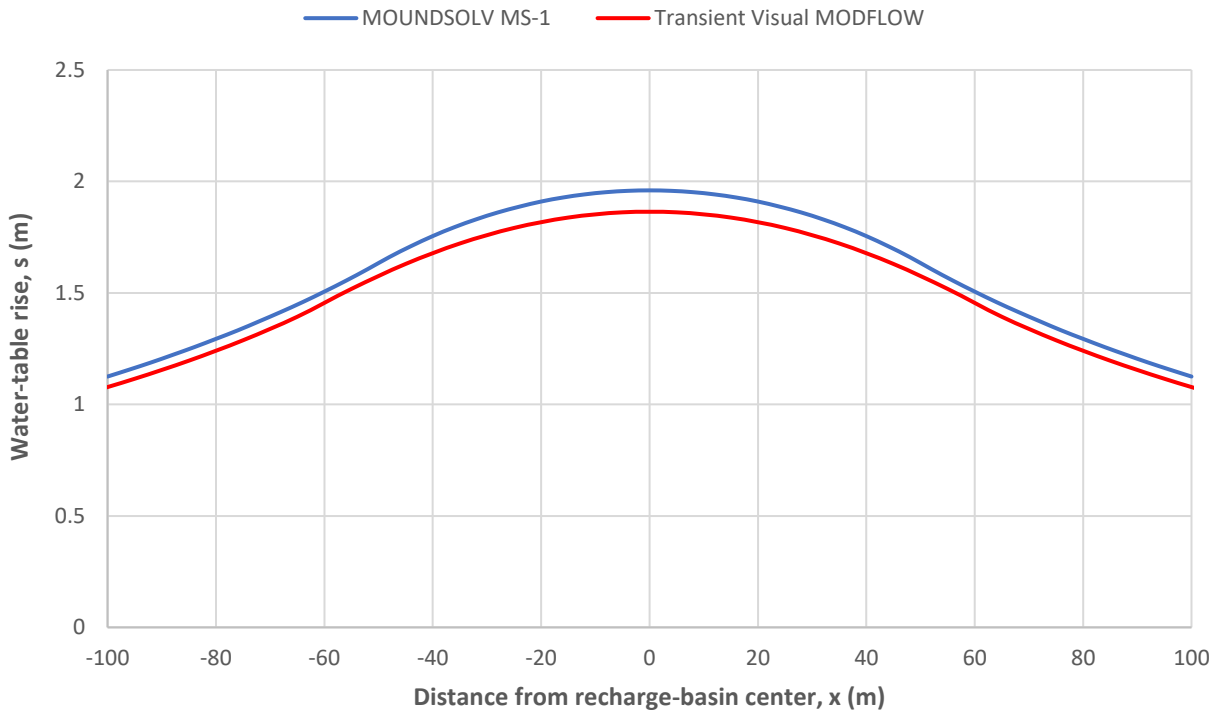

Figure 4.25. Comparison of MOUNDSOLV and transient Visual MODFLOW water-table rise profiles after 365 days for the reference recharge case.

The profile comparison shows that the transient Visual MODFLOW simulation reproduced the general mound shape obtained from MOUNDSOLV. Both approaches produced the maximum water-table rise beneath the recharge area and a gradual decrease away from the recharge-basin center. The Visual MODFLOW profile was slightly lower than the MOUNDSOLV profile over most of the central section, which is consistent with the maximum water-table rise comparison.

The small discrepancy between the two approaches is likely related to differences in model formulation and implementation. MOUNDSOLV uses a simplified analytical transient mounding formulation, while Visual MODFLOW represents the recharge area using a finite-difference grid, model boundaries, and numerical discretization. Therefore, the difference should not be interpreted as a model error, but as the expected effect of comparing two modeling approaches with different assumptions and numerical representations.

As an additional comparison, the transient Visual MODFLOW response was evaluated at the recharge-basin center and at monitoring points located approximately 40, 90, and 200 m from the basin edge. Recharge was applied during the first 365 days and was then stopped. The calculated hydraulic heads were converted to water-table rise relative to the initial groundwater head of −10 m.

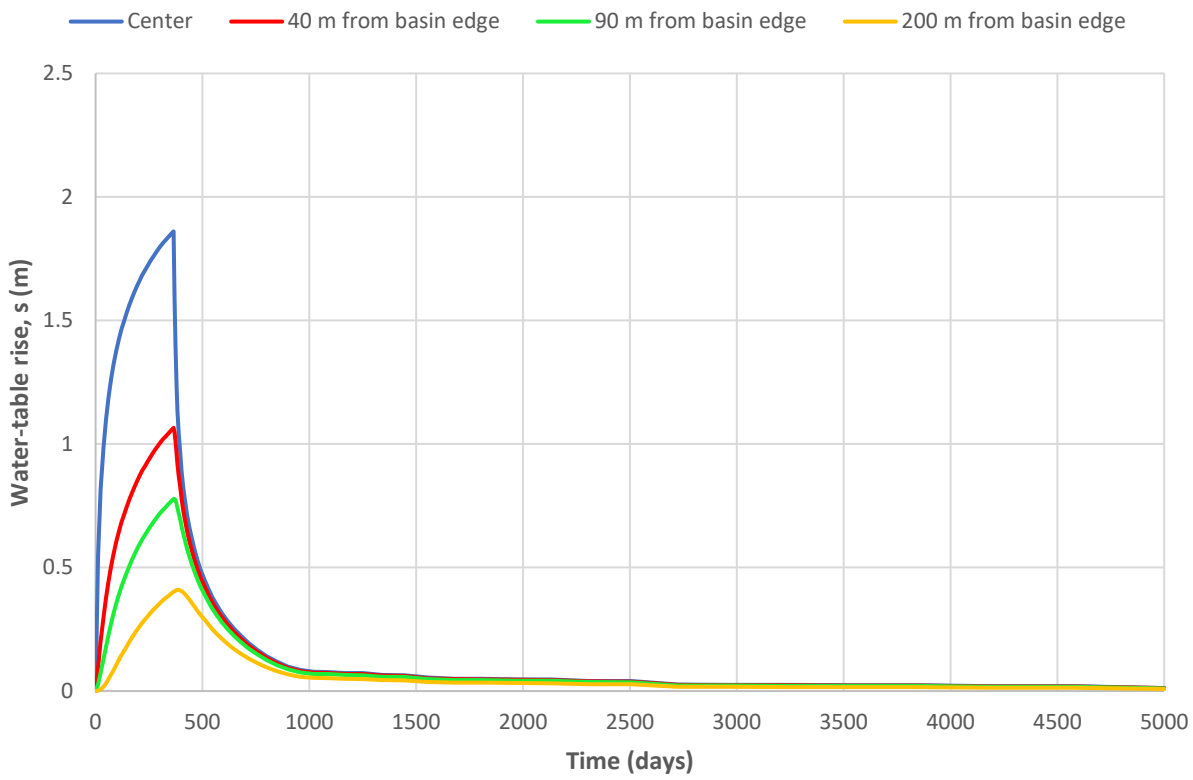

Figure 4.26. Transient Visual MODFLOW water-table rise at the recharge-basin center and at monitoring points located approximately 40, 90, and 200 m from the basin edge. Recharge was applied during the first 365 days and then stopped.

The Visual MODFLOW results show that the water-table rise was highest at the recharge-basin center and decreased with increasing distance from the recharge area. After recharge stopped at day 365, the water-table rise declined at all monitoring locations. The response was larger and faster near the basin, while the more distant monitoring points showed smaller and more gradual changes. This general distance-dependent response was consistent with the pattern obtained from MOUNDSOLV in Figure 4.24.

Overall, the spatial profiles and monitoring-point responses showed similar general patterns in MOUNDSOLV and transient Visual MODFLOW for the reference recharge case. This supports the use of MOUNDSOLV as a practical preliminary tool for evaluating transient groundwater mound development, while Visual MODFLOW provides a more flexible numerical framework when a more detailed representation of the domain, boundary conditions, or recharge geometry is required.

4.6 Main findings of chapter 4

The results show that transmissivity was the main control on groundwater mound development in both the steady-state and transient assessments. Water-table rise decreased as transmissivity increased because higher-transmissivity aquifers allowed recharge-induced head buildup to dissipate more effectively.

Recharge geometry and recharge-area distribution also influenced water-table rise. Under the same total recharge input, the trench configuration produced lower water-table rise than the circular basin, while concentrating recharge over smaller areas produced higher local water-table rise.

The transient MOUNDSOLV results showed that water-table rise increased with recharge duration and could persist after recharge stopped. Overall, the results confirm that analytical calculations, steady-state numerical simulations, and selected transient assessment can be used together as a preliminary framework for comparing infiltration-based MAR configurations.

5. Conclusion

This thesis examined infiltration-based Managed Aquifer Recharge (MAR) as a preliminary water management option for climate-resilient agriculture. In agricultural systems, seasonal water availability, groundwater storage capacity, groundwater depth, and the risk of excessive water-table rise are important factors that need to be considered before recharge systems are implemented. For this reason, the main focus of this study was groundwater mounding beneath two simplified recharge configurations: a circular basin and a trench/strip recharge system.

The main aim of the study was to develop a preliminary sensitivity-based framework for comparing different MAR alternatives. This framework was not intended to provide a final design for a real site. Instead, it was used to improve the initial understanding of how an aquifer may respond to artificial recharge. The study examined how recharge geometry, recharge rate, aquifer transmissivity, hydraulic conductivity, specific yield, recharge duration, and distance from the recharge area affect the magnitude, spatial distribution, and persistence of groundwater mounding.

The assessment used both analytical and numerical methods under steady-state and transient conditions. Steady-state analytical calculations were used for preliminary mound estimates, while MOUNDSOLV was used for the transient analytical assessment. Visual MODFLOW Classic was used for both steady-state simulations and one representative transient simulation. Together, these methods were used to evaluate mound magnitude, spatial distribution, growth, and dissipation.

The analyses confirmed that groundwater mounding is one of the main hydraulic constraints in infiltration-based MAR systems. In both the circular basin and trench configurations, water-table rise decreased as aquifer transmissivity increased. This is because, in low-transmissivity aquifers, the added recharge water spreads less easily through the aquifer and produces a larger increase in hydraulic head beneath the recharge area. In contrast, in higher-transmissivity aquifers, the recharge water can spread more effectively, which reduces the maximum water-table rise. Therefore, the hydraulic properties of the aquifer, especially transmissivity, were found to be the main control on mound development.

Recharge geometry also had an important effect on the magnitude and concentration of groundwater mounding. Under the same total recharge input, the trench configuration produced lower water-table rise than the circular basin. This happened because, in the trench configuration, the recharge was distributed over a longer and narrower area, while in the circular basin the recharge was more locally concentrated. Therefore, elongated recharge configurations can help reduce local groundwater mounding in some conditions. However, the effect of geometry became smaller in aquifers with higher transmissivity, showing again that aquifer properties were more dominant than the shape of the recharge area.

The comparison between analytical and numerical results showed that both methods produced similar general trends, but the calculated values were not always identical. For the circular basin case, the main difference was related to the analytical assumption of constant transmissivity. In the unconfined MODFLOW model, saturated thickness, and therefore effective transmissivity, can change as the water table rises. For the strip/trench case, the differences were mainly related to the fact that the analytical solution assumes an idealized long strip, while the numerical model represents a finite and discretized recharge area within a limited model domain. Therefore, the differences between the methods were mainly caused by modeling assumptions, not simply by numerical error.

The sensitivity analysis showed that recharge loading and recharge-area distribution should be interpreted separately. When the recharge rate or recharge width was increased without keeping the total recharge input constant, water-table rise increased noticeably. Among these cases, increasing the recharge rate produced the strongest response, showing that recharge intensity can have a strong effect on mound development. However, when the total recharge input was kept approximately constant and only the distribution of recharge was changed, the differences were smaller. In the basin cases, concentrating the same total recharge over a smaller area increased local water-table rise, while spreading it over a larger area reduced water-table rise. In the strip cases, when the recharge input per unit strip length was kept approximately constant, the hydraulic-head profiles were very similar.

The supplementary narrow-trench case also showed that reducing the effective trench width caused only limited changes in water-table rise when the total recharge input was kept approximately constant. This suggests that, under the tested conditions, making the recharge area narrower by itself did not strongly change the overall aquifer response. Its effect was smaller than the effect of hydraulic conductivity and transmissivity.

In the transient assessment, the MOUNDSOLV results showed that groundwater mounding depends not only on recharge amount and aquifer properties, but also on time. As recharge duration increased, water-table rise also increased, although the rate of increase became slower over time. Hydraulic conductivity had a strong effect on the transient response. Higher hydraulic conductivity greatly reduced the simulated water-table rise. Specific yield also affected mound development by controlling aquifer storage, but its effect was smaller than the effect of hydraulic conductivity in the tested cases.

The constant-diffusivity comparison showed that diffusivity is an important factor in transient mound behavior, but it cannot fully explain all differences by itself. Even when the diffusivity ratio was kept constant, the responses were not the same. This means that transmissivity, specific yield, and recharge-area geometry all contributed to the transient mound response.

The transient recharge-area distribution cases showed that concentrating the same total recharge over a smaller area produced a higher and more concentrated mound. In contrast, spreading the same recharge over a larger area produced a lower but wider mound. The monitoring-point results also showed that the aquifer response decreased with distance from the recharge area. The highest water-table rise occurred at the center of the basin, while points farther away showed smaller and slower responses.

One important part of the study was the assessment of mound dissipation after recharge stopped. The dissipation analysis indicated that the effect of recharge can remain in the aquifer for several years after recharge ends, especially near the recharge area and under low-conductivity conditions. Using the adopted practical threshold of 0.10 m, the mound at the basin center required several years to become practically negligible after recharge stopped. Therefore, MAR assessment should not only consider the maximum water-table rise during recharge, but also how long the hydraulic effect remains after recharge has ended.

The comparison between transient MOUNDSOLV and Visual MODFLOW for a representative basin case showed good agreement. MOUNDSOLV predicted a maximum water-table rise of 1.960 m, while Visual MODFLOW produced 1.862 m. The difference was about 5%, and the mound profiles from the two models were also similar. This result shows that MOUNDSOLV can be used as a suitable tool for quick preliminary transient mound assessment, while Visual MODFLOW is

more useful for more detailed analyses, especially when more complex boundary conditions or more realistic recharge geometries need to be represented. Overall, the combined modeling framework helped identify the main controls on groundwater mounding and compare alternative recharge configurations for preliminary MAR assessment.

However, the results of this thesis should be interpreted as preliminary guidance, not as final design values. The analytical solutions also rely on simplified representations of recharge geometry, aquifer properties, and hydraulic boundaries, and their assumptions should therefore be considered when interpreting the results**.** The scenarios were synthetic and were not calibrated using field data. The aquifer was assumed to be homogeneous and isotropic, and spatial variations in hydraulic conductivity, storage, aquifer thickness, and boundary conditions were not fully represented. In addition, the study mainly focused on the saturated-zone hydraulic response. Processes such as unsaturated-zone flow, soil infiltration variability, clogging, water quality, salinity, pumping, recovery efficiency, and operational management were not examined in detail.

For future work, this framework should be applied to a real or representative agricultural site using field data. Information such as aquifer thickness, hydraulic conductivity, storage properties, initial groundwater depth, natural gradient, and boundary conditions would improve the reliability of the models. Future studies should also include unsaturated-zone processes, soil infiltration capacity, clogging, water quality, and pumping or recovery scenarios. Combining hydraulic modeling with practical design criteria, such as acceptable groundwater-depth limits, agricultural water demand, land availability, operation schedules, monitoring requirements, and economic feasibility, would help move from preliminary assessment toward a more practical and site-specific MAR design.

In conclusion, this thesis showed that groundwater mounding is a key factor in the assessment of infiltration-based MAR systems and should be carefully evaluated before final design. The results confirmed that aquifer transmissivity is the main control on water-table rise, but recharge geometry, recharge intensity, recharge-area distribution, storage properties, and recharge duration also affect the aquifer response. The proposed framework does not replace detailed field investigation, but it can support preliminary screening, help identify important assumptions, and guide the collection of data needed for MAR planning in climate-resilient agricultural water management.

References

Alkhatib, J., Engelhardt, I., & Sauter, M. (2021). Identification of suitable sites for managed aquifer recharge under semi-arid conditions employing a combination of numerical and analytical techniques. *Environmental Earth Sciences*, *80*(17), 554. https://doi.org/10.1007/s12665-021-09797-y

Alley, W., Dillon, P., & Zheng, Y. (2022). Basic concepts of managed aquifer recharge. In *Managed Aquifer Recharge: Overview and Governance* (pp. 1–12). International Association of Hydrogeologists. https://recharge.iah.org/

Barnett, B., Townley, L. R., Post, V., Evans, R. E., Hunt, R. J., Peeters, L., Richardson, S., Werner, A. D., Knapton, A., & Boronkay, A. (2012). *Australian groundwater modelling guidelines* (Waterlines Report Series No. 82). National Water Commission.

Bouwer, H. (2002). Artificial recharge of groundwater: Hydrogeology and engineering. *Hydrogeology Journal*, *10*(1), 121–142. https://doi.org/10.1007/s10040-001-0182-4

Bouwer, H., Back, J. T., & Oliver, J. M. (1999). Predicting infiltration and ground-water mounds for artificial recharge. *Journal of Hydrologic Engineering*, *4*(4), 350–357. https://doi.org/10.1061/(ASCE)1084-0699(1999)4:4(350)

Caretta, M. A., Mukherji, A., Arfanuzzaman, M., Betts, R. A., Gelfan, A., Hirabayashi, Y., Lissner, T. K., Liu, J., Lopez Gunn, E., Morgan, R., Mwanga, S., & Supratid, S. (2022). Water. In *Climate Change 2022: Impacts, Adaptation and Vulnerability*. Cambridge University Press. https://doi.org/10.1017/9781009325844.006

Dillon, P., Pavelic, P., Page, D., Beringen, H., & Ward, J. (2009). *Managed aquifer recharge: An Introduction* (Waterlines Report Series No. 13). National Water Commission. https://recharge.iah.org/files/2016/11/MAR_Intro-Waterlines-2009.pdf

FAO. (2020). *The State of Food and Agriculture 2020: Overcoming water challenges in agriculture* (The State of Food and Agriculture). Food and Agriculture Organization of the United Nations. https://doi.org/10.4060/cb1447en

FAO & UN-Water. (2024). *Progress on the level of water stress: Mid-term status of SDG Indicator 6.4.2 and acceleration needs, with special focus on food security* [SDG 6 Progress Report]. FAO. https://doi.org/10.4060/cd2179en

Hantush, M. S. (1967). Growth and decay of groundwater-mounds in response to uniform percolation. *Water Resources Research*, *3*(1), 227–234. https://doi.org/10.1029/WR003i001p00227

Harbaugh, A. W. (2005). *MODFLOW-2005, The U.S. Geological Survey Modular Ground-Water Model—The Ground-Water Flow Process* (Techniques and Methods Nos. 6-A16). U.S. Geological Survey. https://doi.org/10.3133/tm6A16

HydroSOLVE, Inc. (n.d.). *MOUNDSOLV: Groundwater Mounding Software*. AQTESOLV. Retrieved June 17, 2026, from https://www.aqtesolv.com/moundsolv.htm

Ingrao, C., Strippoli, R., Lagioia, G., & Huisingh, D. (2023). Water scarcity in agriculture: An overview of causes, impacts and approaches for reducing the risks. *Heliyon*, *9*(8), e18507. https://doi.org/10.1016/j.heliyon.2023.e18507

Levintal, E., Kniffin, M. L., Ganot, Y., Marwaha, N., Murphy, N. P., & Dahlke, H. E. (2023). Agricultural managed aquifer recharge (Ag-MAR)—a method for sustainable groundwater management: A review. *Critical Reviews in Environmental Science and Technology*, *53*(3), 291–314. https://doi.org/10.1080/10643389.2022.2050160

Rosa, L., & Sangiorgio, M. (2025). Global water gaps under future warming levels. *Nature Communications*, *16*, 1192. https://doi.org/10.1038/s41467-025-56517-2

Schlumberger Water Services. (n.d.). *Visual MODFLOW Premium Demo Tutorial: Includes New Features of Visual MODFLOW and a Step-by-Step Tutorial* [Software tutorial]. Schlumberger Water Services.

Thompson, A., Nimmer, M., & Misra, D. (2007). *Groundwater Mounding and Contaminant Transport Beneath Stormwater Infiltration Basins* [Technical report / Project report]. University of Wisconsin–Madison, Department of Biological Systems Engineering.

Turral, H., Burke, J., & Faurès, J.-M. (2011). *Climate Change, Water and Food Security* (No. 36; FAO Water Reports). Food and Agriculture Organization of the United Nations. https://www.fao.org/4/i2096e/i2096e.pdf

WMO. (2025). *State of Global Water Resources 2024* (WMO Report No. 1380; State of Global Water Resources, p. 98). World Meteorological Organization. https://doi.org/10.59327/WMO/WATER/2024

Xu, Y., Lü, H., Yagci, A. L., Zhu, Y., Liu, D., Wang, Q., Xu, H., Pan, Y., & Su, J. (2024). Influence of groundwater on the propagation of meteorological drought to agricultural drought during crop growth periods: A case study in Huaibei Plain. *Agricultural Water Management*, *305*, 109122. https://doi.org/10.1016/j.agwat.2024.109122

Zheng, Y., Vanderzalm, J., Hartog, N., Fernández Escalante, E., & Stefan, C. (2023). The 21st century water quality challenges for managed aquifer recharge: Towards a risk-based regulatory approach. *Hydrogeology Journal*, *31*(1), 31–34. https://doi.org/10.1007/s10040-022-02543-z

Zlotnik, V. A., Kacimov, A., & Al-Maktoumi, A. (2017). Estimating Groundwater Mounding in Sloping Aquifers for Managed Aquifer Recharge. *Groundwater*, *55*(6), 797–810. https://doi.org/10.1111/gwat.12530

APPENDIX A. Additional figures for the circular recharge scenarios.

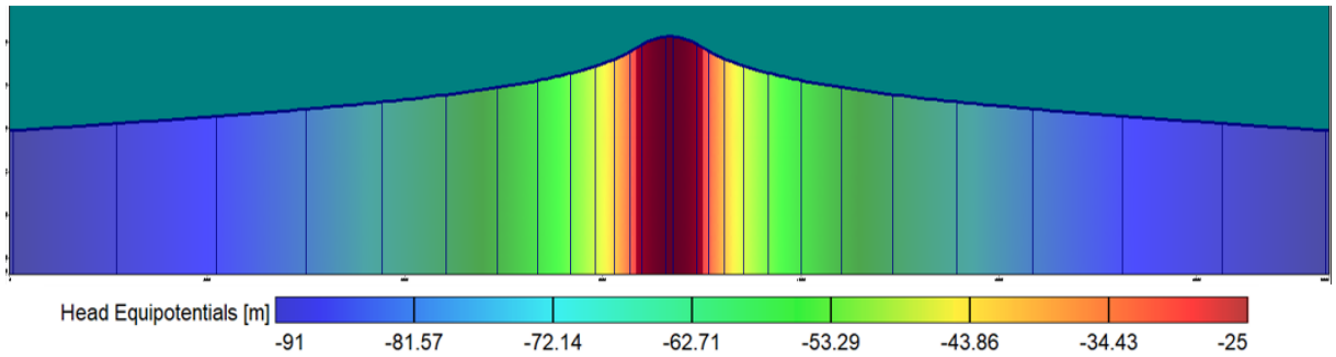

Figure A.1. Central cross-sectional hydraulic-head distribution for the corrected literature-based circular recharge scenario.

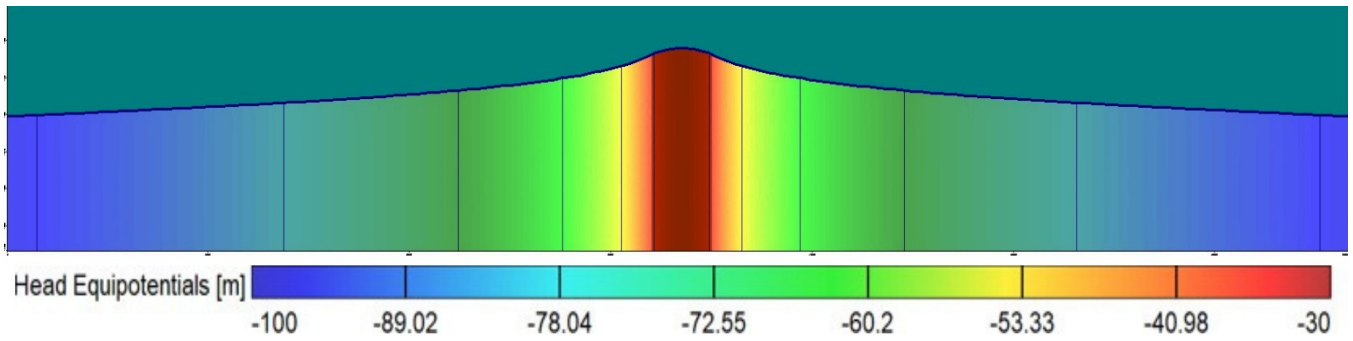

Figure A.2. Central cross-sectional hydraulic -head distribution for the square diagnostic scenario.

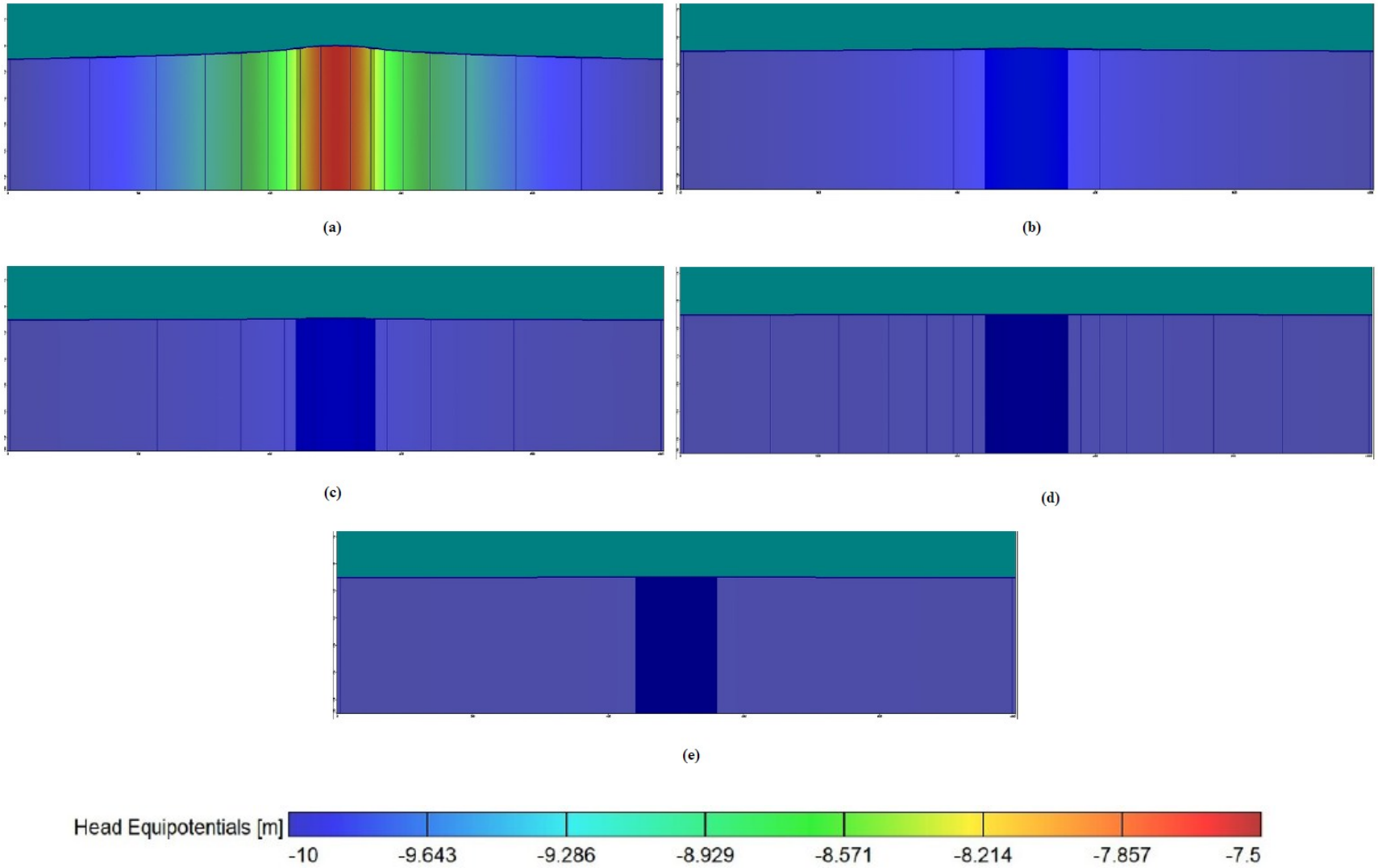

Figure A.3. Comparison of simulated central cross-sectional hydraulic-head distributions for the circular scenario at different transmissivity values.

(a) K = 1 m/day, T = 20 m²/day; (b) K = 5 m/day, T = 100 m²/day; (c) K = 10 m/day, T = 200 m²/day;

(d) K = 50 m/day, T = 1000 m²/day; and (e) K = 100 m/day, T = 2000 m²/day

APPENDIX B. Additional figures for the strip/trench recharge scenarios.

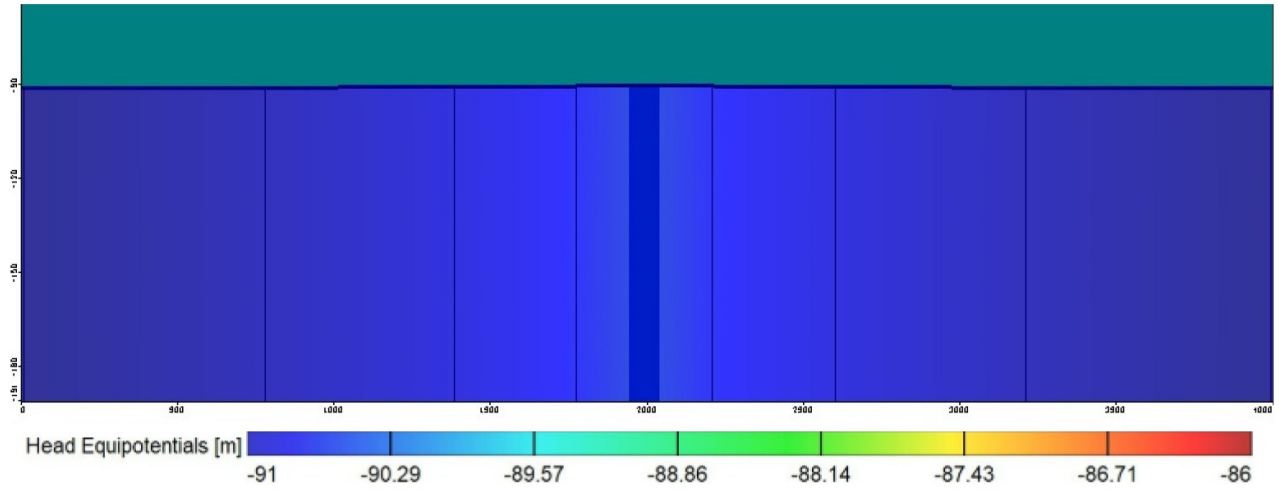

Figure B.1. Central cross-sectional hydraulic-head distribution for the literature-based strip recharge scenario.

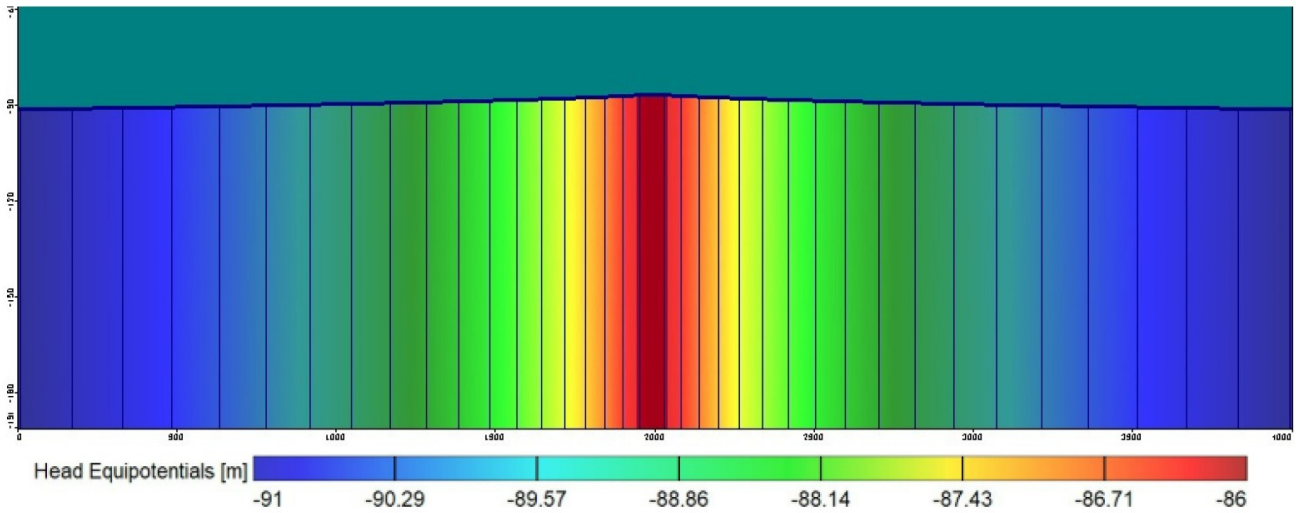

Figure B.2. Central cross-sectional hydraulic-head distribution for the modified recharge-rate strip scenario.

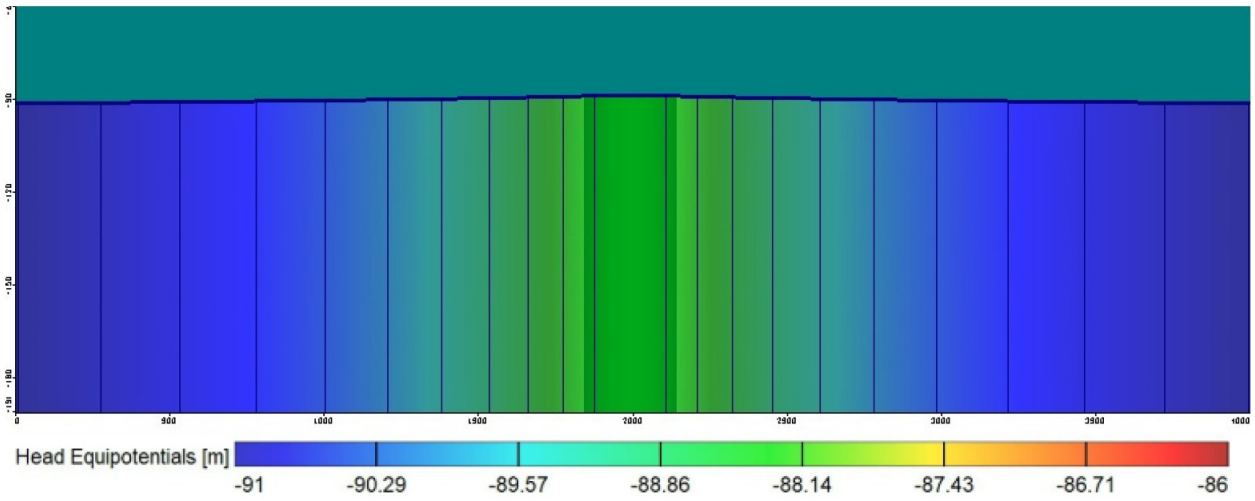

Figure B.3. Central cross-sectional hydraulic head distribution for the modified strip-width scenario.

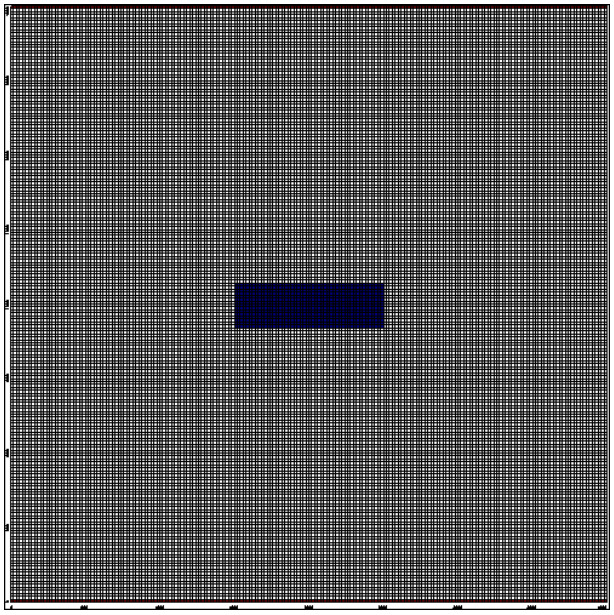

Figure B.4. Numerical model setup for the modified strip-width scenario.

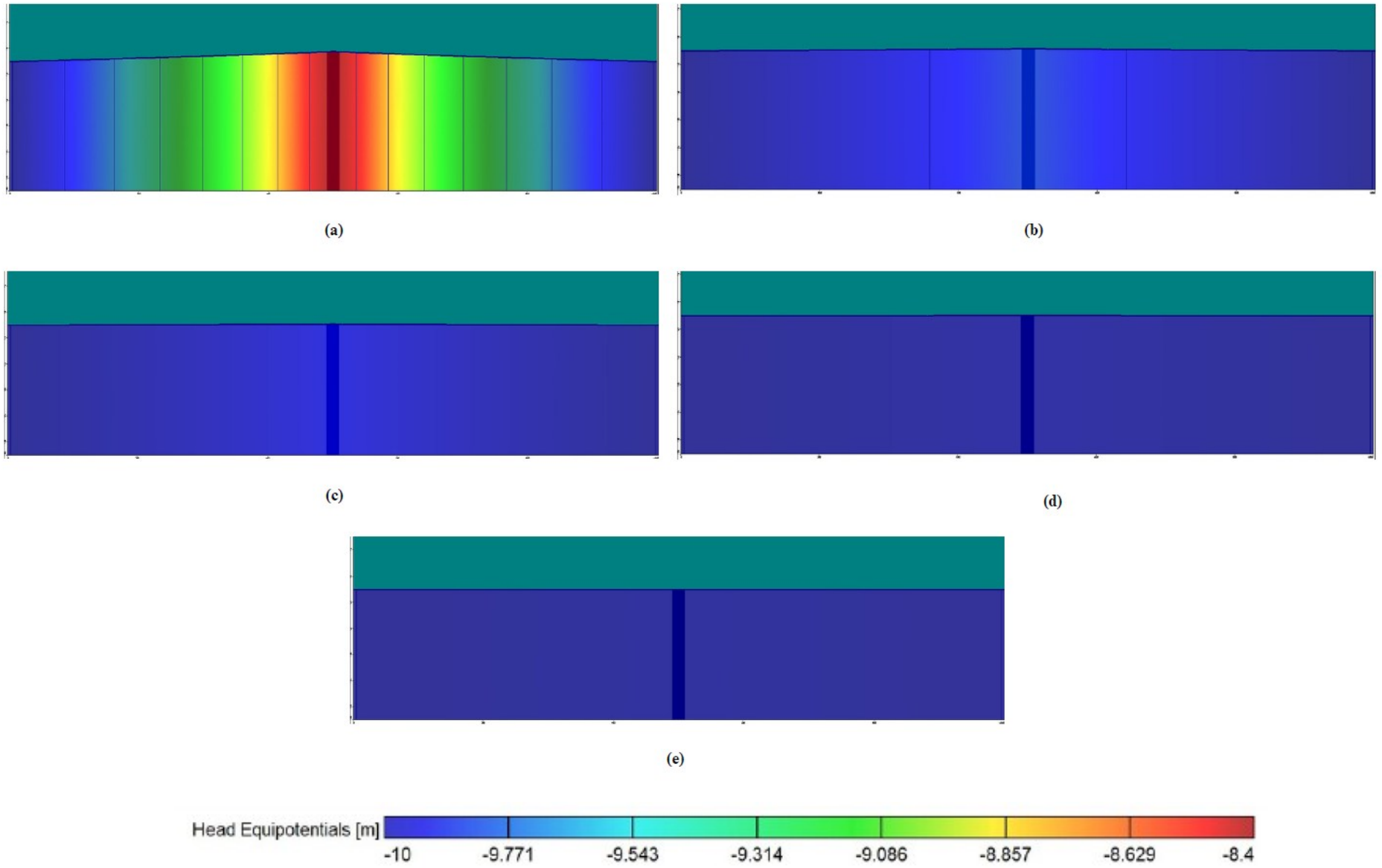

Figure B.5. Comparison of simulated central cross-sectional hydraulic head distributions for the trench scenario at different transmissivity values.

(a) K = 1 m/day, T = 20 m²/day; (b) K = 5 m/day, T = 100 m²/day; (c) K = 10 m/day, T = 200 m²/day;

(d) K = 50 m/day, T = 1000 m²/day; and (e) K = 100 m/day, T = 2000 m²/day

APPENDIX C. Supplementary MOUNDSOLV recovery simulations.

Figures C.1 and C.2 show the preliminary recovery simulations using a 0.05 m threshold. Since this threshold was too strict, a 0.10 m threshold was adopted for the final dissipation-time assessment in Section 4.4.5 and Table 4.23.

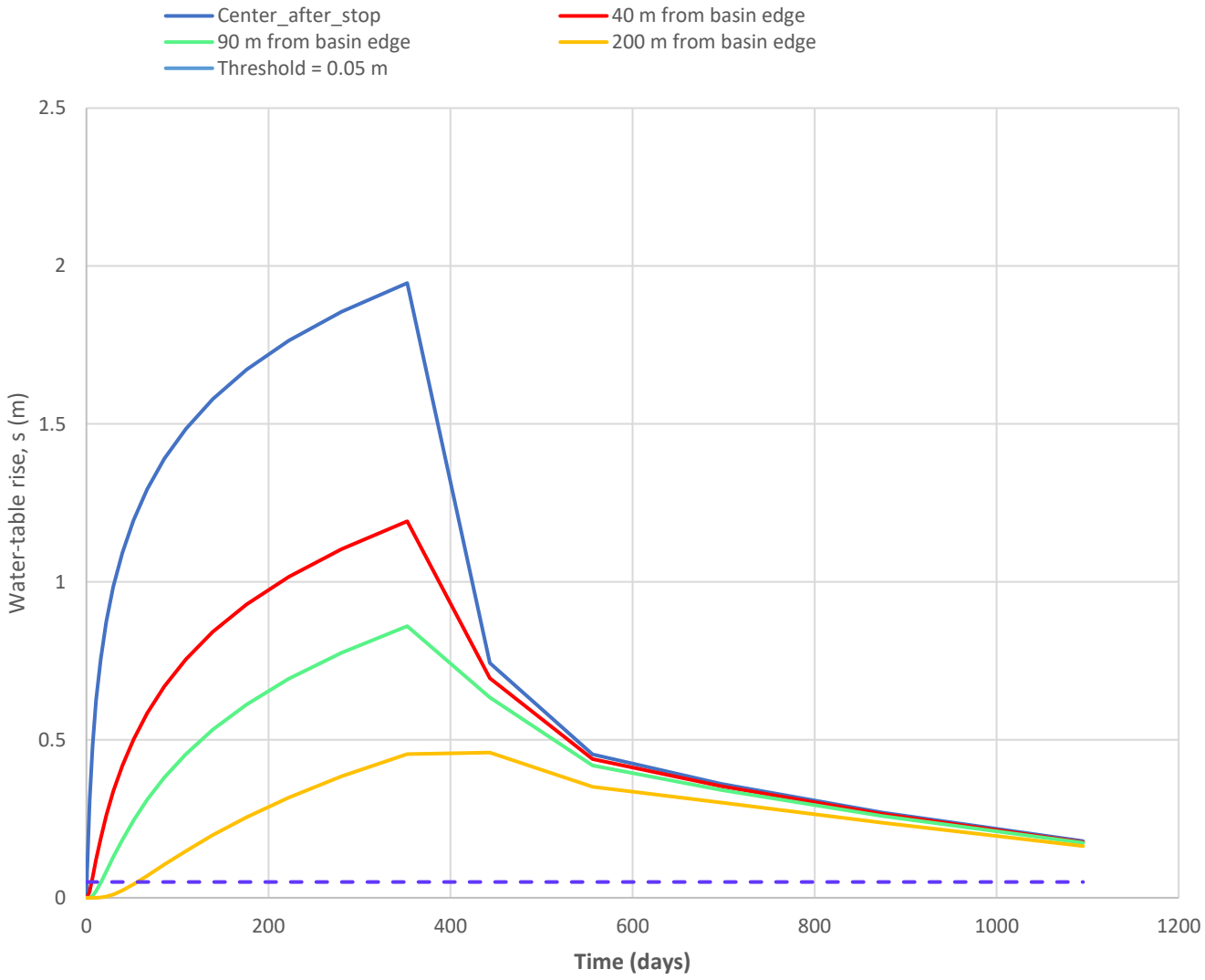

Figure C.1. Preliminary mound dissipation simulation for the 1095-day recovery period. The mound decreased after recharge cessation but did not provide enough long-term information for defining the practical dissipation threshold.

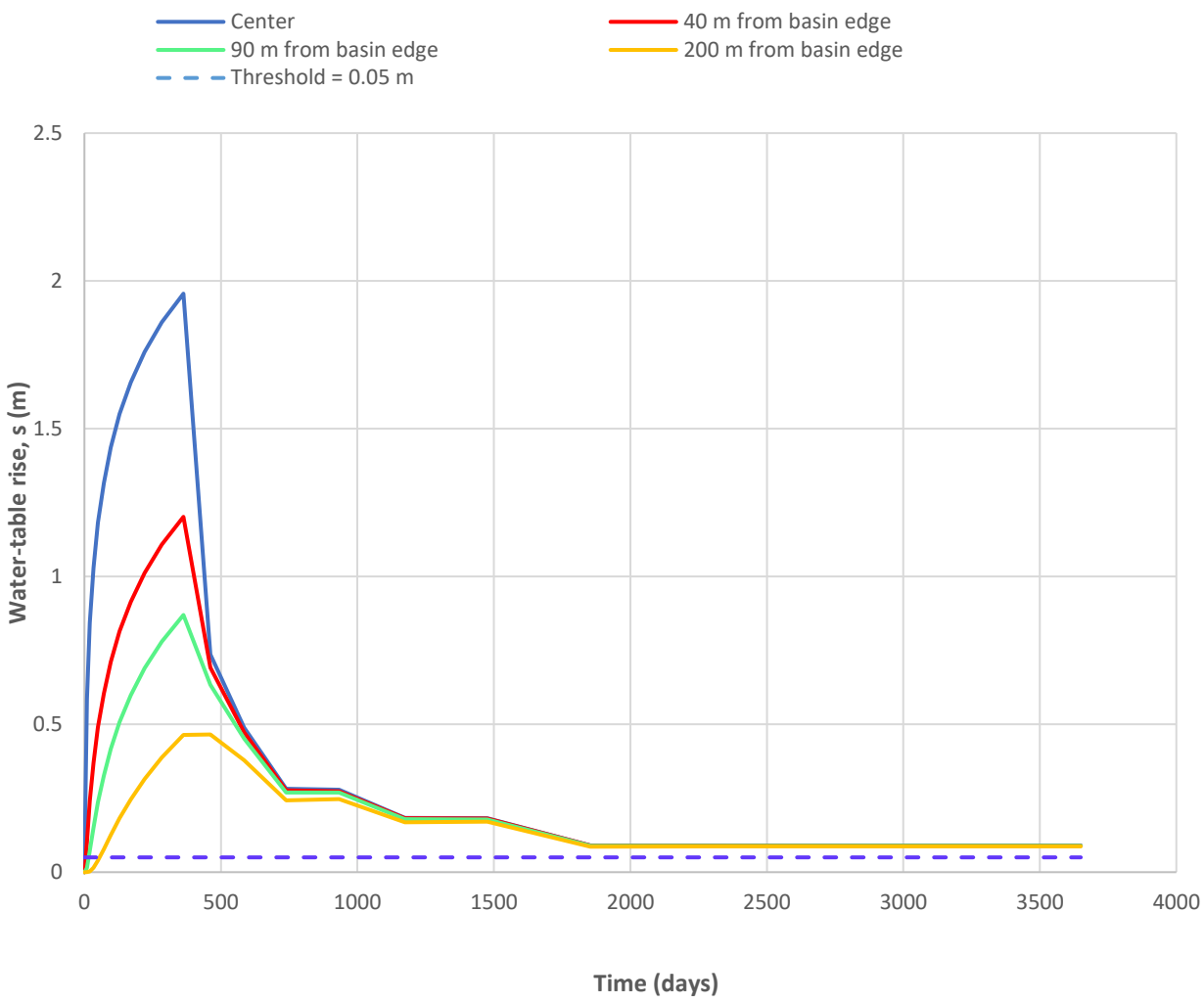

Figure C.2. Preliminary mound dissipation simulation for the 3650-day recovery period. The mound approached the selected threshold, but the extended 36500-day simulation was used for the final dissipation-time assessment.